AN ABSTRACT OF THE THESIS OF

Sutaporn Boon-intra for the degree of Master of Science in Civil Engineering presented on November 30, 2010

Title: Development of a Guideline for Estimating Tsunami Forces on Bridge Superstructures

Abstract approved:

_____

Solomon C. Yim

Infrastructures along the Oregon Coast are vulnerable to seismic events in the Cascadia Subduction Zone that could generate large tsunamis. Bridges along the coast are an important part of the transportation and lifeline system in the area. The major damages on these bridges due to earthquake and/or tsunami would result in traffic disruption along the coast which in turn could significantly damage the economic in the region. Most of these bridges, built between the 1950's and 1970's, were not designed to withstand such large seismic and tsunami loads; thus, they are at risk of being damaged. Since specific design codes for tsunami impact on bridge superstructures are currently not available in general, and in the State of Oregon in particular, this thesis develops and presents a guideline for estimating tsunami forces on bridge superstructures along the Oregon Coast for practical use in engineering design. These guidelines are generally expected to be applicable in other locations under similar situations.

In the development of the guideline, numerical models based on a finite-element code (LS-DYNA) were developed to analyze tsunami impact on full-scaled bridge superstructures of four selected bridges on the Oregon coast - Schooner Creek Bridge, Drift Creek Bridge, Millport Slough Bridge, and Siletz River Bridge. The numerical models were analyzed for a better understanding of the interaction between tsunamis and bridge superstructures and to calculate tsunami forces time-histories on the bridges. Two different types of bridge superstructure, deck-girder and box section, were developed in the case of the Schooner Creek Bridge to study the performance of both the cross-sectional configuration subjected to identical tsunami load conditions. The results showed that the tsunami forces on box section are significantly higher than the forces on deck-girder section; thus, the box section might not be appropriate to be used in a tsunami run-up zone. Moreover, numerical testing of bridge superstructures with rails and without rails under identical tsunami loads are performed to examine an effect of rails to tsunami forces. The results suggested that horizontal and vertical tsunami forces on bridge without rails is smaller than on bridge with rigid rails up to 20% and 15%, respectively. Furthermore, results obtained from the numerical models are incorporated into the mathematical formulations from the existing literature to develop a simplified method for estimating tsunami forces on bridge superstructures. Appropriate empirical coefficients for bridge superstructures under tsunami loads were evaluated in this study based on an average value of the scattering data from the numerical results. However, the guideline is intended to be used as a preliminary guidance for design only as it did not accounted for uncertainties, therefore, an

appropriate factor of safety must be included in the design. A previous analysis of tsunami forces on the Spencer Creek Bridge on the Oregon Coast, also performed by the research group in which the author is a member, is revisited to examine the applicability of the developed guideline. This thesis also presents computational performance studies and an optimal number of CPUs for running fluid-structure interaction (FSI) numerical models of bridge superstructures using LS-DYNA software on high-performance computing (HPC) systems.

Development of a Guideline for Estimating Tsunami Forces on Bridge Superstructures

by

Sutaporn Boon-intra

A THESIS

submitted to

Oregon State University

in partial fulfillment of
the requirements for the
degree of

Master of Science

Presented November 30, 2010

Commencement June 2011

Master of Science thesis of Sutaporn Boon-intra

presented on November 30, 2010.

APPROVED:

_____

Major Professor, representing Civil Engineering

_____

Head of the School of Civil and Construction Engineering

_____

Dean of the Graduate School

I understand that my thesis will become part of the permanent collection of Oregon State University libraries. My signature below authorizes release of my thesis to any reader upon request.

_____

Sutaporn Boon-intra, Author

ACKNOWLEDGEMENTS

I am grateful to all those who made this thesis possible. I would like to thank Dr. Solomon C. Yim for being a great mentor and advisor during the time of research. I am deeply appreciated a great opportunity that you offered. It is a pleasure to thank Seshu B. Nimmala and Holly M. Winston for interested in my research and your contributions. Without your help this research would be a lot more difficult. I am indebted to my colleagues for their friendship and supports.

To Sirikarn Woracheewan, Mathukorn Sanwanich, Wipada Sompong, and so many people that I did not mention your name: you have been such a great friend here in Corvallis. Thank you for being here and help me get through this challenging time. To all my best friends in Thailand (you know who you are), I thank you for your friendship and for being there when I needed the most. It is an honor for me to have you in my life. I owe my deepest gratitude to Tipakorn Greigarn for always be there for me. You are my best friend and my family. I would've never been this far without you. Finally, my family, your unconditional love and supports help me get through this challenging time. Who I am in my life, I owe it to you.

CONTRIBUTION OF AUTHORS

The author would like to show gratitude to Prof. Kwok Fai Cheung of the Department of Ocean and Resources Engineering, University of Hawaii, USA for providing tsunami inundation data as input sources in the numerical models. It is a pleasure to thank Seshu B. Nimmala for his availability to assist in running numerical models and his advice. I am indebted to Holly M. Winston for her supervision and reviewing this work despite her busy schedule. Finally, the author shows deepest gratitude to people from ODOT for their comments and suggestions that helped directing this thesis.

TABLE OF CONTENTS

Page

General Introduction 1

Development of a Guideline for Estimating Tsunami Forces on Bridge Superstructures 4

Abstract 5

Introduction 6

Background 6

Tsunami Flow Field 8

Literature Review 10

Wave Forces Equations 10

Literature of Tsunami Forces 12

Summary of Literature Review 13

Numerical Models of Tsunami Impact Load on Bridge Superstructures 14

Model Description 15

Bridge Descriptions and Tsunami Flow Fields 16

Tsunami Force Time-Histories 18

Effect of Cross-Sectional Bridge Type 20

Effect of Rails 21

Cumulative Probability of Maximum Tsunami Forces 22

Computational Efforts 23

Estimation of Tsunami Forces on Bridge Superstructures 26

Horizontal Forces 26

Vertical forces 29

Discussion and Limitation of Recommended Approach 31

Case study of the Spencer Creek Bridge – revisited 32

Computational Performance 34

Concluding Remarks 36

TABLE OF CONTENTS (Continued)

Page

Future Research 38
References 41
General Conclusion 75
Bibliography 78
Appendices 80
Appendix A Simulation Models 81
Appendix B Tsunami Time-History Forces of the Selected Bridge Superstructures 104
Appendix C Example Calculations of Tsunami forces on Bridge Superstructure 113
Appendix D A case study of the Spencer Creek Bridge, Oregon – revisited: 118
Appendix E Drawing of the Selected Bridges 125

LIST OF FIGURES

Figure Page

1. Top view map of Siletz bay area and location of the selected bridges 43
2. Boundaries of Cascadia Subduction zone inferred from the National Seismic Hazard Map (2008) 43
3. An example of numerical model of Millport Slough Bridge 44
4. Comparisons of predicted horizontal tsunami force (lb/in) time-history on different bridge geometry 45
5. Comparisons of predicted vertical tsunami force (lb/in) time-history on different bridge geometry 46
6. Comparisons of predicted overturning moment (kip-ft/ft) time-history on different bridge geometry 47
7. Time-Histories of predicted horizontal tsunami force (lb/in) on Schooner Creek Bridge (Deck-Girder) 48
8. Time-Histories of predicted vertical tsunami force (lb/in) on Schooner Creek Bridge (Deck-Girder) 49
9. Time-Histories of predicted overturning moment (kip-ft/ft) on Drift Creek Bridge 50
10. Time-Histories of predicted horizontal tsunami force (lb/in) on Drift Creek Bridge 51
11. Time-Histories of predicted vertical tsunami force (lb/in) on Drift Creek Bridge 52
12. Time-Histories of predicted overturning moment (kip-ft/ft) on Drift Creek Bridge 53
13. Time-Histories of predicted horizontal tsunami force (lb/in) on Millport Slough Bridge 54
14. Time-Histories of predicted vertical tsunami force (lb/in) on Millport Slough Bridge 55
15. Time-Histories of predicted overturning moment (kip-ft/ft) on Millport Slough Bridge 56

LIST OF FIGURES (Continued)

Figure Page

16. Water elevation time-histories at Siletz River Bridge 57

17. Cumulative probability of Maximum Horizontal Tsunami Force 58

18. Cumulative probability of Maximum Vertical Tsunami Force 59

19. A relationship between maximum flux momentums and maximum predicted horizontal tsunami forces 61

20. Parameters definition used in the recommended equations for estimating tsunami forces 64

21. Relationships between total horizontal force and flux momentum (flux momentum-dependent part) 65

22. Comparisons between estimated maximum horizontal tsunami force and predicted maximum horizontal tsunami force 66

23. Relationship between horizontal water velocity with and without obstruction 67

24. Comparisons between the estimated maximum vertical force and the predicted numerical maximum vertical force 68

25. Maximum percentage of pressure distribution under each girder along the cross-section at Schooner Creek Bridge 69

26. Maximum percentage of pressure distribution under each girder along the cross-section at Drift Creek Bridge 70

27. Maximum percentage of pressure distribution under each girder along the cross-section at Millport Slough Bridge 71

28. Empirical drag coefficients for Spencer Creek Bridge 72

29. Relationships between consumed computational time and number of computer CPU 73

30. Relationships between computational time, unit cost, and number of computer CPU 74

31. Boundary conditions. 82

LIST OF FIGURES (Continued)

Figure Page

32. Simulation model of Schooner Creek Bridge (deck-girder) cross-section with one-inch thickness in z-direction....85

33. Simulation model of Schooner Creek Bridge (box-section) cross-section with one-inch thickness in z-direction....85

34. Simulation model of Millport Slough Bridge cross-section with one-inch thickness in z-direction....86

35. Input conditions for simulation models of Schooner Creek Bridge under GA M_w 9.0 tsunami scenario....87

36. Input conditions for simulation models of Schooner Creek Bridge under GA M_w 9.2 tsunami scenario....87

37. Input conditions for simulation models of Schooner Creek Bridge under LZ M_w 9.0 tsunami scenario....88

38. Input conditions for simulation models of Schooner Creek Bridge under MT M_w 9.0 tsunami scenario....88

39. Input conditions for simulation models of Schooner Creek Bridge under TZ M_w 9.0 tsunami scenario....89

40. Input conditions for simulation models of Drift Creek Bridge under GA M_w 9.2 tsunami scenario....89

41. Input conditions for simulation models of Drift Creek Bridge under LZ M_w 9.0 tsunami scenario....90

42. Input conditions for simulation models of Drift Creek Bridge under MT M_w 9.0 tsunami scenario....90

43. Input conditions for simulation models of Millport Slough Bridge under GA M_w 9.2 tsunami scenario....91

44. Input conditions for simulation models of Millport Slough Bridge under LZ M_w 9.0 tsunami scenario....91

45. Input conditions for simulation models of Millport Slough Bridge under MT M_w 9.0 tsunami scenario....92

LIST OF FIGURES (Continued)

Figure Page

46. Captured of Schooner Creek Bridge (box-section) under GA M_w 9.0 tsunami scenario 93

47. Captured of Schooner Creek Bridge (box-section) under LZ M_w 9.0 tsunami scenario 94

48. Captured of Schooner Creek Bridge (box-section) under MT M_w 9.0 tsunami scenario 95

49. Captured of Schooner Creek Bridge (box-section) under TZ M_w 9.0 tsunami scenario 96

50. Captured of Schooner Creek Bridge (deck-girder) under GA M_w 9.0 tsunami scenario 96

51. Captured of Schooner Creek Bridge (deck-girder) under GA M_w 9.2 tsunami scenario 97

52. Captured of Schooner Creek Bridge (deck-girder) under LZ M_w 9.0 tsunami scenario 98

53. Captured of Schooner Creek Bridge (deck-girder) under MT M_w 9.0 tsunami scenario 99

54. Captured of Schooner Creek Bridge (deck-girder) under TZ M_w 9.0 tsunami scenario 100

55. Captured of Drift Creek Bridge under GA M_w 9.2 tsunami scenario 101

56. Captured of Drift Creek Bridge under LZ M_w 9.0 tsunami scenario 102

57. Captured of Millport Slough Bridge under GA M_w 9.2 tsunami scenario 103

58. Captured of Millport Slough Bridge under LZ M_w 9.0 tsunami scenario 103

59. Time-history forces of Schooner Creek Bridge (box-section) under GA M_w 9.0 tsunami conditions 105

60. Time-history forces of Schooner Creek Bridge (box-section) under GA M_w 9.2 tsunami conditions 105

LIST OF FIGURES (Continued)

Figure Page

61. Time-history responses of Schooner Creek Bridge (box-section) under LZ M_w 9.0 tsunami conditions 106

62. Time-history forces of Schooner Creek Bridge (box-section) under MT M_w 9.0 tsunami conditions 106

63. Time-history forces of Schooner Creek Bridge (box-section) under TZ M_w 9.0 tsunami conditions 107

64. Time-history forces of Schooner Creek Bridge (deck-girder) under GA M_w 9.0 tsunami conditions 107

65. Time-history forces of Schooner Creek Bridge (deck-girder) under GA M_w 9.2 tsunami conditions 108

66. Time-history forces of Schooner Creek Bridge (deck-girder) under LZ M_w 9.0 tsunami conditions 108

67. Time-history forces of Schooner Creek Bridge (deck-girder) under MT M_w 9.0 tsunami conditions 109

68. Time-history forces of Schooner Creek Bridge (deck-girder) under TZ M_w 9.0 tsunami conditions 109

69. Time-history forces of Drift Creek Bridge under GA M_w 9.2 tsunami conditions 110

70. Time-history forces of Drift Creek Bridge under LZ M_w 9.0 tsunami conditions110

71. Time-history forces of Drift Creek Bridge under MT M_w 9.0 tsunami conditions 111

72. Time-history forces of Millport Slough Bridge under GA M_w 9.2 tsunami conditions 111

73. Time-history forces of Millport Slough Bridge under LZ M_w 9.0 tsunami conditions 112

74. Model of Spencer Creek Bridge [ref: ftp://ftp.wsdot.wa.gov/public/Bridge/WBES2007] 118

LIST OF FIGURES (Continued)

Figure Page

75. Spencer Creek Bridge [ref: http://bridgehunter.com/photos/].....119

76. Horizontal and vertical force time-histories based on Cornell tsunami model 120

77. Horizontal and vertical force time-histories based on FVWAVE tsunami model120

78. Preliminary drawing of Schooner Creek Bridge (deck-girder).....125

79. Preliminary drawing of Schooner Creek Bridge (box-section).....126

80. Preliminary drawing of Drift Creek Bridge 127

81. Plan and elevation view of new Millport Slough Bridge 128

82. Staging plan of new Millport Slough Bridge 129

83. Plan and elevation view of Siletz River Bridge 130

LIST OF TABLES

Table Page

1. Maximum forces and moments due to tsunami loads on superstructure of Schooner Creek Bridge 24
2. Maximum forces and moments due to tsunamis on Drift Creek Bridge (with rigid rails) 24
3. Maximum forces and moments due to tsunamis on superstructure of Millport Slough Bridge (including rails) 24
4. Joint Probability of Rupture Scenarios (After Cheung et al. 2010) 25
5. Computational efforts for performing the simulation models 25
6. Summary of computational time 36

General Introduction

The Oregon Coast is vulnerable to seismic events in the Cascadia Subduction Zone (CSZ) that could generate large tsunamis, which could damage the infrastructures along the coastal area. Bridges along the coast are an important part of the transportation and lifeline system in the area. They were mostly built in the 1950's through the 1970's and were not designed to withstand such large seismic or tsunami loads. Hence the Oregon Department of Transportation (ODOT) is preparing for replacements or retrofits of these bridges to avoid potential major damages that could cause traffic disruption and economic losses in the area due to those loads. However, unlike seismic loads, currently there is no specific design standard for estimating tsunami forces on bridge superstructures in general and in the State of Oregon in particular. The existing literature focused mainly on computing tsunami forces on vertical structures – such as vertical wall, column, and pile – and wave forces on bridge decks due to storm surge or river floods. Therefore, an understanding of the fluid loads on bridge superstructures under tsunamis is of major interest to the practicing engineering community.

In this context, this thesis developed numerical models of tsunami impact on bridge superstructures to study the interaction between the fluid and the structure. The models were developed to perform numerical testing of tsunami impact on bridge superstructures whereas the alternative of performing laboratory experiments could be more expensive and difficult to control. The numerical models were developed by

using general purpose multi-physics simulation software, LS-DYNA, which has a capability to handle fluid-structure interaction (FSI) problems.

This Master thesis is written in a manuscript document format and contains a manuscript titled “Development of a Guideline for Estimating Tsunami Forces on Bridge Superstructures”. The presented manuscript consists of two major works extended from a previous study of tsunami design criteria on the Spencer Creek Bridge, Oregon, conducted by Nimmala et al. (2006). The first part of this research includes development of numerical models of tsunami impact on the selected bridge superstructures. The second part presents the development of a guideline for estimating tsunami forces on bridge superstructures in a tsunami run-up zone based on the numerical results obtained in the first part of this research. The previous analysis of the Spencer Creek Bridge is revisited in this thesis to examine the impact of the guideline so developed and evaluate the applicability of the formulations suggested in the guideline. In addition, this manuscript also presents a performance testing of LS-DYNA software with FSI models. The performance testing was intentionally performed to determine an optimal number of processors (i.e., CPUs) for solving FSI problems with LS-DYNA software on high-performance computing (HPC) system.

The appendices consist of five sections describing the details development of the numerical models, bridge descriptions, and time-history forces on the bridge superstructures under the selected tsunami load conditions. The first section describes boundary conditions used in the numerical models, a summary of the theoretical background of the calculation performed by LS-DYNA, the selected input tsunami

flow fields, and snapshots of tsunami impact on the bridge superstructures. The second section shows plots of horizontal force and vertical force time-histories of the bridge superstructures under various tsunami flow fields. The third section presents example calculations of tsunami forces on bridge superstructures. The fourth section summarizes a case study of the Spencer Creek Bridge conducted by Nimmala et al. (2006) and a study of the guideline applicability. Finally, the fifth section contains preliminary drawing of the selected bridges that were used for constructing the bridge part in the numerical models.

Development of a Guideline for Estimating Tsunami Forces on Bridge Superstructures

Sutaporn Boon-intra, Solomon C. Yim, Seshu B. Nimmala, Holly M. Winston

School of Civil and Construction Engineering, Oregon State University, Corvallis, Oregon USA

Kwok Fai Cheung

Department of Ocean and Resources Engineering, University of Hawaii, Honolulu, Hawaii, USA

1. Abstract

The Pacific Northwest is vulnerable to seismic events in the Cascadia Subduction Zone (CSZ) that could generate large tsunami to devastate coastal infrastructures such as bridges. In this context, this paper describes a development of a guideline for estimating tsunami forces on bridge superstructures along the Oregon Coast. A multi-physics based numerical code is used to perform numerical testing of tsunami impact on full-scaled bridge superstructures of four selected bridges – Schooner Creek Bridge, Drift Creek Bridge, Millport Slough Bridge, and Siletz River Bridge – located on Highway 101 in the Siletz Bay area on the Oregon Coast. Two different types of bridge superstructure, deck-girder and box sections, are developed in the case of the Schooner Creek Bridge to study an effect of geometry of bridge cross-section. The results show that tsunami forces on box section are significantly higher than the forces on deck-girder section; therefore, the box section might not be appropriate to be used in a tsunami run-up zone. Moreover, numerical testing of deck-girder bridge with rigid rails and without rails subjected to identical tsunami loads are performed to examine an effect of rails to tsunami forces. The results suggested that horizontal and vertical tsunami forces on bridge with rails are larger than those on bridge without rails up to 20% and 15%, respectively. These numerical results are finally incorporated into the mathematical formulations from the existing literature to develop a simplified method for estimating tsunami forces on bridge superstructures. Appropriate empirical coefficients for bridge superstructures under tsunami loads were evaluated based on an average value of the scattering data from the numerical results. The developed

guideline is intended to be used as a preliminary guidance for design only as it did not accounted for uncertainties; thus, an appropriate factor of safety must be included in the calculations. A previous analysis of tsunami forces on the Spencer Creek Bridge on the Oregon Coast is revisited to examine the applicability of the guideline developed in the present work. This paper also presents the results of a study on the optimal number of CPUs for running fluid-structure interaction (FSI) numerical models of bridge superstructures using LS-DYNA on high-performance computing (HPC) systems.

2. Introduction

2.1. Background

The Oregon coast is vulnerable to large seismic events in the Cascadia Subduction zone (CSZ) which shares common seismic characteristics with those at Sumatra that generated large tsunamis in the Indian Ocean in December 2004. Studies of tsunami deposits and evidences of coastal subsidence indicate that an average of large seismic events in CSZ occurs once every 500 years (Goldfinger et al. 2003). The most recent large seismic event in the CSZ occurred in 1700; therefore, there is a relatively high probability that a large seismic event will occur in the near future that could damage the infrastructures along the coastal area in the Pacific Northwest.

The bridges along the Oregon Coast are an important part of the transportation and lifeline system in the area. Any major damages to these bridges would result in traffic disruption and impede post-event emergency response. Since these bridges, mostly

built in the 1950-70's, were not designed to resist such large seismic or tsunami loads, they are at the risk of being severely damaged during large seismic events. However, unlike seismic loads, currently there is no specific design standard for estimating tsunami forces on bridge superstructures in the US in general and in Oregon in particular. Therefore, an understanding of tsunami impact on bridge superstructures is of major interest to the practicing engineering community. Consequently, the Oregon Department of Transportation (ODOT) initiated a research program to develop a guideline for estimating tsunami forces on bridge superstructures in the tsunami run-up zone along the Oregon Coast. This guideline is also expected to be applicable in other locations under similar situations.

Nonlinear finite element analysis (NL-FEA) is an essential analysis tool as a less expensive alternative to perform a prototype model testing. It increasingly replaces prototype testing in many industries because of its advantages in providing a better understanding of basic physical behavior of interested structures under controlled environments by providing time-history responses that are not measurable – such as stress, strain, reaction forces, and other variables – while laboratory experiment of prototype provides globally important results. Therefore, it is used to analyze tsunami impact on bridge superstructures, and determine time-history forces on the bridge under various tsunami load conditions in this study. The numerical models are developed by using a multi-physics finite element based code, LS-DYNA, which is one of very accurate software for analyzing fluid-impact on structure with free surface.

This study is divided into two major parts. The first part is to develop numerical models to perform full-scale simulation of tsunami impact on bridge superstructures, and calculate reaction forces due to tsunami loads on four selected bridges on the Oregon Coast. The four bridges – Schooner Creek Bridge, Drift Creek Bridge, Millport Slough Bridge, and Siletz River Bridge – are located on Highway 101 in the Siletz bay area as shown in Figure 1. The second part is to develop a guideline for estimating tsunami forces on bridge superstructures to be used as preliminary guidance for design of bridges in the tsunami run-up zone. The developed guidance base on existing literature and time-history results obtained from the numerical models calculated in the first part.

This research is an extension of a previous case study of tsunami design criteria on the Spencer Creek Bridge, Oregon, conducted by Nimmala et al. (2006). The Spencer Creek project was conducted by developing numerical models of tsunami impact on bridge deck to determine the time-history forces on the bridge by using LS-DYNA software. The analysis is revisited late in this paper to examine the applicability of the guideline developed in the present work.

2.2. Tsunami Flow Field

The input tsunami flow fields, water surface elevation and water velocity time-histories, for the simulation models were obtained from tsunami numerical models developed by Cheung and associates from University of Hawaii (Cheung et al. 2010). The nonlinear shallow-water model by Yamazaki et al (2009) was utilized to capture

hydraulic processes – wave overtopping, hydraulic jump formation, and bore propagation – describing flow conditions at the interested bridge sites. The development of a rupture model based on 500-year Cascadia earthquake scenarios from the National Seismic Hazard Maps is illustrated in Figure 2. The rupture boundaries extend approximately 1,100 km from Cape Mendocino in northern California to Vancouver Island in British Columbia. The western boundary of the rupture is specified along the trench at the base of the continental slope. Additional conditions are provided by Wang et al (2003) to define the eastern rupture boundaries at the midpoint of the transition zone (MT) and the base of the transition zone (BT). Moreover, a global analog (GA) of shallow-dipping subduction zones, from Tichelaar and Ruff (1993), is used to define the eastern rupture boundary at 123.8°W at 30 km depth.

Four hours duration of tsunami flow field data of a 500-year Cascadia tsunami event at the Siletz bay were provided in six different scenarios. The six tsunami scenarios base on four rupture configurations at moment magnitude (M_w) 9.0 and two additional moment magnitude 8.8 and 9.2 at the rupture based on global analog zone. The first configuration assumes the rupture occurs within the locked zone (LZ, black line in Figure 2) only. The eastern rupture occurs at the midpoint of the transition zone (MT, yellow line in Figure 2) and at the base of the transition zone (TZ, pink line in Figure 2). The fourth rupture configuration is assumed to occur at 30 km depth based on global analog (GA, blue line in Figure 2).

A relative weight distribution probability of occurrence for the rupture configurations (0.1, 0.2, 0.2 and 0.5 for LZ, MT, BT and GA, respectively) and moment magnitudes (0.6, 0.2 and 0.2 for M_w 9.0, 8.8 and 9.2) are assigned based on the logic tree in the Pacific Northwest seismic source model in Cheung et al. (2010).

3. Literature Review

Currently, there is no specific code of practice to obtain the information of forces on bridge superstructures due to tsunami loads. However, there is an availability of some relevant literature of wave forces on highway bridge decks and offshore platforms, and some literature on tsunami forces for other type of structures such as vertical wall, elevated slab, and columns of different shapes.

3.1. Wave Forces Equations

3.1.1. Wave Forces on Decks of Offshore Platforms

Bea et al. (1999) presented a modification of the American Petroleum Institute (API) guidelines for estimating wind-induced wave forces on a platform deck of offshore structures by separating the total wave force into two components, horizontal force and vertical force. The horizontal force consisted of slamming force ($F_s = 0.5C_s\rho A_h u_x^2$), drag force ($F_d = 0.5C_d\rho A_h u_x^2$), and inertia force ($F_i = C_m\rho Va$). The slamming force and drag force depended on horizontal velocity of the waves while the inertia force depended on the acceleration. The vertical force consisted of buoyant

force ($F_b = \rho V g$) and lifting force ($F_l = 0.5 C_l \rho A_v u_y^2$), which depended on vertical velocity of the waves.

3.1.2. Wave Forces on Bridge Decks

Douglass et al. (2006) presented a method for estimating wave forces on typical U.S. coastal bridge spans due to wind waves and storm surge to offer a preliminary guidance for design engineers. The estimated horizontal and vertical forces in that method mainly depended on the elevation of the wave crest as shown in equation (3.1.1) and (3.1.2), respectively. Other than water elevation, the horizontal force also depended on the number of girders supporting the bridge deck. This recommended approach was verified with post-storm damages on U.S. 90 Bridge across Biloxi bay, Mississippi by Hurricane Katrina.

$$F_H = [1 + C_r(N-1)](C_{h-va} + C_{h-im})\gamma(\Delta h)A_h \quad (3.1.1)$$

$$F_V = (C_{v-va} + C_{v-im})\gamma(\Delta h)A_v \quad (3.1.2)$$

where C_r is a reduction factor for forces distribution on the internal girders; N is number of girders supporting bridge deck; C_{h-va} and C_{v-va} are empirical coefficients for slow varying horizontal and vertical force respectively; C_{h-im} and C_{v-im} are empirical coefficients for horizontal and vertical impact force respectively. The other parameters are generally defined in notation.

3.2. Literature of Tsunami Forces

3.2.1. Guidelines for Design of Structures for Vertical Evacuation from Tsunamis

FEMA P646 (2008), guidelines for design of structures for vertical evacuation from tsunamis, summarized the relevant design code, and presented equations for estimating tsunami forces on vertical evacuation structures. It also provided some suggestions on how to combine tsunami force with other loads such as dead load and live load. Load effects that had to be considered for tsunami forces consisted of hydrostatic ($F_h = 0.5\gamma b h_{max}^2$), hydrodynamic ($F_d = 0.5 C_d \rho b (hu^2)_{max}$), impulsive ($F_i = 1.5 F_d$), buoyant ($F_b = \rho V g$) and uplift forces ($F_l = 0.5 C_u \rho A_v u_y^2$). The hydrostatic force depended on water elevation and would be considered to be zero when water fills up on two opposite sides. Unlike the wave forces due to storm surge, the hydrodynamic force due to tsunamis depended on flux momentum (hu^2) where h is elevation of water crest and u is horizontal velocity. The impulsive force due to tsunami could be estimated by taking 1.5 times the corresponding hydrodynamic force for conservatism.

3.2.2. Performance-Based Tsunami Engineering

Performance-Based Tsunami Engineering (PBTE, 2010) was developed by a team of ocean, hydraulic and structural engineers to establish guidelines for the design of future coastal infrastructure. In this research, laboratory experiments and simulation models were performed to obtain information of tsunami bore formation, energy dissipation, and coastal inundation. The obtained tsunami flow field was used to study

interaction between tsunamis and structural components, such as vertical walls and elevated slabs. Differ from FEMA (2008), the equation for estimating hydrodynamic uplift force presented in this method is a function of horizontal water velocity. A study of sediment transportation due to tsunamis and scour was also included.

3.3. Summary of Literature Review

The existing literature does not provide adequate information for estimating tsunami forces on bridge superstructures. The existing approaches are mostly applicable for wave force and tsunami force estimation in specific situations. Bea et al. (1999)'s method is recommended in API guidelines to estimate wave forces on lower deck of offshore platforms. The equations presented therein are mostly depended on the wave velocity while neglecting the relevance of the wave crest elevation. Moreover, the empirical coefficients were evaluated from laboratory testing on platform deck models which may not be applicable in estimating forces on a highway bridge deck. Douglass et al. (2006) developed a method for the Federal Highway Administration (FHWA) to estimate wave forces on highway bridge decks due to storm surge. Their approach was developed based on laboratory experiments of a scaled bridge deck model in a 3D wave basin. The resulting predictions were shown to be adequate for estimating the wave force induced by storm as verified by measured field damages from Hurricane Ivan and Katrina. However, the equations presented in that method depended only on wave crest elevation without considering the importance of water velocity, which is an important factor in tsunamis. Finally, the guideline for design of structures for vertical evacuation from tsunamis provided by FEMA P646 (2008) and PBTE (2010)

presented details of load effects that had to be considered in estimating the tsunami design forces. These guidelines were developed for vertical structures and elevated slabs only, thus, it might not directly apply to the horizontal structures such as bridge superstructures.

Even though the existing methods are not appropriate to be used directly for estimating tsunami forces on bridge superstructures, they provided background knowledge on wave force characterization, and a general idea on how to develop appropriate guideline for fluid load estimation. These approaches, thus, are modified and incorporated with numerical tsunami force data to develop a guideline for estimating tsunami forces on bridge superstructures along the coast.

4. Numerical Models of Tsunami Impact Load on Bridge Superstructures

The models are developed to perform numerical testing of tsunami impact on realistic bridge superstructures to predict the magnitude of tsunami forces that could occur on specific types of bridge superstructure. This section presents details development of the numerical models, bridge descriptions as well as time-history of fluid loads on bridge superstructures under various tsunami flow fields. Effect of different cross-sectional bridge type and effect of rails to fluid loads are discussed followed by cumulative probabilities of tsunami forces and overturning moments. Furthermore, computational efforts are also summarized and presented in this section.

4.1. Model Description

Two-dimensional (2-D) numerical models are developed using a finite-element based code. The provided tsunami flow velocities are assumed to be uniform over depth and resolved in the direction perpendicular to the longitudinal span of the bridge. The cross-section of the bridge superstructure normal to the longitudinal span is modeled by assuming simply supported under external girders.

In general, a simulation model consists of two major material parts: a fluid part and a rigid structure part. The fluid part is a composition of water and air materials which are demonstrated by appropriate material type combining with equation of states (explained in Appendix A). For computational efficiency, an approximating rigid body material was used to represent bridge part and reaction forces are determined by replacing four rigid elements at supports by elastic material. As mentioned earlier, this study focuses on quantifying the maximum value of the horizontal force, vertical force, and overturning moment due to tsunami loads on the selected bridges; thus, it is appropriate to begin the simulation at a time immediately prior to first water impact the superstructure and terminate the simulation after obtaining the peak values of the time-history of the loads.

The Lagrangian-Eulerian coupling algorithm combined with an Arbitrary Lagrangian-Eulerian (ALE) solver was used in the numerical models as it is the most mature formulation to simulate the problem involving interaction between fluid with high velocity and rigid structure. The basic concept of the Lagrangian-Eulerian coupling algorithm is to track the relative displacements of the corresponding coupling points

defined at the interfaced between the Lagrangian surface (bridge superstructure part) and inside the Eulerian elements (fluid part).

Figure 3 shows an example of the numerical model of the Millport Slough Bridge developed in this research. The model consists of three material parts: water, air, and bridge parts. Material properties for each part – such as material mass density, pressure cut-off, fluid viscosity, modulus of elasticity, and Poisson's ratio – are specified appropriately as they are used in the ALE differential equation and in calculating of interface stiffness. Even though the numerical model is two dimensioned, it could be thought of a three dimensional rectangular cross-section with unit thickness in z-direction. The cross-section composes of water and air material parts with a bridge part inside. The boundaries setting up for the numerical models are described later in Appendix A-1 .

4.2. Bridge Descriptions and Tsunami Flow Fields

Numerical models of four selected bridges in the Siletz bay are developed for this tsunami load estimation study. The first is the Schooner Creek Bridge located close to the open channel of the bay facing directly toward the incoming tsunamis as shown in Figure 1. Two types of bridge geometry – deck-girder and box section – under identical tsunami flow fields are examined to determine the effects of bridge cross-sectional geometry. The cross-section of the Schooner Creek Bridge is not symmetrical as the west edge (tsunami impact face) is lower than the east edge due to a 4% slope for the deck-girder section and a 3% slope for the box section, as shown in

Figure 81 and Figure 82, respectively. The reference bridge elevation measured at the support of the lowest (west-most) bridge girder is approximately 18 feet above mean sea level (MSL). The second bridge is the Drift Creek Bridge located southeast of the Schooner Creek in a more open area. The bridge geometry is similar to that of the Schooner Creek Bridge (deck-girder section) with a smaller cross-sectional width and less number of girders supporting the bridge deck. The bridge is designed for a 2% slope with a reference elevation of approximately 14 feet above MSL, as shown in Figure 83. The third bridge is the Millport Slough Bridge located at the south end of the Siletz Bay on Highway 101. The bridge, which has a 2% slope crown with a reference elevation of 15 feet above MSL, as shown in Figure 84 and Figure 85, is currently under replacement construction (at the time of the writing, December 2010). Finally, the fourth bridge is the Siletz River Bridge. This bridge, which is currently under designed as a box section, with a reference elevation of approximately 33 feet above MSL, is high compared to that of the other three bridges.

As mentioned earlier, six different tsunami flow fields are provided for each bridge site (GA M_w 8.8, GA M_w 9.0, GA M_w 9.2, LZ M_w 9.0, MT M_w 9.0 and TZ M_w 9.0). However, the maximum water surface elevations generated in some scenarios are lower than the reference bridge elevation, and can be neglected because tsunamis in these scenarios would not induce forces on the superstructures. In particular, five tsunami scenarios – GA M_w 9.0, GA M_w 9.2, LZ M_w 9.0, MT M_w 9.0 and TZ M_w 9.0 – are applicable to the Schooner Creek Bridge, and the same three scenarios – GA M_w 9.2, LZ M_w 9.0 and MT M_w 9.0 – are applicable to the Drift Creek Bridge and the

Millport Slough Bridge. On the other hand, all six tsunami scenarios can be neglected for the Siletz River Bridge as it is designed for such a high elevation that prevents the tsunami flow from reaching the superstructure. The input tsunami flow fields of the applicable scenarios at each bridge site are shown in Appendix A-2

4.3. Tsunami Force Time-Histories

Figure 4 to Figure 15 show the time-histories of the predicted reaction forces – horizontal force and vertical force – and overturning moments due to tsunami loads on the three affected bridges calculated from the numerical models. The horizontal tsunami forces on the box section, black line in Figure 4, show a pattern of a short duration high intensity force at the time immediately after water impacting the bridge followed by fluctuating drag forces similar to those reported by Yeh et al. (2005). The impact forces on the box section are approximately 1 to 2.5 times the corresponding drag forces; whereas the maximum impact horizontal forces on the deck-girder section are sometimes smaller than the corresponding maximum drag force. The Millport Slough Bridge is under construction as deck-girder bridge section, while the Drift Creek Bridge is designed to be of the same type. The simulated horizontal reaction forces on these two bridges are shown in Figure 10 and Figure 13, respectively. A comparison of the vertical tsunami force time-histories on both box section and deck-girder at the Schooner Creek is shown in Figure 5. The vertical tsunami forces on both sections show similar pattern as they are rapidly increased at the time water impacting the structure followed by considerably steady forces for a while until the water subsided.

To summarize, tsunami forces on the superstructure of the selected bridges are quite difference given the same tsunami scenario. According to the results discussed above, the Siletz River Bridge could survive a 500-years Cascadia tsunami event because the designed reference elevation of the bridge superstructure is sufficiently high to avoid tsunami loads while the other three bridges are inundated in some scenarios. The Schooner Creek Bridge and the Drift Creek Bridge were subjected to large tsunami forces, compared to the forces on the Millport Slough Bridge, because it is located in an open area close to the inlet channel of the bay facing directly to the incoming tsunamis while the Millport Slough is located far from the inlet channel. A regression line relating the maximum horizontal forces and the corresponding maximum flux momentums is plotted in Figure 20. It is reasonable to assume that the maximum horizontal force is approximately linearly proportional to the maximum flux momentum as suggested in FEMA (2008) and PBTE (2010).

According to the numerical results, the magnitude of the tsunami forces on a bridge superstructure generated from different rupture configurations and moment magnitudes can be significantly different. Mostly, the forces are extremely high and it may not be reasonable to design a bridge to resist such large forces that occur rarely. The joint probability distribution of the rupture configurations and their corresponding earthquake moment magnitude which provides a basis for probabilistic design for a 500-year Cascadia tsunami event is shown in Table 4 (Cheung et al. 2010). Observe that the GA rupture with M_w 9.0 has the highest probability of occurrence in the

Pacific Northwest seismic event and the predicted loads represent reasonable tsunami design forces.

4.4. Effect of Cross-Sectional Bridge Geometry

The maximum horizontal and vertical reaction forces, and the maximum overturning moments on two different bridge types – deck-girder and box section – of the Schooner Creek Bridge are summarized in Table 1. It can be observed that the maximum forces and moments on the box section superstructure are significantly higher than those of the deck-girder section. One of the major load effects that must be considered for tsunami forces calculation is the hydrostatic pressure which is a function of distance between water surface elevation and the reference elevation of the bridge cross-section (Δh). Unlike the box-section, chambers between girders supporting the deck allow water to flow in, which help in reducing encountered hydrostatic pressures under the bridge superstructure. Moreover, a study of the effects of air compression to wave forces on coastal bridge decks (Cuomo et al. 2009) suggested that the air compression trapped in a chamber behaved as a cushion opposing the violent flow. Cuomo et al. (2009) suggested that wave energy was lost in compression of the air trapped which reduced wave impact pressures. Therefore, it is reasonable that tsunami forces on a box section bridge are higher than those on deck-girder section under identical incoming tsunami flow fields. The time-histories of the horizontal and vertical tsunami forces on the box section and the deck-girder section are plotted in Figure 7 and Figure 8, respectively appear to confirm the above observations.

4.5. Effect of Rails

To examine an effect of the presence of the bridge rails, numerical models of deck-girder without rails are developed subjected to tsunami loads identical to those on the bridges with rigid rails. Figure 7 to Figure 12 show comparisons of the fluid forces and moments on the bridge superstructures with and without rails. It can be observed that the presence of rigid rails does not significantly affect the magnitude of the impact force but induces a slightly larger drag force for fully inundated bridge superstructures. The results appear reasonable since having the rails would increase the projected vertical area encountering horizontal flows which results in an increase in the maximum horizontal force. The results show that horizontal tsunami force on a bridge with rigid rails is higher than the force on a bridge without rails up to approximately 20%. Furthermore, in practice, the rails should not significantly affect the vertical uplift force on an inundated bridge because the vertical force depends mostly on the horizontal projected area under the bridge superstructure, water velocity, and inundation depth and the water passes through between the rails. However, the model of bridge with rigid rails in this study is selected at the rail post and assumed that water cannot flow through spaces between the rails; thus, the vertical tsunami force on the bridge with rails could be higher than that on the bridge without rails because rails prevent water from overtopping the superstructure, hence increases the buoyancy force. According to the numerical results, vertical tsunami force on bridge with rigid rails could be higher than the force on bridge without rails up to 15%.

4.6. Cumulative Probability of Maximum Tsunami Forces

Joint probability of 12 scenarios based on four rupture configurations and three earthquake moment magnitudes from the 2008 National Seismic Hazard Maps were provided by Cheung et al. 2010 (see Table 4). The provided probability on each scenario is assigned to the corresponding maximum tsunami forces and moments generated on the superstructures. Figure 17, Figure 18, and Figure 19 illustrate cumulative probabilities of the predicted maximum horizontal force, vertical force and overturning moment due to tsunamis, respectively. Note that six tsunami data from LZ, MT and BT rupture at M_w 8.8 and M_w 9.2 were not available for this study as they have considerably low probability of occurrence and ODOT and Cheung decided not to generate them. For this study, tsunami forces generated in the three ruptures with M_w 8.8 are assumed equal to the minimum predicted forces while the forces generated in the ruptures with M_w 9.2 are assumed equal to the maximum predicted forces on each bridge.

According to these cumulative probabilities, the Schooner Creek Bridge has the highest probability of being subjected to relatively large tsunami forces while the Millport Slough Bridge has the lowest probability. These results correspond to the location of the bridges since the Schooner Creek Bridge is located closest to the inlet channel in the bay while the Millport Slough located far most. However, the result forces on the Siletz River Bridge are exception because the designed reference elevation of the superstructure is very high compared to the other three bridges, which help preventing tsunami flows from reaching the superstructure. Therefore, it may be

concluded that location and reference elevation of the bridge superstructure are important factors for tsunami load estimation.

4.7. Computational Efforts

Two computational platforms were used to analyze the developed numerical models. The first is an eight processors workstation, Intel Xeon with 34 GB memory, while the second is a parallel cluster system consisting of 1100 two processor socket dual-core with 16 GB memory each. The processors on the parallel cluster system operate at 3.0 GHz frequency. A record of the computational efforts – number of CPU node, and CPU time – is summarized in Table 5.

As mentioned earlier, the time-marching algorithm in the numerical models is based on explicit integration. An average time step size (Δt) used in calculation of the models is approximately 5×10^{-6} which results in long computational time up to approximately 190 hours depending on number of CPU used for calculation and the specified problem termination time. The total numbers of cycle of the models range from approximately 20×10^6 to 120×10^6 depending on the corresponding termination time (but independent of the number of CPU used). A linear relationship between the total number of cycle and the termination time is shown in Figure 21. When the CPU run time is scaled to a 300-seconds termination time, the correlation between the CPU run time and the number of CPU (shown in Figure 22) is observed to decrease parabolically with increasing number of CPU.

Table 1 Maximum forces and moments due to tsunami loads on superstructure of Schooner Creek Bridge

Tsunami Scenario	Horizontal Force (kip/ft)		Vertical Force (kip/ft)		Overturning Moment (k-ft/ft)	
	Deck-Girder	Box Girder	Deck-Girder	Box Girder	Deck-Girder	Box Girder
GA 9.0	6.0	150	25.0	600	1570.0	40600
GA 9.2	80	150	370	720	18900	49600
LZ 9.0	71	200	360	840	18200	51700
MT 9.0	52	230	230	685	14200	47600
TZ 9.0	12	190	85.0	630	8200.0	43600

Table 2 Maximum forces and moments due to tsunamis on Drift Creek Bridge (with rigid rails)

Tsunami Scenario	Horizontal Force (kip/ft)	Vertical Force (kip/ft)	Overturning Moment (k-ft/ft)
GA 9.2	96.0	147	6090
LZ 9.0	77.0	156	6420
MT 9.0	29.0	120	5110

Table 3 Maximum forces and moments due to tsunamis on superstructure of Millport Slough Bridge (including rails)

Tsunami Scenario	Horizontal Force (kip/ft)	Vertical Force (kip/ft)	Overturning Moment (k-ft/ft)
GA 9.2	8.0	47.0	1760
LZ 9.0	8.0	34.0	1265
MT 9.0	5.0×10^{-3}	0.04	1.2

Table 4 Joint Probability of Rupture Scenarios (After Cheung et al. 2010)

Rupture	Moment Magnitude, M_w			Total
	8.8	9	9.2	
LZ	0.02	0.06	0.02	0.1
MT	0.04	0.12	0.04	0.2
BT	0.04	0.12	0.04	0.2
GA	0.1	0.3	0.1	0.5
Total	0.2	0.6	0.2	1

Table 5 Computational efforts for performing the simulation models

Tsunami Scenario	Computer System	Number of CPU (ncpu)	Problem Termination Time (s)	CPU Run Duration (hrs)	Number of Cycle
Schooner Creek Bridge: Deck-Girders (with rigid rails)					
GA M_w 9.0	8-processor workstation	6	98	117	2.0E+07
GA M_w 9.2	parallel cluster	32	365	86	7.3E+07
LZ M_w 9.0	parallel cluster	64	335	83	6.8E+07
MT M_w 9.0	parallel cluster	32	305	68	6.2E+07
TZ M_w 9.0	8-processor workstation	6	185	111	2.4E+07
Schooner Creek Bridge: Box Section (with rigid rails)					
GA M_w 9.0	8-processor workstation	6	125	53	2.5E+07
GA M_w 9.2	parallel cluster	64	365	63	7.3E+07
LZ M_w 9.0	8-processor workstation	6	257	N/A	N/A
MT M_w 9.0	8-processor workstation	6	305	121	6.2E+07
TZ M_w 9.0	8-processor workstation	6	185	76	3.7E+07
Drift Creek Bridge (with rigid rails)					
GA M_w 9.2	parallel cluster	16	275	99	5.6E+07
LZ M_w 9.0	parallel cluster	16	335	120	6.8E+07
MT M_w 9.0	Parallel cluster	16	155	51	3.1E+07
Millport Slough Bridge (with rigid rails)					
GA M_w 9.2	parallel cluster	32	363	N/A	N/A
LZ M_w 9.0	parallel cluster	32	612	190	1.2E+08
MT M_w 9.0	8-processor workstation	6	125	N/A	N/A

5. Estimation of Tsunami Forces on Bridge Superstructures

This section presents a development of a guideline for estimating tsunami forces on superstructures for preliminary design of bridges in a tsunami run-up zone along the Oregon Coast. This approach is developed by incorporating the relevant existing literature and the tsunami forces obtained from the numerical models developed in Section 4.

The total tsunami force on a bridge superstructure can be considered separately as horizontal and vertical components. The horizontal component acts perpendicularly to the longitudinal span of the bridge superstructure while the vertical component acts in upward and downward directions normal to the wave direction. The estimated total tsunami forces are assumed to apply to the bridge superstructure through the centroid of the cross-sectional area as shown in Figure 23.

5.1. Horizontal Forces

The total horizontal forces on the bridge superstructures due to tsunami loads are basically a combination of hydrostatic and hydrodynamic pressures. The hydrostatic pressure is induced by gravity, and increases with water depth. The total force due to hydrostatic pressure is a result of imbalanced pressure, which could be considered zero when water filled up both side of the structure. The hydrodynamic pressure is induced by horizontal water velocity which is a significant factor in the tsunami events. The hydrostatic and hydrodynamic forces are considered linearly proportional to the water elevation and the flux momentum (hu^2), respectively.

The total horizontal wave-induced force on bridge superstructures presented by Douglass et al. (2006) is estimated by combining the hydrostatic pressure on the seaward external girder and the total pressure on the internal girders. The total force on the internal girders can be estimated by multiplying reduction factor with the corresponding force on the seaward external girder. The horizontal force due to hydrostatic (Douglass et al. 2006) and hydrodynamic (Yeh 2007) pressures, therefore, can be formulated as shown in equation (5.1.1) and (5.1.2), respectively.

$$F_h = (1 + C_r(N-1))C_h F_h^* \tag{5.1.1}$$

$$F_d = 0.5 C_d \rho b (\Delta h u^2)_{\max} \tag{5.1.2}$$

where $C_r = 0.4$ reduction coefficient for pressure on internal girders; N = number of girder supporting bridge deck; $F_h^* = \gamma(\Delta h_{max})A_h$; C_d = empirical drag coefficient; ρ = seawater mass density; and $(hu^2)_{max}$ = maximum flux momentum.

As mentioned earlier, the total horizontal force due to tsunami loads consists of hydrostatic force (water elevation-dependent term) and hydrodynamic force (flux momentum-dependent term). Even though the maximum of these forces might not occur exactly at the same time, combining these maximum forces together is considered reasonable (and conservative) for design purpose. Therefore, the maximum horizontal force on bridge superstructure due to tsunamis can be estimated by combining equation (5.1.1) and (5.1.2) as follows:

$$\begin{aligned} F_H &= F_h + F_d \\ &= (1 + C_r(N-1))F_h^* + 0.5 C_d \rho b (\Delta h u^2)_{\max} \end{aligned} \tag{5.1.3}$$

An empirical drag coefficient, C_d, for bridge superstructures were evaluated in this research based on the time-history results obtained from the numerical models. A plot between the total horizontal force and flux momentum can be considered separately into two parts. The first part is where the horizontal force increases rapidly with a small change in the flux momentum (flux momentum-independent part). The second part is where the horizontal force increases proportionally to the corresponding flux momentum (flux momentum-dependent part) as shown in Figure 24. The empirical coefficient was estimated from slope of the graph between flux momentum and the total horizontal force as $0.5C_d\rho b\ (= slope)$. Therefore, the drag coefficient is approximately 1.0 for the deck-girder bridge type.

In determination of wave forces due to wind wave and storm surge, it is recommended that the total horizontal pressure on internal girders could be estimated as 40% of the pressure on the external seaward girder. However, horizontal pressure time-history results at the bottom of bridge girders are determined to evaluate an appropriate reduction coefficient for the distributed pressure on the internal girders under tsunami loads. The results show that the maximum pressure on the internal girders is approximately 20% to 50% of the corresponding pressure on the external seaward girder. Therefore, the reduction coefficient, C_r, can be used as 0.4 until further information.

A comparison between the estimated maximum horizontal forces and the predicted forces calculated from the numerical models are shown in Figure 25. The straight line in Figure 25 represents a perfect fit between estimated force and the predicted force. It

can be observed that the estimated forces could be overestimated or underestimated in some cases because the recommended empirical coefficients are based on an average value of the scattering data as shown above.

5.2. Vertical forces

Load effects due to tsunamis that must be considered for estimating vertical force under bridge girders consist of hydrostatic and hydrodynamic pressure. The hydrostatic pressure is induced by water elevation as mentioned earlier while the hydrodynamic pressure is induced by horizontal and vertical water velocity. The summation of estimated pressures under the bridge superstructure can be estimated by equation (5.2.1).

$$P = \gamma(\Delta h) + \frac{1}{2}\rho u_x^2 + \frac{1}{2}\rho u_y^2 \tag{5.2.1}$$

However, the hydrodynamic force induced by the vertical component of water velocity is relatively small compared to the corresponding hydrostatic and hydrodynamic forces due to horizontal velocity; thus, it can be neglected. Consequently, the maximum vertical force due to tsunami loads can be estimated by equation (5.2.2).

$$F_V = \{\gamma(\Delta h_{\max}) + \frac{1}{2}\rho u_{x,\max}^2\}A_v \tag{5.2.2}$$

As mentioned earlier, these maximum forces might not occur at exactly the same time, but it is considered conservative to combine these maximum forces together for design purpose.

Mostly, the provided tsunami flow field data – water velocity and water elevation – bases on tsunami flow without obstruction (which is a bridge superstructure in this study). The results from the numerical models suggest that the output water elevation and water velocity of tsunami waves near the bridge are higher than the input values. Figure 26 shows a plot between input value of water velocity and the output value of water velocity obtained from the numerical models. The output water velocities are measured near the bottom of the seaward external girder as pressures at this location represent up to 80% of total pressure under the bridge cross-section (explained later in this section). It can be interpreted that the output water velocity near the bridge superstructure is approximately 3.5 times the input water velocity, based on scattering data shown in Figure 26. The relationship between these input and output water velocity can be formulated as shown in equation (5.2.3).

$$u_{x,\max} \cong 3.5 u^{*}_{x,\max} \tag{5.2.3}$$

where $u_{x,max}$ = adjusted horizontal water velocity (output water velocity); and $u^{*}_{x,max}$ = input horizontal water velocity. Figure 27 shows a comparison between the estimated maximum vertical force and the predicted maximum vertical force obtained from the simulations. The estimated vertical forces are observed to be overly conservative for small values and slightly under-estimated for large values. However, the recommended equation is considered appropriate for estimating vertical force due to tsunamis until further study.

The maximum percentage values of pressure distribution time-histories under each girder along the cross-section of the deck-girder Bridges are plotted in Figure 28, Figure 29, and Figure 30. The pressure under bridge girders are not uniformly distributed along the cross-section. The maximum 70 to 100% of total pressure is applied to the external seaward girder and rapidly decreased for the internal girders. However, the total vertical force, equation (5.2.2), is assumed to interact with the bridge at the centroid of the cross-section at this time.

5.3. Discussion and Limitation of Recommended Approach

The recommended approach is intended to be used for estimating tsunami forces on bridge superstructures as a preliminary guidance for design. This approach is developed by incorporating those literatures proposed in section 3. and the time-history of the tsunami forces on bridge superstructures calculated from the numerical models developed in this research. Given the uncertainties in tsunami flow field and lacking of laboratory results on realistic bridge model, an appropriate factor of safety should be added into these equations.

The input parameters required for estimating tsunami forces by the recommended approach consist of maximum water elevation, horizontal water velocity, maximum flux momentum, and elevation of bridge superstructure. Moreover, tsunami waves usually loosen sediment saturated with seawater while surging inland increasing the effective fluid density above that of typical seawater. Thus, FEMA (2008)

recommended the fluid density to be equal to 1.2 times typical freshwater density for tsunami forces calculation.

The recommended empirical coefficients are given here. The reduction factor for forces on internal girders, C_r, is given as 0.4 which corresponds to that presented in Douglass et al. (2006) as the maximum fluid pressure on the internal girders is approximately 20% to 50% of the pressure on the seaward external girder. The drag coefficient $C_d = 1$ was obtained for bridge superstructures under tsunami loads in this study.

The recommended approach is developed based on the deck-girder bridge section only. It might not be appropriate to apply these recommended equations directly to calculate tsunami forces on other types of bridge superstructure. A comparison between maximum tsunami forces on deck-girders section and box section (Table 1) shows that maximum forces on box-sections are significantly higher than those on deck-girder sections. Therefore, the box-section bridge type is not recommended to be placed in the tsunami run-up zones.

6. Case study of the Spencer Creek Bridge – revisited

It is of technical interest to revisit the Spencer Creek Bridge analysis for a more complete presentation of the ODOT bridges taken up by the authors, particularly because both the projects were awarded with a similar goal, although the scope has evolved, of developing a set of guidelines for the design of coastal bridges. Firstly, this extension will provide an evaluation of the guideline with regards to an

application to another bridge which is at a different location and thus subjected to different tsunami loads. Secondly, it will help study the application of the recommended formulations to a bridge with a different structural configuration (with an arch-type of structure in place of longitudinal girders).

The chosen critical section for the Spencer Creek Bridge was at the middle of the longitudinal span consisting of a deck and a cross-beam. Even though the recommended approach (in this paper) for estimating tsunami forces on the bridge superstructures is developed for the deck-girder bridge type only, similar logic can be applied to the deck of the Spencer Creek Bridge with modified coefficients.

Since there is no girder supporting the bridge deck in this case, the term that accounts for additional horizontal force on internal girders will be zero; i.e., it can be considered that the bridge superstructure consists of a deck with one girder (N = 1). Therefore, equation (5.1.3) can be modified as follows:

$$F_H = \gamma(\Delta h_{\max})A_h + 0.5\rho C_d b(\Delta hu^2)_{\max} \qquad (6.1.1)$$

Other than setting the number of girders equal to one, the empirical drag coefficient, C_d, must be modified for this case because the recommended value provided in section 5. is evaluated based on the tsunami forces of deck-girder bridge type. Considering the numerical results of tsunami impact on the Spencer Creek Bridge from Nimmala et al. (2006), the drag coefficient can be evaluated by taking $C_d = 2 \times F_H/(\rho bhu^2)$. Thus the recommended drag coefficient for the Spencer Creek Bridge is 3.5 as shown in Figure 31. Consequently, estimated maximum horizontal force due to tsunami loads

on the Spencer Creek Bridge deck calculated by equation (6.1.1) is approximately 18 kip/ft while the predicted maximum force is approximately 23 kip/ft. Note that the drag coefficient used to estimate the maximum horizontal force is based on a single set of data only; therefore, additional data is required to confirm the appropriateness of the drag coefficient for this type of bridges.

The equation for estimating maximum vertical force, equation (5.2.2), can be directly applied to the Spencer Creek Bridge. Unlike the deck-girder bridge type, an observation from the numerical model of the Spencer Creek Bridge suggests that the local velocity near the bridge support is approximately equal to the input value of water velocity ($u_x \cong 1.0u_x^*$) which can be directly used in equation (5.2.2). Consequently, the estimated maximum vertical force due to tsunami loads on the Spencer Creek Bridge deck is approximately 67 kip/ft while the predicted maximum vertical force is approximately 40 kip/ft. An example calculation of tsunami forces on the Spencer Creek Bridge using the recommended approach is shown in Appendix C.

7. Computational Performance

This section presents a performance study of the numerical code (LS-DYNA) by performing FSI simulation models on a high-performance computing system. In this study, the parallel cluster system consists of 1,100 two processor socket dual-core computer nodes with 8 GB of memory each. The core processor specification on parallel cluster is 4,400 with 3.0 GHz Intel Woodcrest.

Three FSI models with different finite element nodes – 12k, 30k, and 48k nodes – are tested with 20 seconds termination time. The test was conducted by running each FSI model with varying number of computer CPU (CPU node) and keeps the record of the computational time consumed. The purpose of this study is to determine an optimal number of CPU for calculating FSI problem with LS-DYNA software on high performance computer system. The consumed computational time for each simulation are summarized in Table 6.

A comparison between the computational time and the number of CPU of three different FSI models are plotted in Figure 32. The number of CPU axis (x-axis) is shown in log scale for a better demonstration purpose. According to Figure 32, the computational time decreased rapidly as the number of CPU increases at the small number of CPU, and continues to decrease slowly until reaching its optimal point. It can be observed that using number of CPU more than the optimal number could increase the computational time for running these models. The optimal number of CPU for Model 1 and Model 2 are approximately at 32 CPU nodes while the optimal number of CPU for Model 3 is approximately at 64 nodes. However, the computational time used for simulating Model 1 with 16 CPU nodes is only slightly higher than using 32 CPU as shown in Table 6. Thus, it might be more appropriate to use 16 CPU nodes for simulating Model 1 considering the cost of computational. Furthermore, relationships between computational time, unit cost, and number of CPU are shown in Figure 33. It can be observed that by considering the consuming time along with the unit cost, the optimal number of CPU for all three models are 16 nodes.

According to this performance study, it can be concluded that an appropriate number of CPU for simulating FSI problem by the simulation code depends on size of each FSI model. Moreover, the optimal number of CPU for small model (Model 1: 12k) is smaller than the optimal number of CPU for large model (Model 3: 48k).

Table 6 Summary of computational time

Number of CPU	Computational Time (min)		
	Model 1: 12k	Model 2: 30k	Model 3: 48k
2	863.3	2382.7	3675.7
4	436.9	1210.6	1792.6
8	244.6	647.6	933.7
16	161.2	388.9	502
32	158.2	278.9	333.2
64	196.6	303.3	313
128	379.3	461.9	466.8

8. Concluding Remarks

Bridges along the Oregon coast are an important part of the transport system in the area; however, they were not designed to resist large tsunami loads. Based on the studies of tsunami deposits, there is a high possibility that large tsunamis could occur in the vicinity of the Oregon Coast. To mitigate major damages that could occur to these bridges, ODOT initiated a research program to perform a tsunami vulnerability study of the bridge superstructures along the coast. Four bridges in the Siletz bay area, Oregon, were selected to perform this study.

This study was divided into two major parts. The first part is to develop numerical models to perform numerical testing of tsunami impact on full-scaled bridge

superstructures. The provided tsunami flow fields at each bridge location consisted of six different scenarios based on rupture configurations and earthquake moment magnitudes. However, the maximum elevations of wave crest in some scenarios were lower than the reference bridge elevation; therefore, only the cases in which the maximum wave crest elevation higher than the reference elevation were selected to perform the numerical testing. The selected tsunami scenarios consisted of five scenarios at Schooner Creek, and three scenarios at Drift Creek and Millport Slough. At the Schooner Creek, two different bridge superstructure cross-sections, deck-girder and box section, were developed to perform numerical testing subjected to identical tsunami flow field. The time-history of the numerical results show that, given identical tsunami conditions, box section bridges have to resist significantly larger forces (both horizontal and vertical forces) than the deck-girder section bridges. Therefore, it would be more appropriate to select deck-girder section bridges in the tsunami run-up zone instead of a box section. Furthermore, an effect of bridge rails to tsunami forces was examined in this research. The results showed that rigid rails on the superstructure could increase horizontal and vertical tsunami forces up to 20% and 15%, respectively.

The second part of this study was to develop a guideline to estimate tsunami forces on a bridge superstructure. The guideline was developed based on a review of wave force related literature and time-history results obtained from numerical models conducted in the first part of this research. The horizontal force due to tsunamis is considered to be linearly proportional to the water elevation and the flux momentum ($F_H \propto \Delta z; F_H \propto$

$(\Delta z)u_x^2$), while the vertical force is linearly proportional to the water elevation and the square of water velocity in horizontal direction ($F_V \propto \Delta z; F_V \propto u_x^2$). The water pressure due to water velocity in vertical direction is relatively small compared to the pressure due to water elevation and the water velocity in horizontal direction; thus, it can be neglected. The recommended approach provided simplified equations for estimating tsunami forces due to fluid loads only. Impact force from floating objects was not included in these equations.

The recommended approach was developed to be used as a preliminary guideline for design engineers. An appropriate factor of safety should be incorporated into these equations in design given uncertainties in the tsunami flow fields, and lacking of laboratory experiments on realistic bridge models to validate the numerical results.

9. Future Research

The current study is developed based on tsunami time-history loads calculated from finite-element models without verification with laboratory test data. A recommendation for future research is to perform laboratory experiments of tsunami impact on bridge superstructures and compare the test results with the numerical predictions. Furthermore, the numerical models developed in this study are two-dimensional. The longitudinal span lengths of the bridge are not taken into account. Three-dimensional models of tsunami impact on bridge superstructures should be developed for a better understanding of an interaction between them, and to study the effect of longitudinal span length in computing the tsunami forces. Other than total

tsunami forces on bridge superstructure, force distribution on each girder along the cross-section could be evaluated for a better design aspect by tracking reaction forces at connections between deck and girders in the future model.

The recommended approach for estimating the tsunami forces on bridge deck is developed as a preliminary guidance for design of new bridges in the tsunami run-up zone, and for performing a tsunami vulnerability study of the existing bridges as well. A survey of the tsunami vulnerability for existing bridges should be conducted to initiate plans for retrofit, or replacement if necessary, of these bridges to be able to withstand possible tsunami events.

Notation

A_h	Projected are of bridge superstructure distributed to horizontal pressure (vertical plane)
A_v	Projected area under bridge superstructure distributed to vertical pressure (horizontal plane)
b	A unit width of bridge superstructure on the longitudinal span
C_d	Empirical Drag Coefficient
C_r	Reduction Coefficient for internal girders
CSZ	Cascadia Subduction Zone

F_d	Drag Force or Hydrodynamic Force
F_h	Hydrostatic Force
F_h^*	Reference Horizontal Force ($F_h^* = \gamma(\Delta z_h)A_h$)
GA	Global Analog
h	Water Elevation
LZ	Locked Zone
MT	Midpoint of Transition zone
P	Total Pressure
TZ	Transition Zone
u_x	Horizontal Water Velocity
u_x^*	Input horizontal water velocity (flow without obstruction)
u_y	Vertical Water Velocity
Δz_v	A difference between water surface elevation and under bridge superstructure
ρ	Mass density of seawater
γ	Unit Weight of seawater

10. References

Arnason, H. *Interaction between an Incident Bore and a Free-Standing Coastal Structure.* PhD Thesis, Seattle: University of Washington, 2005.

Bea, R.G., Xu T., Stear J., and and Ramos R. "Wave Forces on Decks of Offshore Platforms." *Journal of Waterway, Port, Coastal and Ocean Engineering*, 1999: 136-144.

Belytschko, T., B Moran, and W. K. Liu. *Nonlinear Finite Elements for Continua and Structures.* Chichester, NY: John Wiley, c2000, 2000.

Chen, Q., L. Wang, and H. Zhao. "Hydrodynamic Investigation of Coastal Bridge Collapse during Hurricane Katrina." *Journal of Hydraulic Engineering*, 2009: 175-186.

Cuomo, Giovanni, K. Shimosako, and S. Takahashi. "Wave-in-deck loads on coastal bridges and the role of air." *Coastal Engineering*, 2009: 793-809.

Douglass, S. L., Q. Chen, and J. M. Olsen. *Wave Forces on Bridge Decks.* Washington: Federal Highway Administration, 2006.

Francis, M. J., and H. Yeh. *Tsunami Inundation Scour of Roadways, Bridges and Foundations.* EERI/ FEMA NEHRP Professional Fellowship Report, 2006.

Goldfinger. "Deep-water turbidites as Holocene earthquake proxies: the Cascadia subduction zone and Northern San Andreas Fault systems." *Annals of Geophysics*, 2003: 1169-1194.

Hallquist, John O. *LS-DYNA Theory Manual.* Livermore, CA: Livermore Software Technology Corporation, 2006.

Haritos, N., T. Ngo, and P. Mendis. "Evaluating Tsunami Wave Forces on Structures." *Monash University*. Melbourne, Australia, 2005.

Hsiao, S., and T. Lin. "Tsunami-like solitary waves impinging and overtopping an impermeable seawall: Experiment and RANS modeling." *Coastal Engineering*, 2010: 1-18.

Huang, W., and H. Xiao. "Numerical Modeling of Dynamic Wave Force Acting on Escambia Bay Bridge Deck during Hurricane Ivan." *Journal of Waterway, Port, Coastal, and Ocean Engineering*, 2009: 164-175.

Jung, J. K. *Using a Finite-Element Based Software LS-DYNA for Modeling and Simulation of Nonlinear Contact/Impact Structural and Fluid Mechanics Problems.* MS project report, Corvallis, OR: Oregon State University.

Livermore Software Technology Corporation (LSTC). *LS-DYNA Keyword User's Manual Volume I.* Livermore, CA: Livermore Software Technology Corporation (LSTC), 2007 Version 971.

Mcconnell, K., W. Allsop, and I. Cruickshank. *Piers, jetties and related structures exposed to waves Guidelines for hydraulic loadings.* London: Thomas Telford Publishing, 2004.

Nimmala, S. B., Solomon C. Y., K. F. Cheung, and Yong W. *Tsunami Design Criteria for Coastal Infrastructure: A case study for Spencer Creek Bridge, Oregon.* Technical Report, Salem: Oregon Department of Transportation (ODOT), 2006.

Oregon Department of Transportation, Bridge Engineering Section. *Seismic Vulnerability of Oregon State Highway Bridges.* Oregon Department of Transportation, 2009.

Palermo, D., I. Nistor, Y. Nouri, and A. Cornett. "Tsunami loading of near-shoreline Structures: a primer." NRC Research Press, 2009. 1804-1815.

Reid, John D. *LS-DYNA Examples Manual.* Livermore, CA: Livermore Software Technology Corporation, 2001.

Tichelaar, B. W., and L. J. Ruff. "Depth of seismic coupling along subduction zone." *Journal of Geophysical Research*, 1993: 15829-15831.

Winston, H. *Tsunami Design Criteria Analysis of Coastal Highway Bridges.* Master Report, Corvallis: Oregon State University, 2010.

Yeh, H. "Design Tsunami Forces for Onshore Structure." *Journal of Disaster Research Vol.2 No.6*, 2007: 531-536.

Yeh, H. "Maximum Fluid Forces in The Tsunami Runup Zone." *Journal of Waterway, Port, Coastal, and Ocean Engineering*, 2006: 496-500.

Yeh, H., I. Robertson, and J. Preuss. *Development of Design Guidelines for Structures that Serve as Tsunami Vertical Evacuation Sites.* Olympia: Washington State Department of Natural Resources, 2005.

Zhang, W. *An Experimental Strudy and a Three-Dimensional Numerical Wave Basin Model of Solitary Wave Impact on a Vertical Cylinder.* Master Thesis, Corvallis: Oregon State University, 2009.

Zienkiewicz, O. C., R.L. Taylor, and P. Nithiarasu. *The finite element method for fluid dynamics.* Oxford; Boston: Elsevier Butterworth-Heinemann, 2005.

Figure 1 Top view map of Siletz bay area and location of the selected bridges

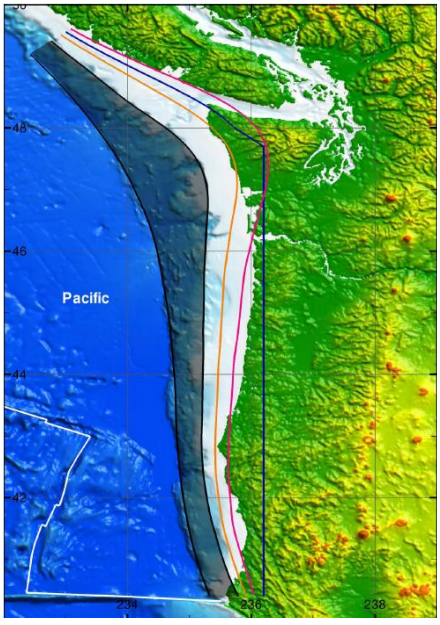

Figure 2 Boundaries of Cascadia Subduction zone inferred from the National Seismic Hazard Map (2008)

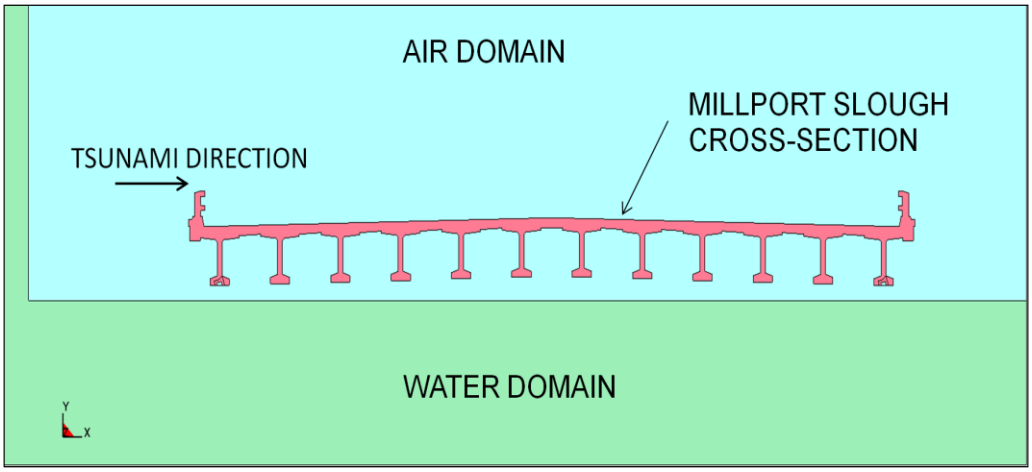

Figure 3 An example of numerical model of Millport Slough Bridge

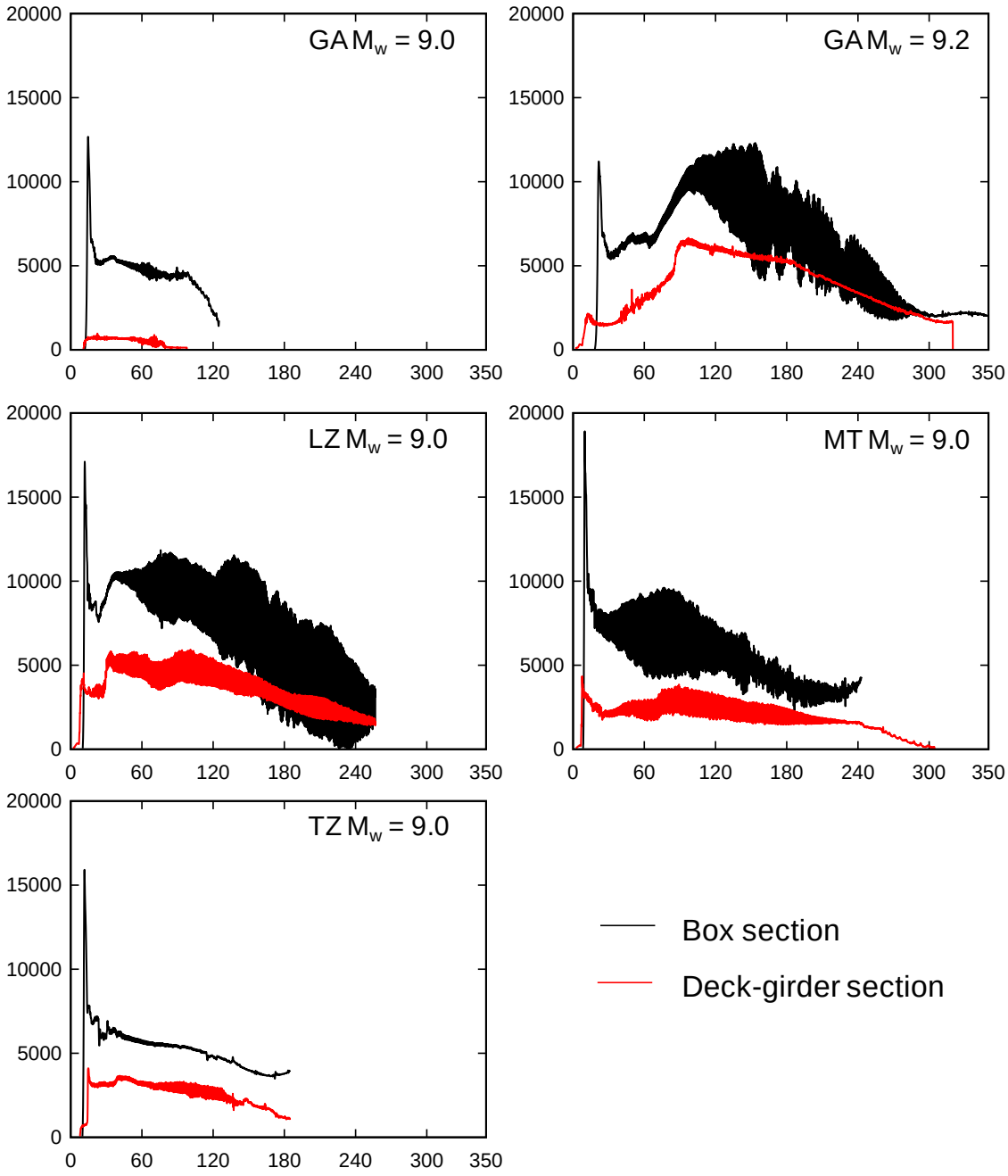

Figure 4 Comparisons of predicted horizontal tsunami force (lb/in) time-history on different bridge geometry

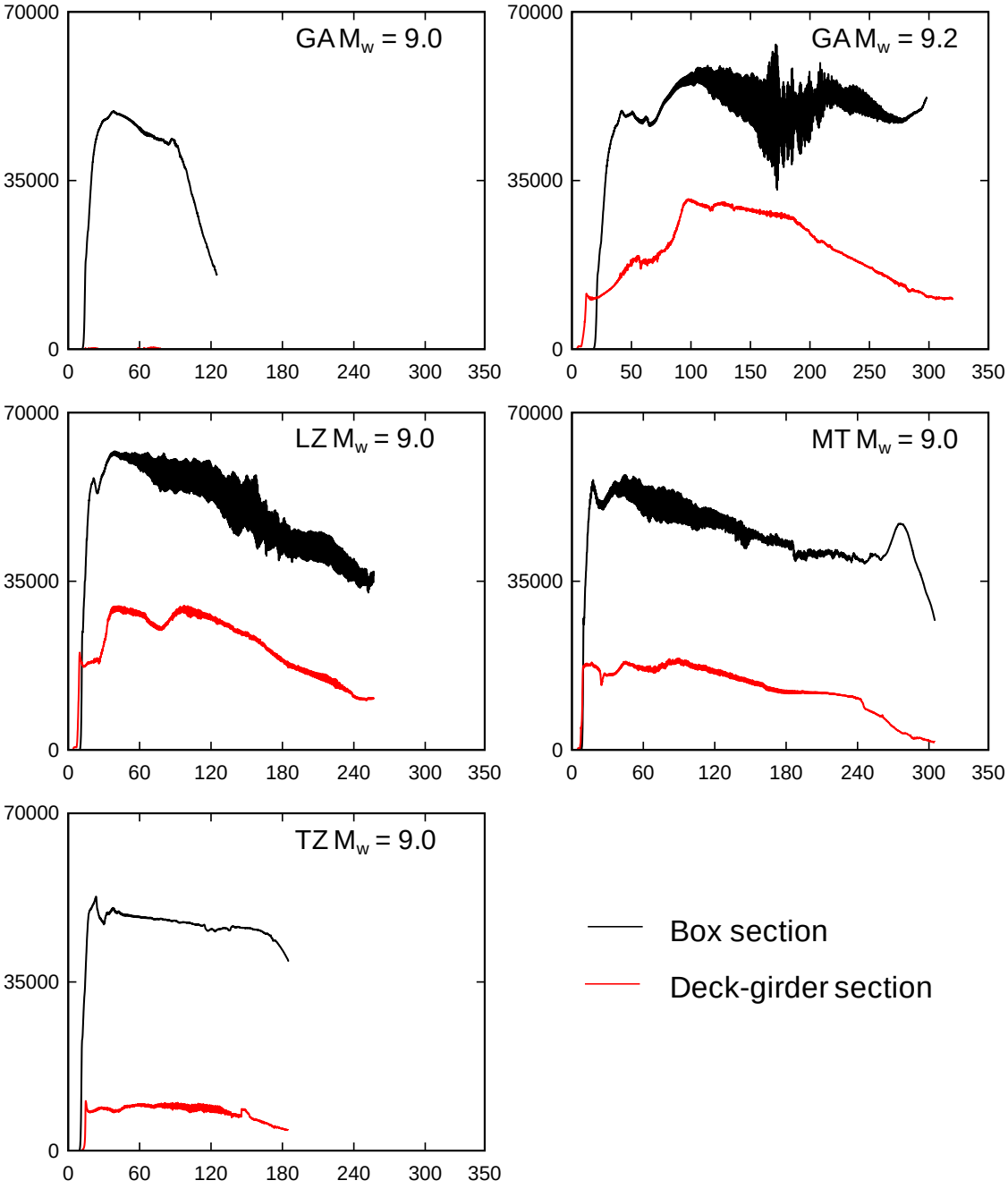

Figure 5 Comparisons of predicted vertical tsunami force (lb/in) time-history on different bridge geometry

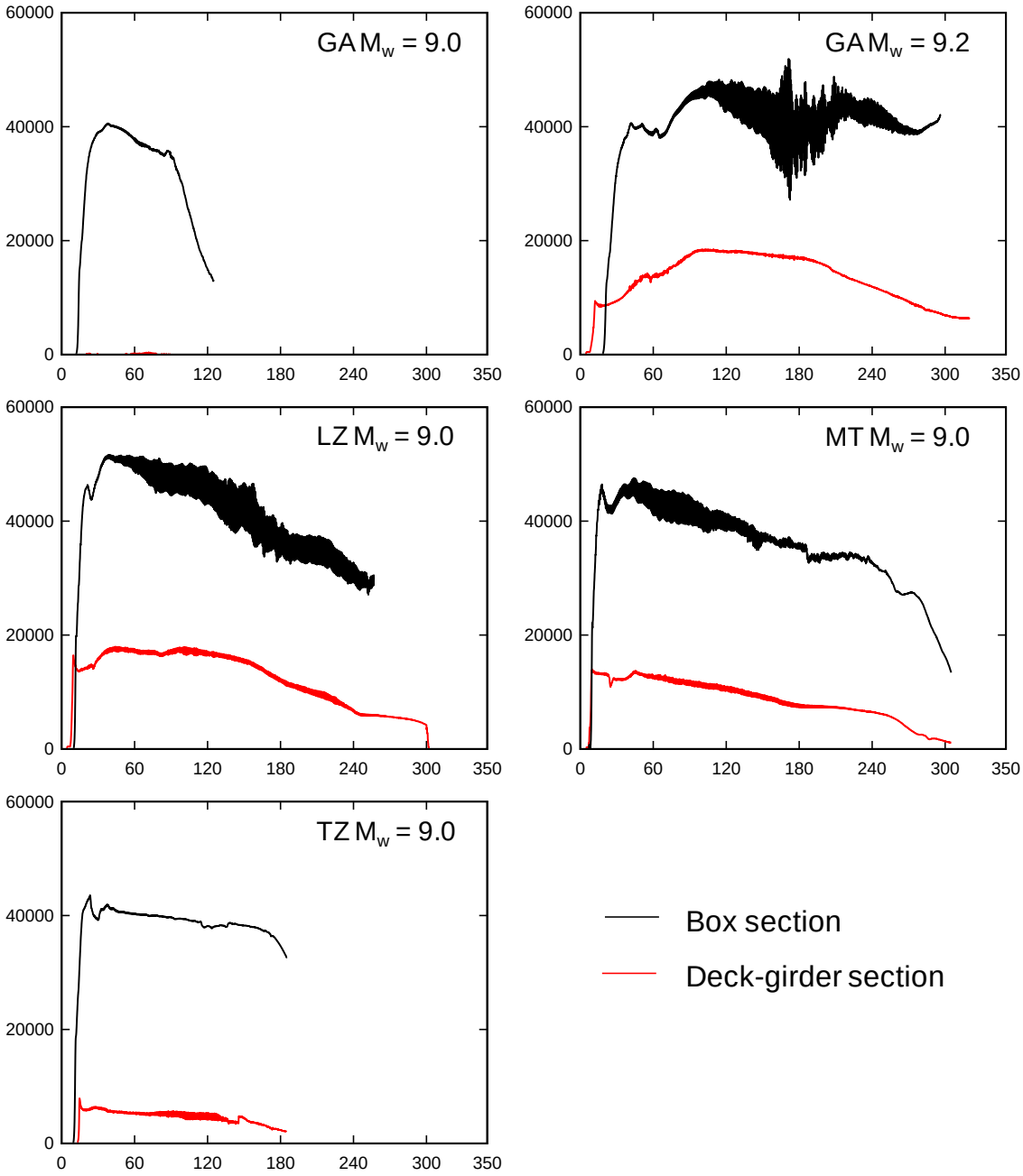

Figure 6 Comparisons of predicted overturning moment (kip-ft/ft) time-history on different bridge geometry

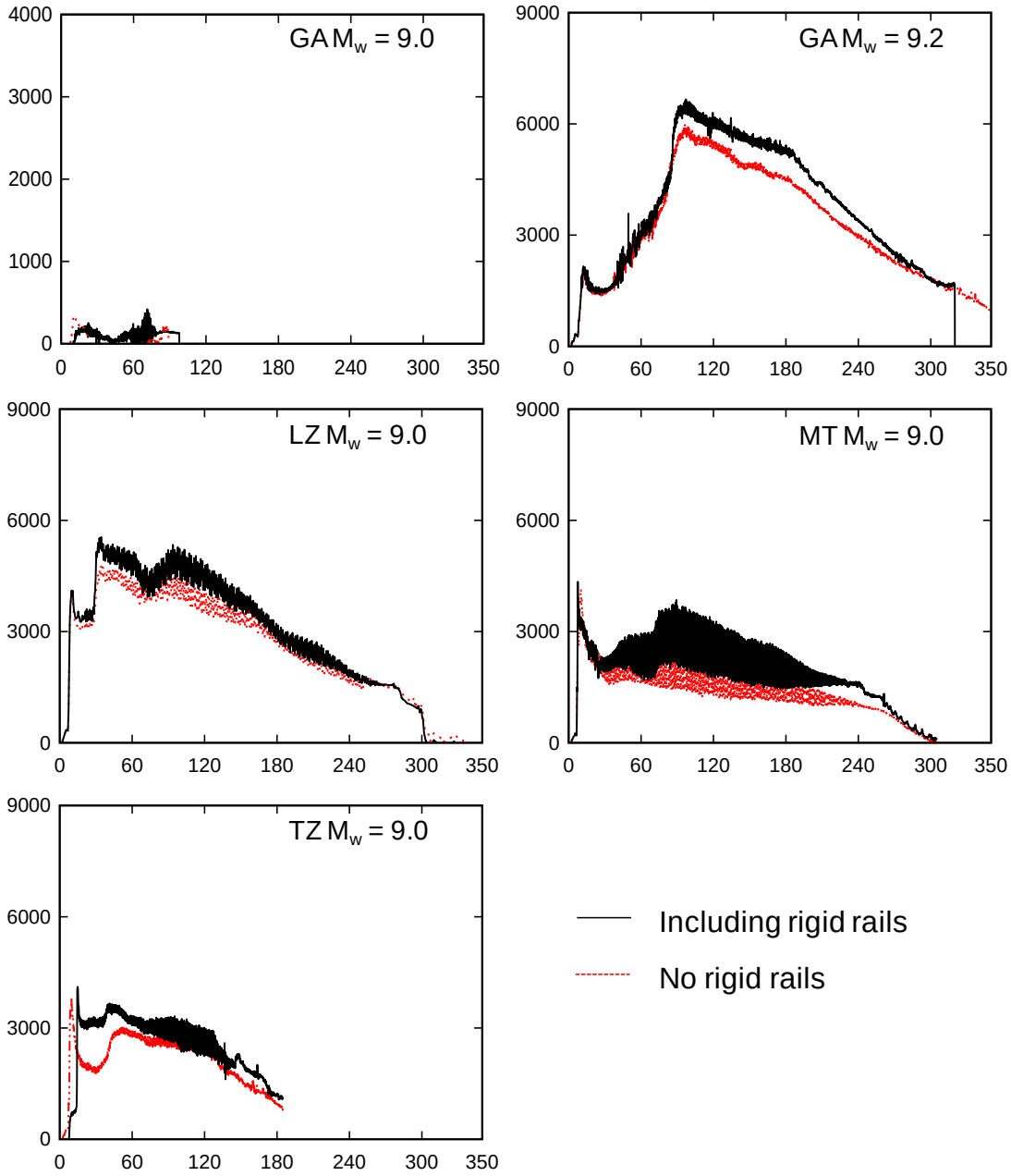

Figure 7 Time-Histories of predicted horizontal tsunami force (lb/in) on Schooner Creek Bridge (Deck-Girder)

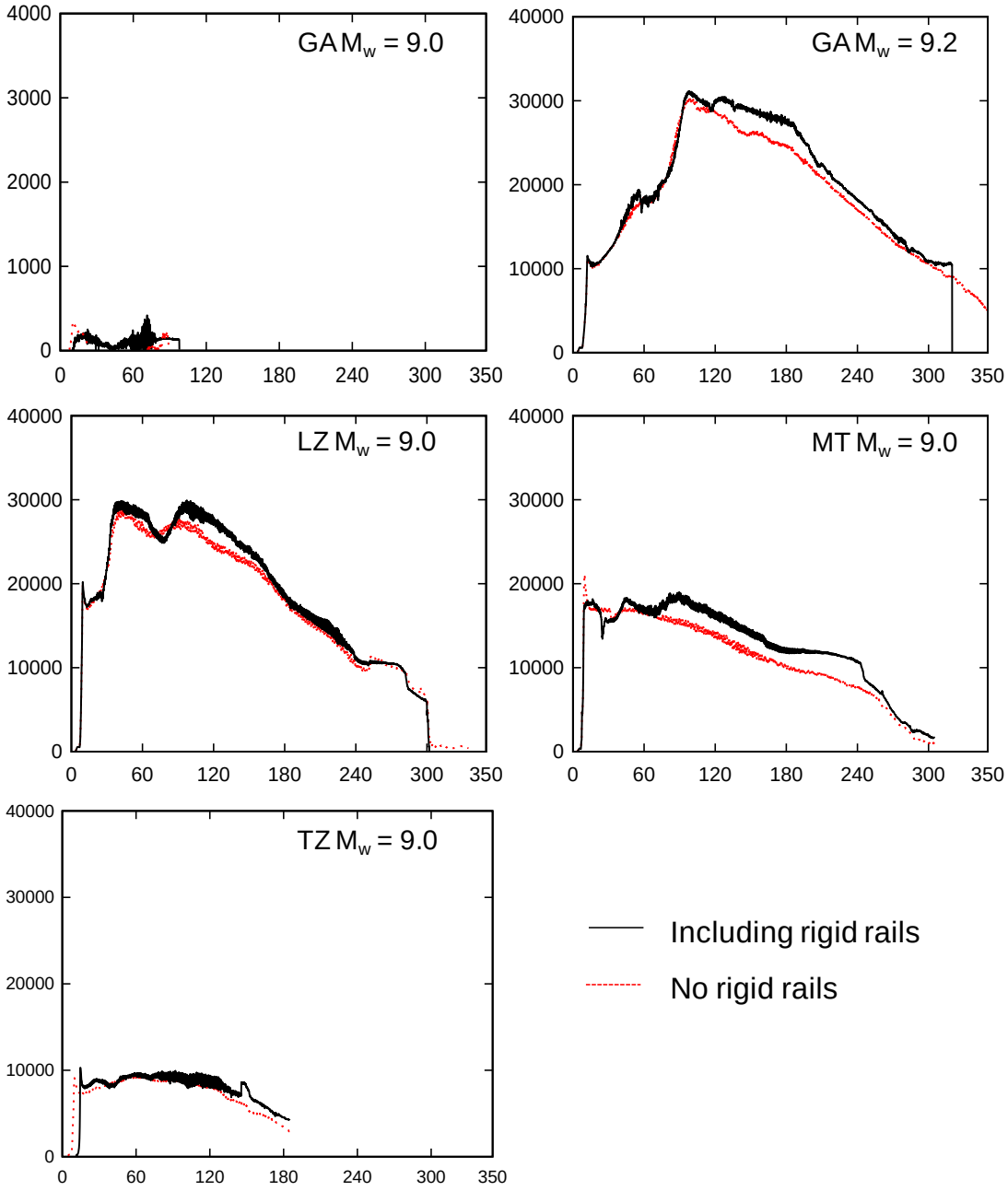

Figure 8 Time-Histories of predicted vertical tsunami force (lb/in) on Schooner Creek Bridge (Deck-Girder)

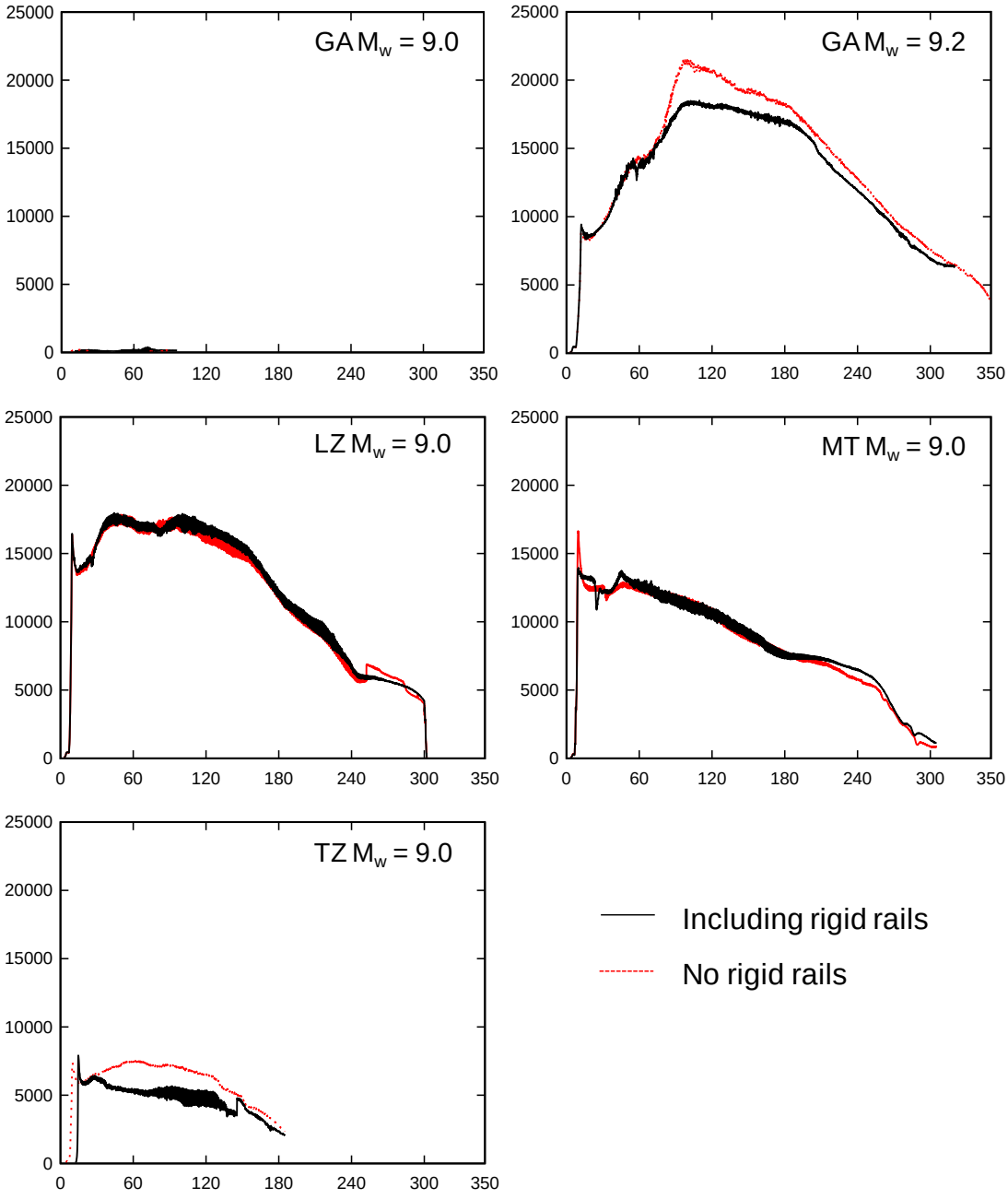

Figure 9 Time-Histories of predicted overturning moment (kip-ft/ft) on Schooner Creek Bridge (Deck-Girder)

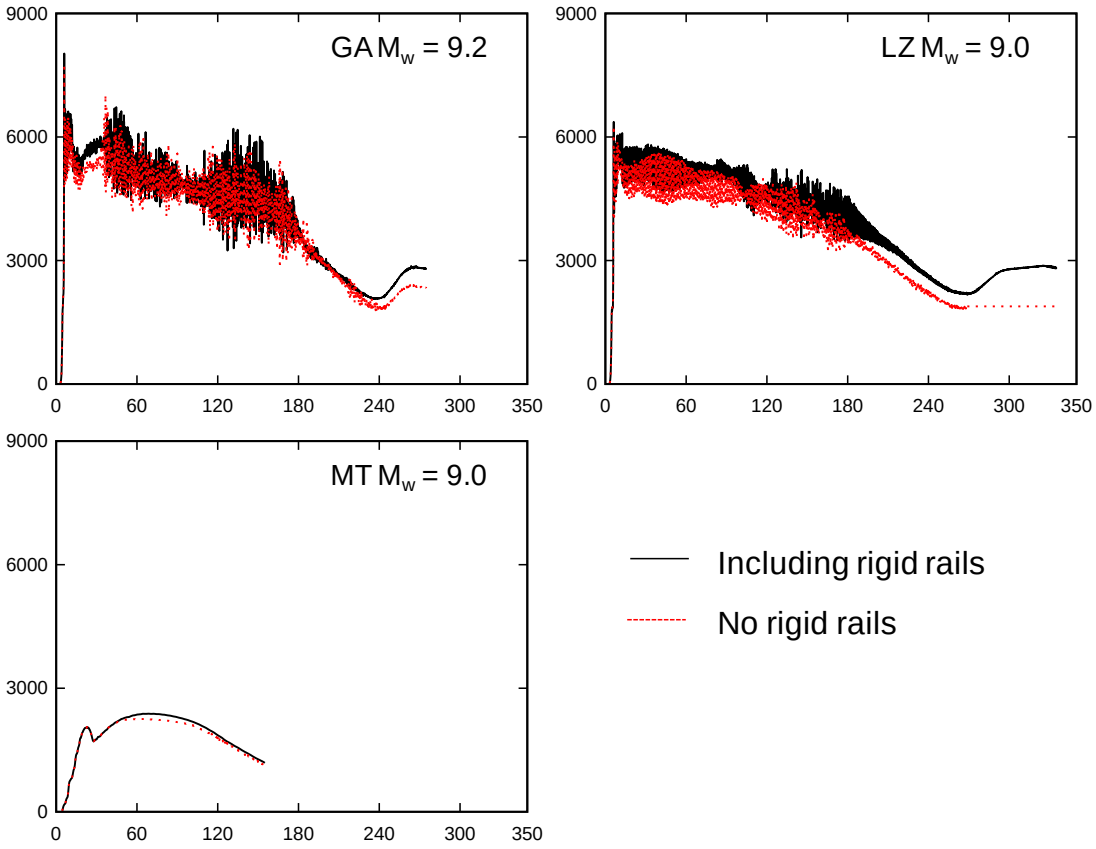

Figure 10 Time-Histories of predicted horizontal tsunami force (lb/in) on Drift Creek Bridge

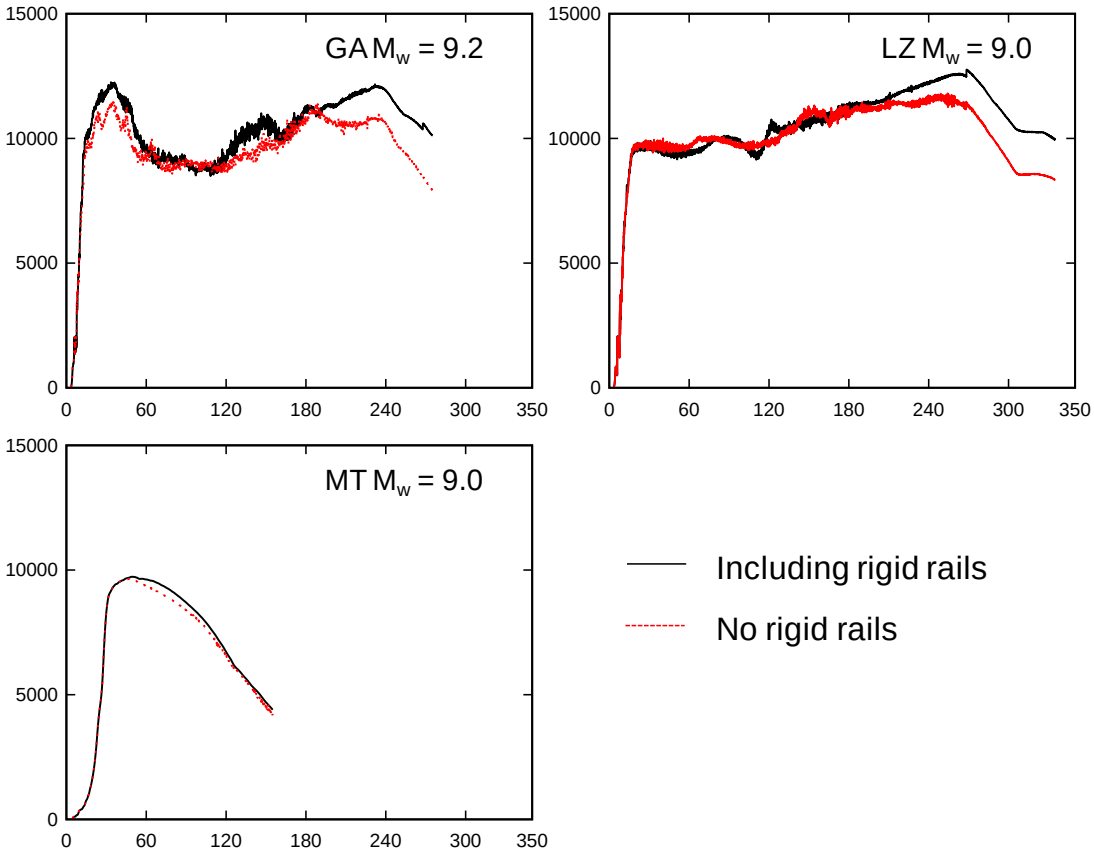

Figure 11 Time-Histories of predicted vertical tsunami force (lb/in) on Drift Creek Bridge

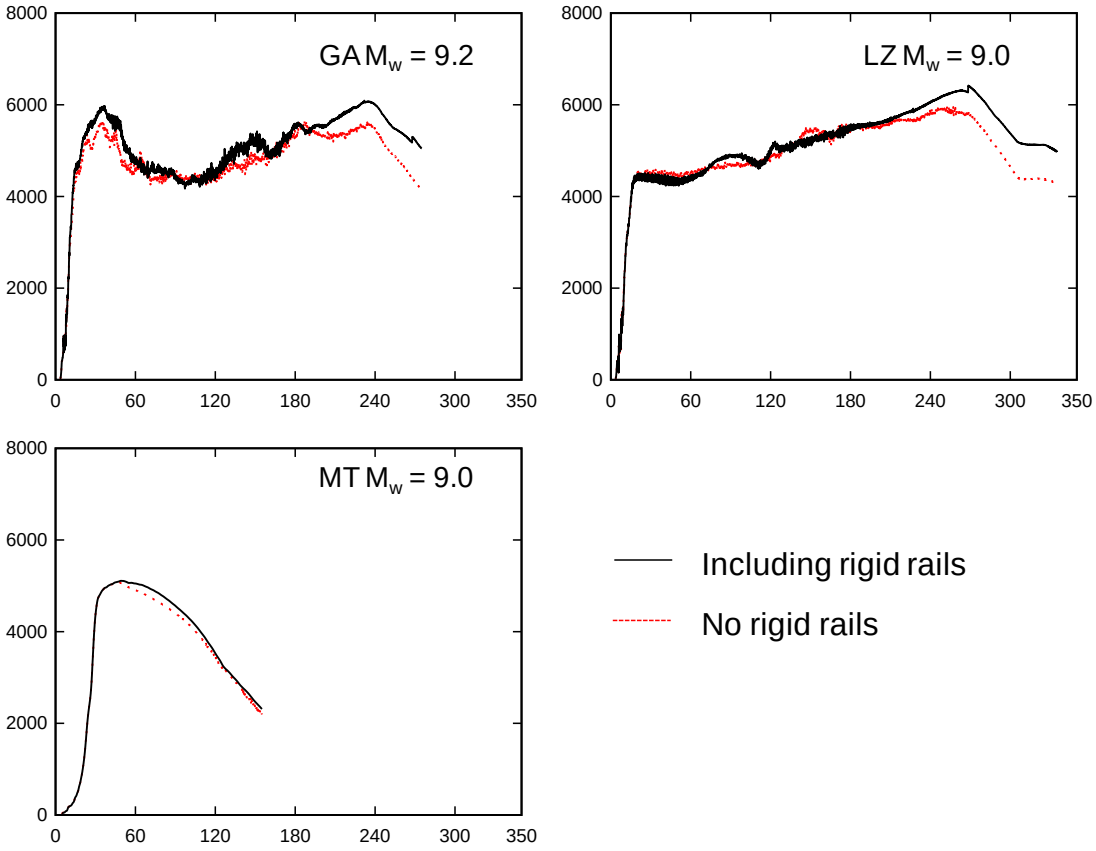

Figure 12 Time-Histories of predicted overturning moment (kip-ft/ft) on Drift Creek Bridge

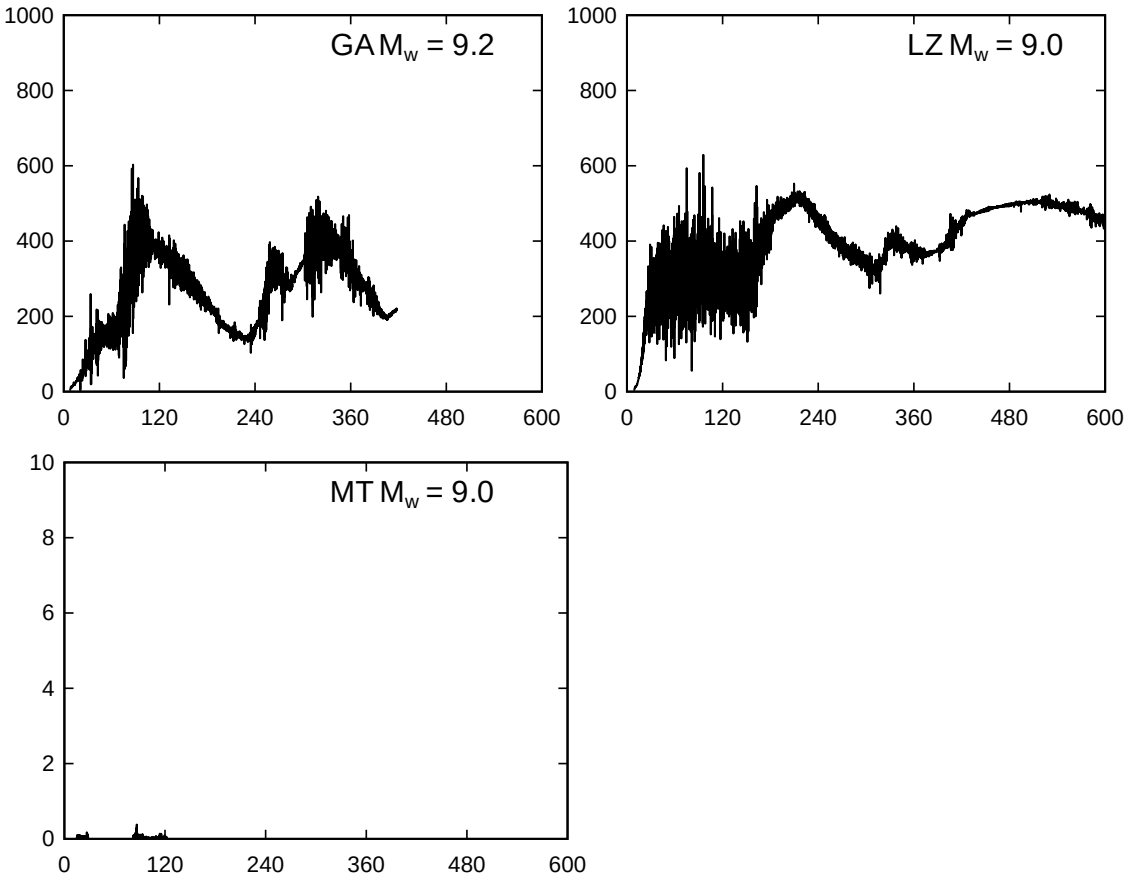

Figure 13 Time-Histories of predicted horizontal tsunami force (lb/in) on Millport Slough Bridge

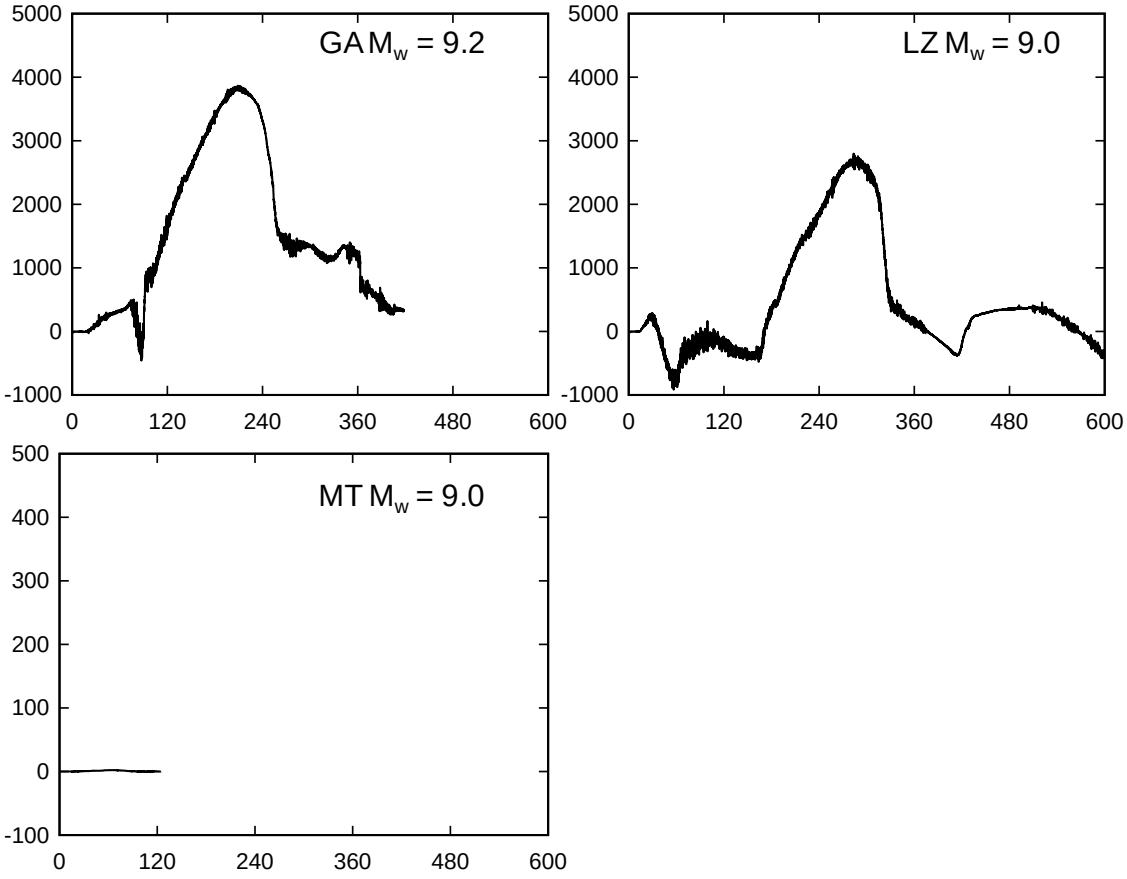

Figure 14 Time-Histories of predicted vertical tsunami force (lb/in) on Millport Slough Bridge

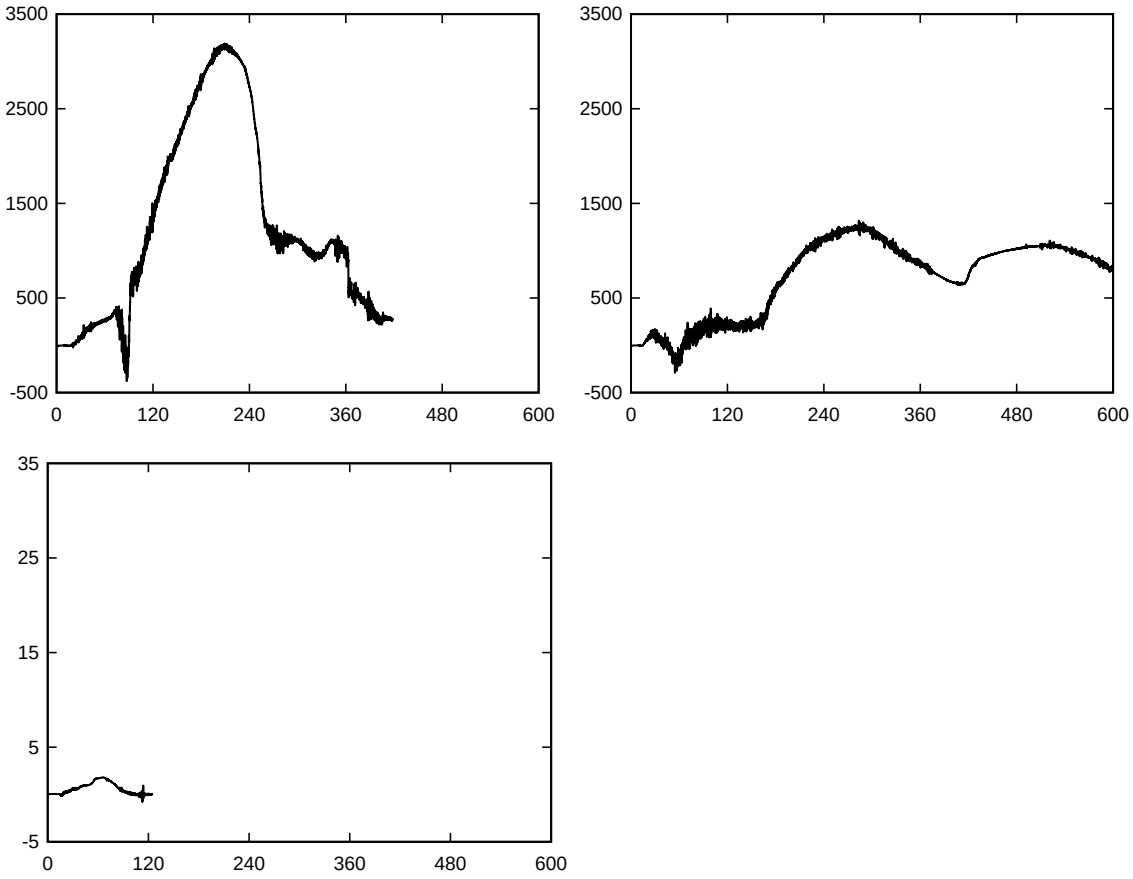

Figure 15 Time-Histories of predicted overturning moment (kip-ft/ft) on Millport Slough Bridge

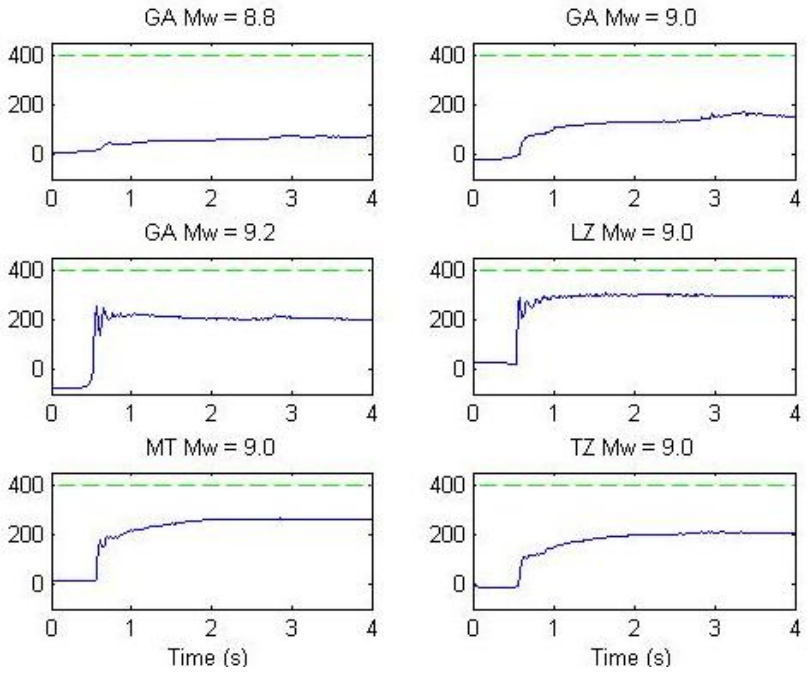

Figure 16 Water elevation time-histories at Siletz River Bridge: ____, water surface elevation (in); _ _ ., reference bridge elevation (in)

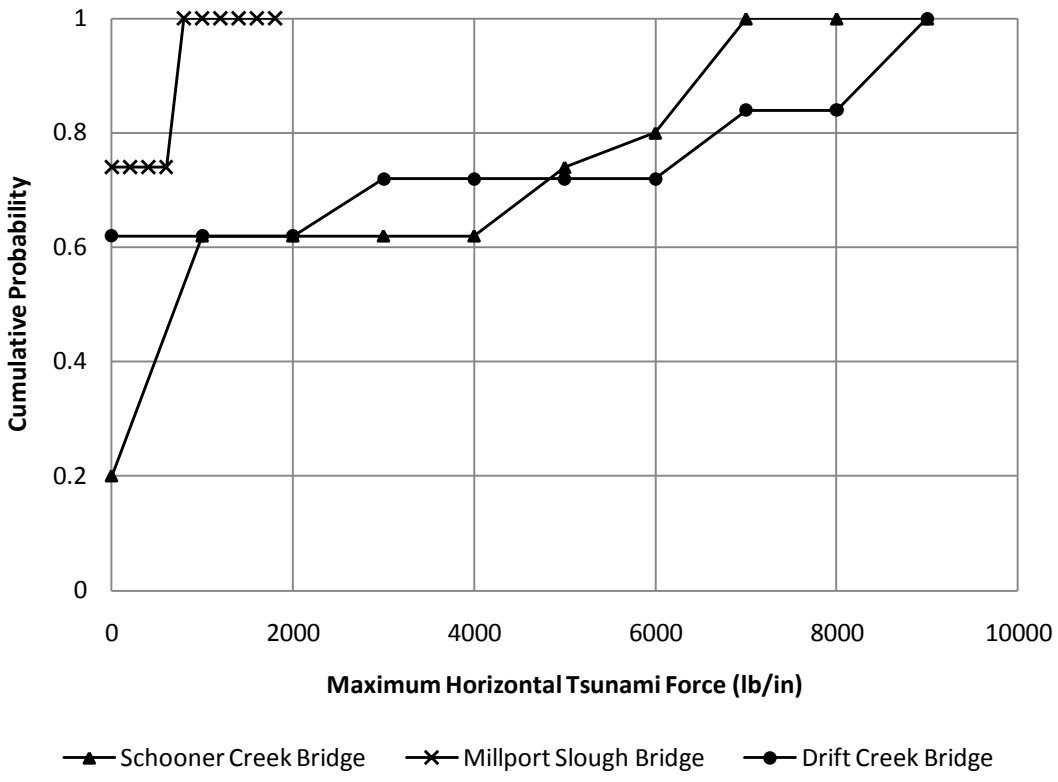

Figure 17 Cumulative probability of Maximum Horizontal Tsunami Force

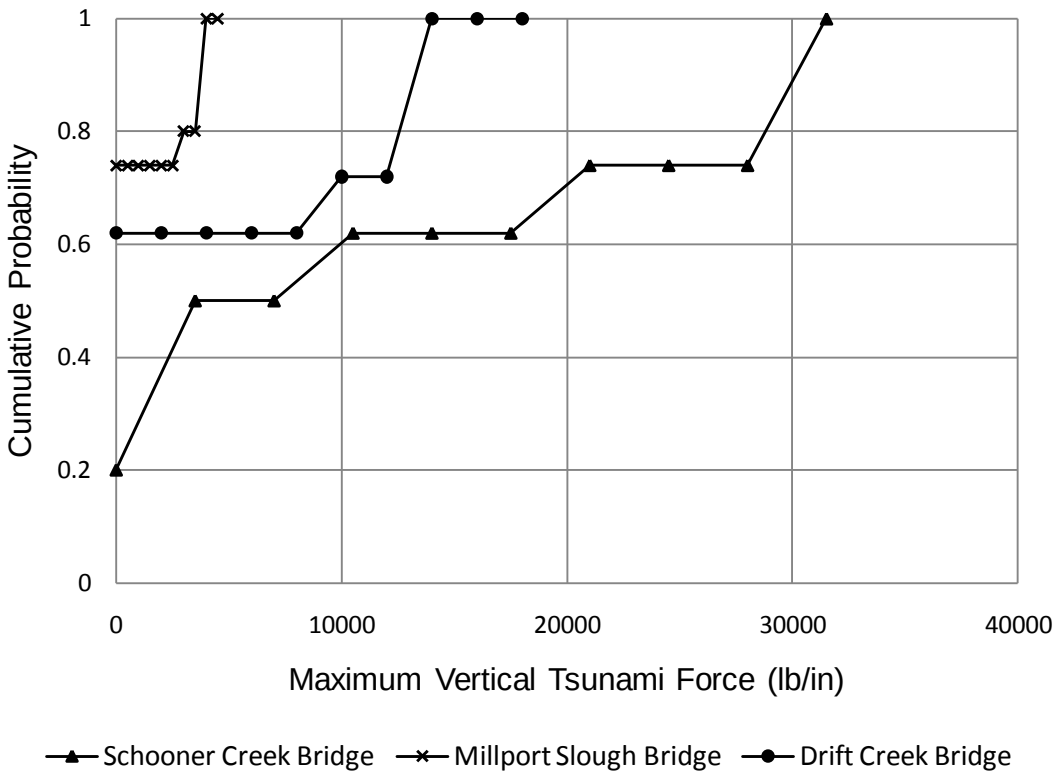

Figure 18 Cumulative probability of Maximum Vertical Tsunami Force

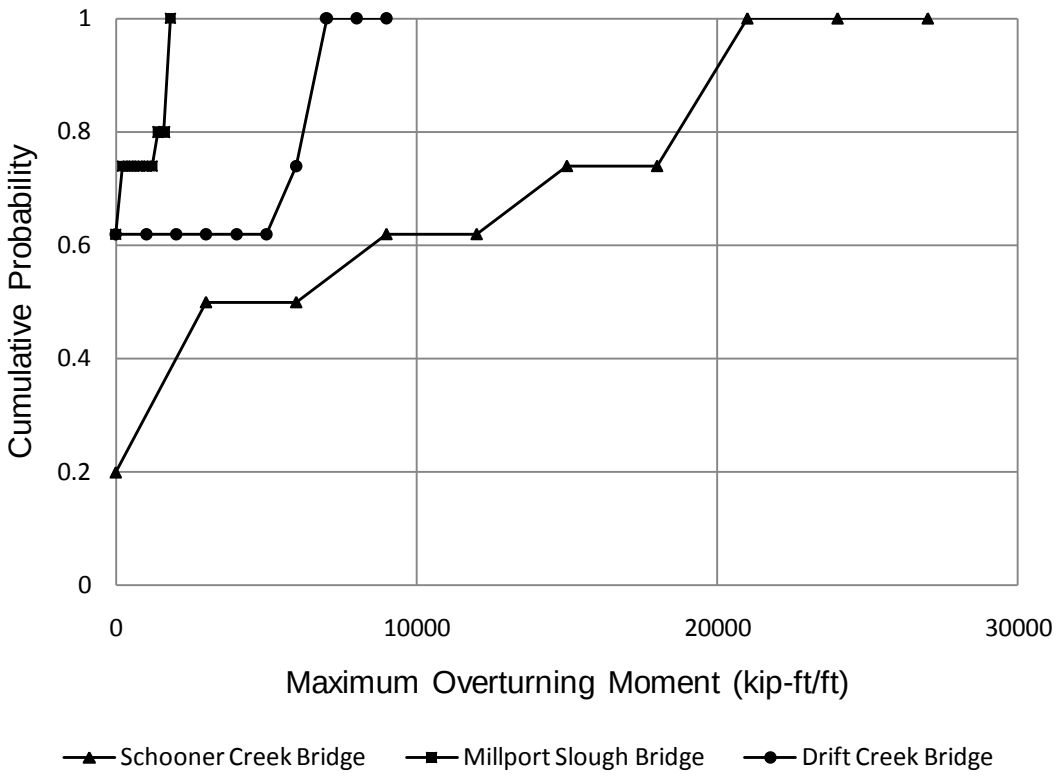

Figure 19 Cumulative probability of Maximum Overturning Moment due to Tsunamis

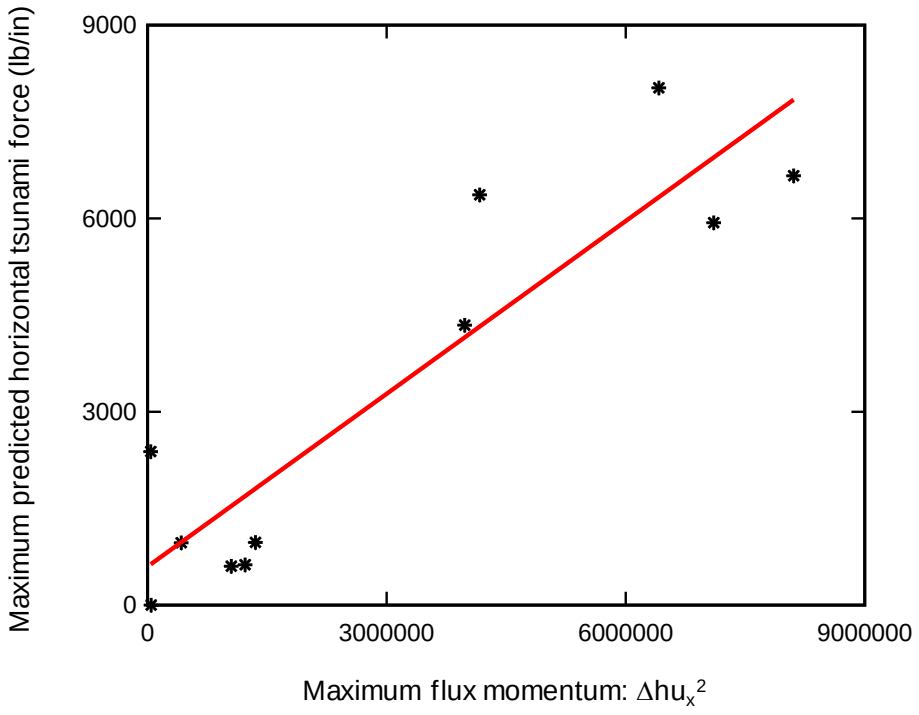

Figure 20 Correlation between maximum flux momentums and maximum predicted horizontal tsunami forces

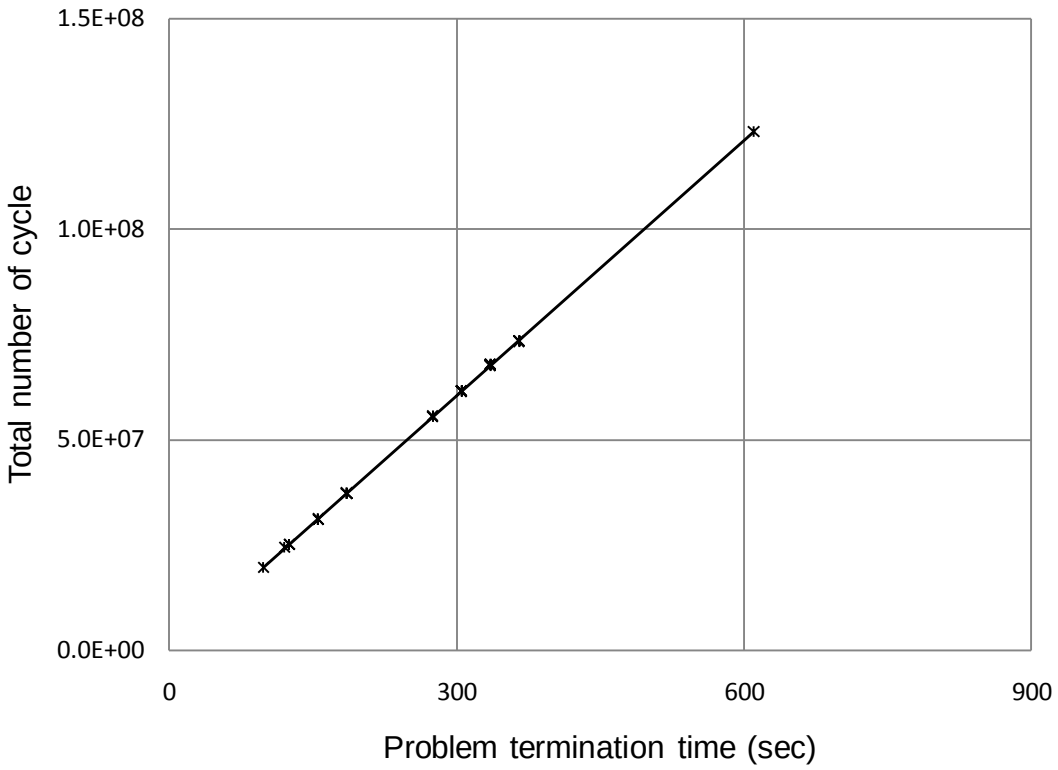

Figure 21 Correlation between problem termination time and total number of cycle

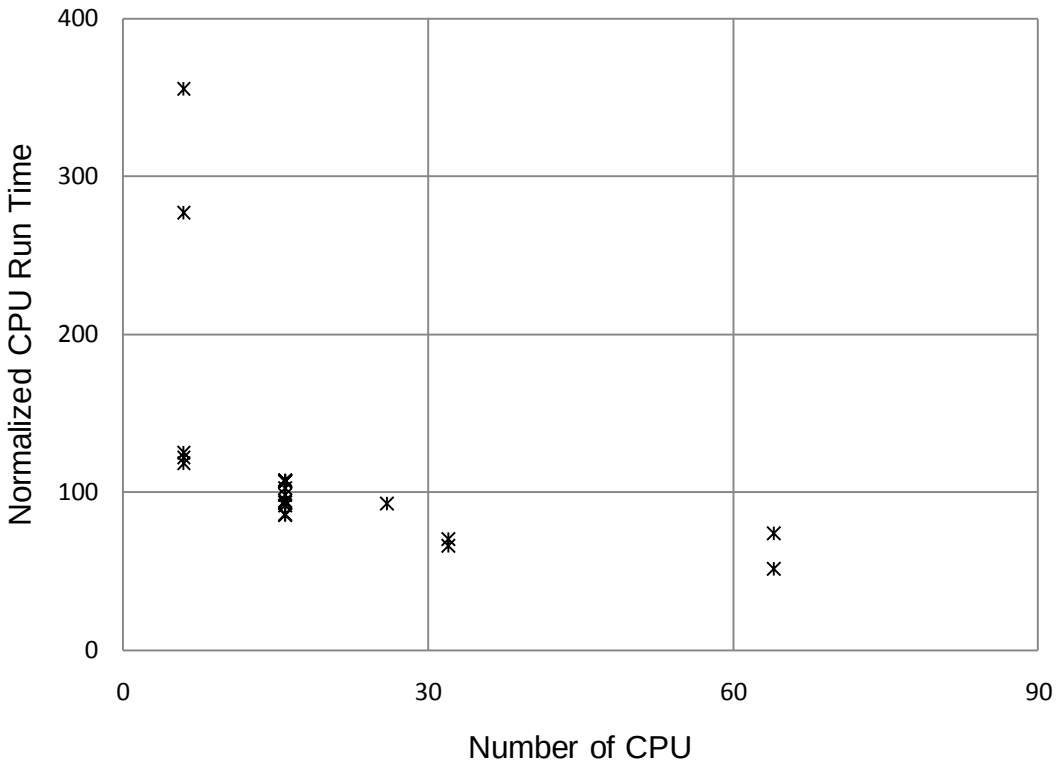

Figure 22 Relationship between number of CPU and consumed CPU time scaled for 300 seconds problem termination time

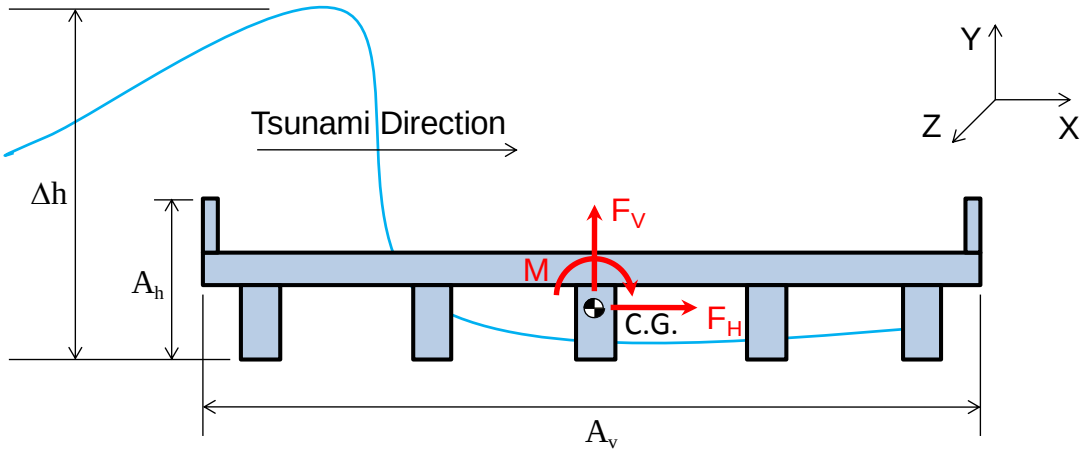

Figure 23 Parameters definition used in the recommended equations for estimating tsunami forces

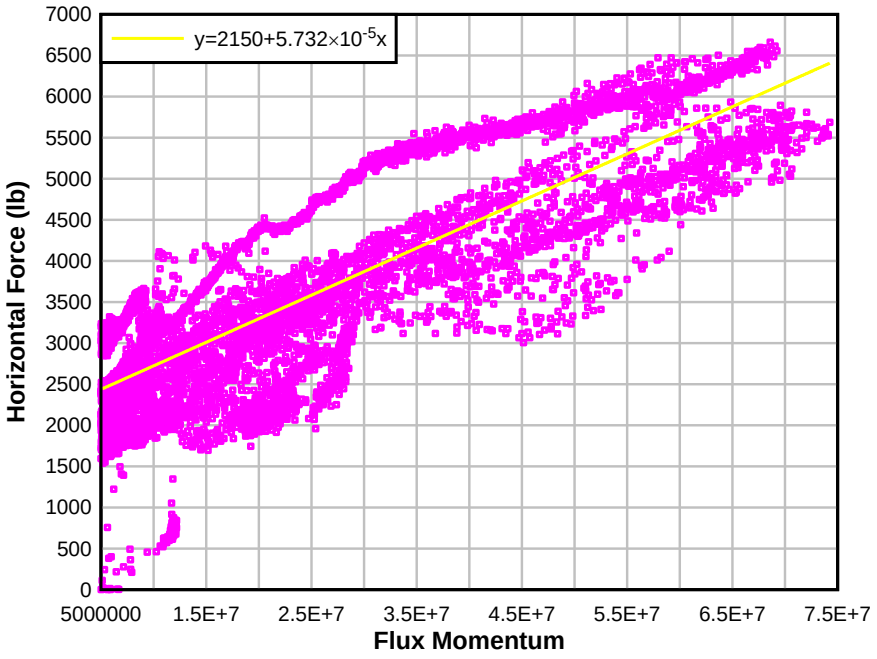

Figure 24 Relationship between total horizontal force and flux momentum (flux momentum-dependent part)

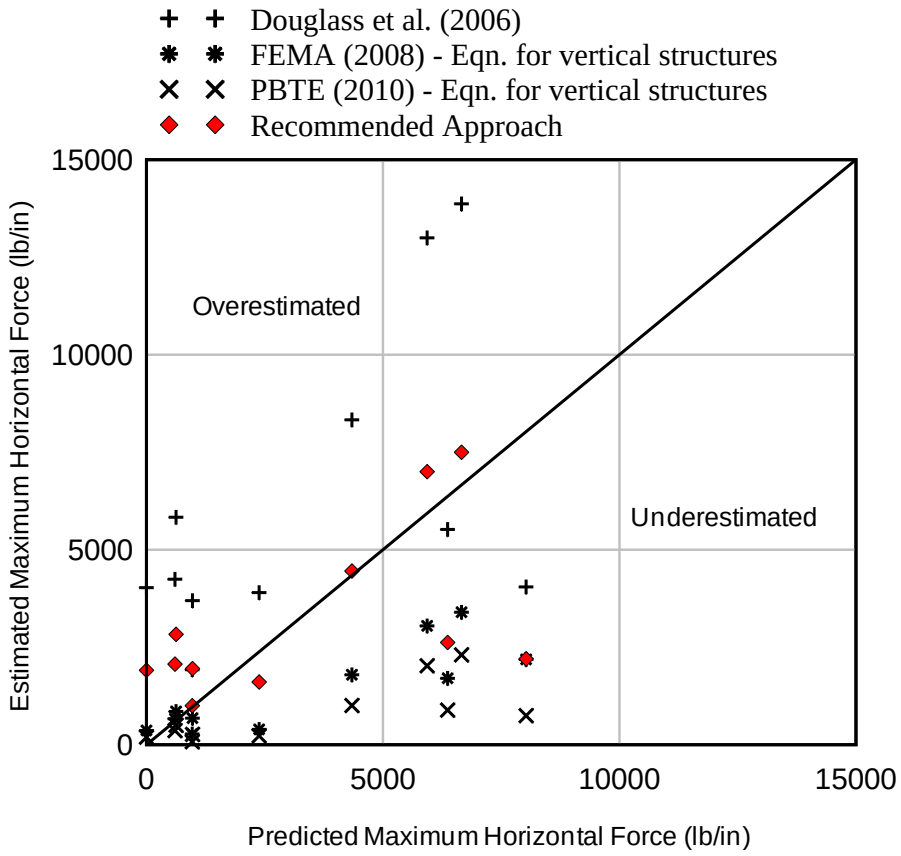

Figure 25 Comparison between estimated maximum horizontal tsunami force and predicted maximum horizontal tsunami force

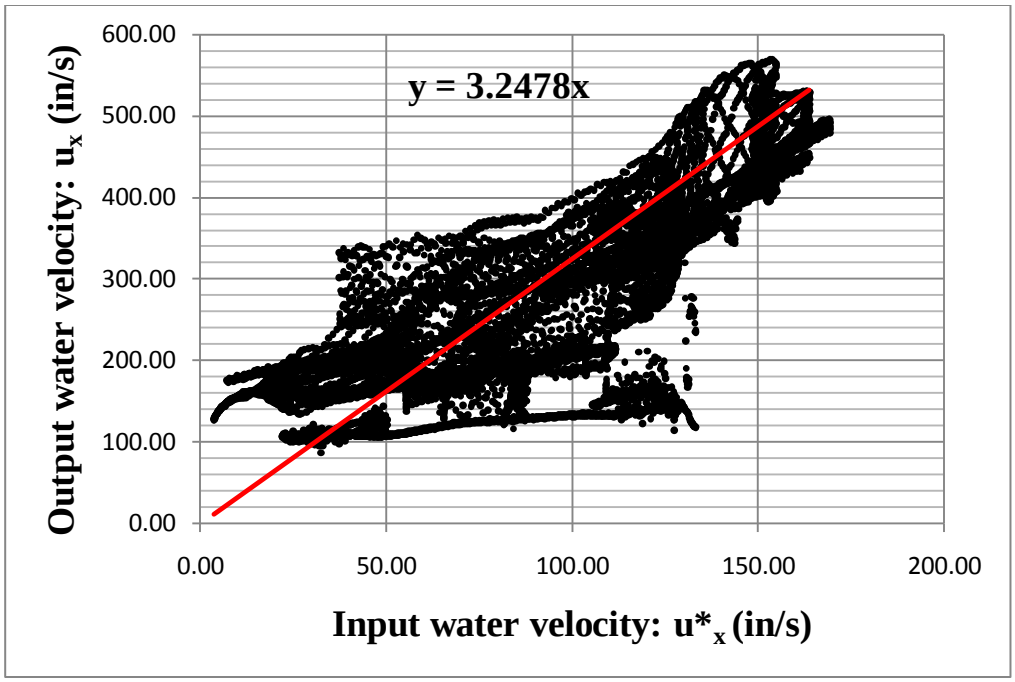

Figure 26 Correlation between horizontal water velocity with and without obstruction

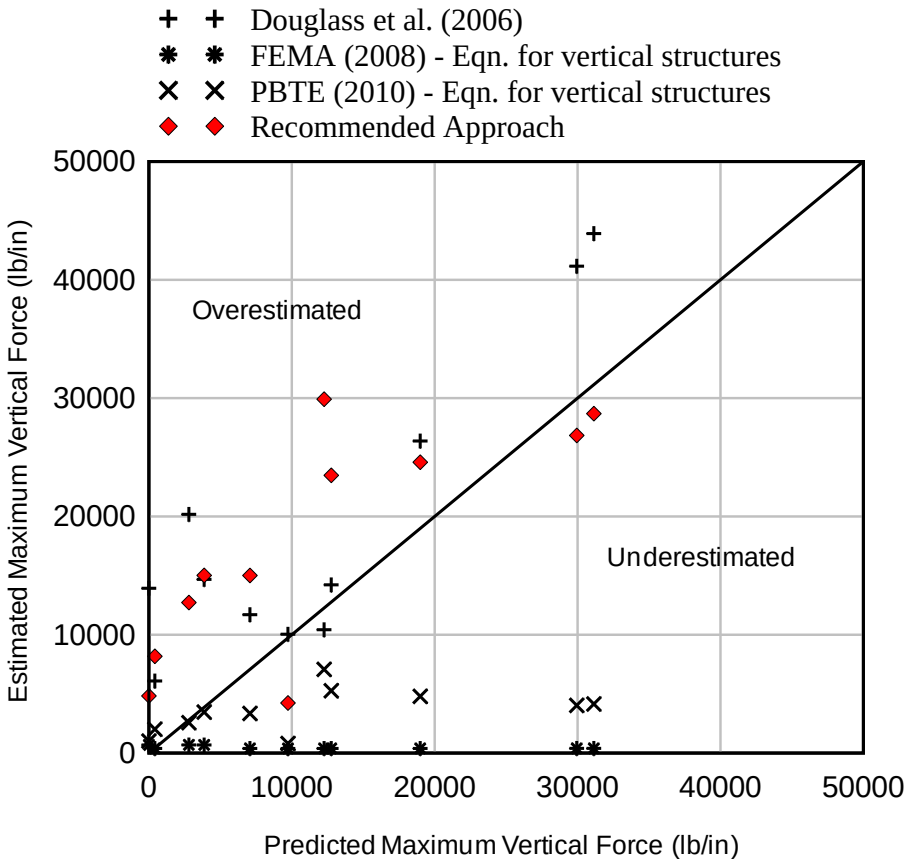

Figure 27 Comparison between the estimated maximum vertical force and the predicted numerical maximum vertical force

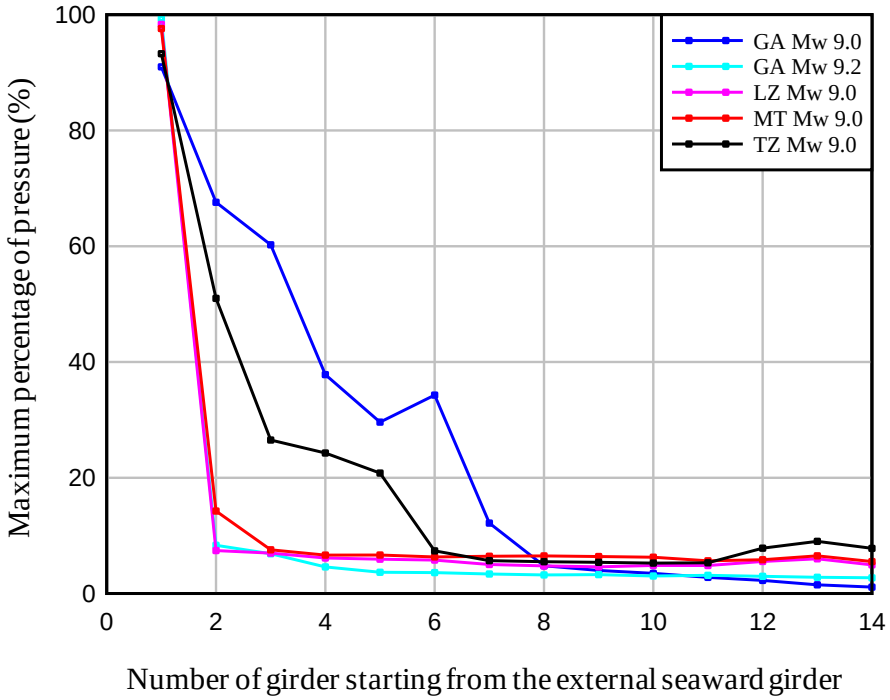

Figure 28 Maximum percentage of pressure distribution under each girder along the cross-section at Schooner Creek Bridge

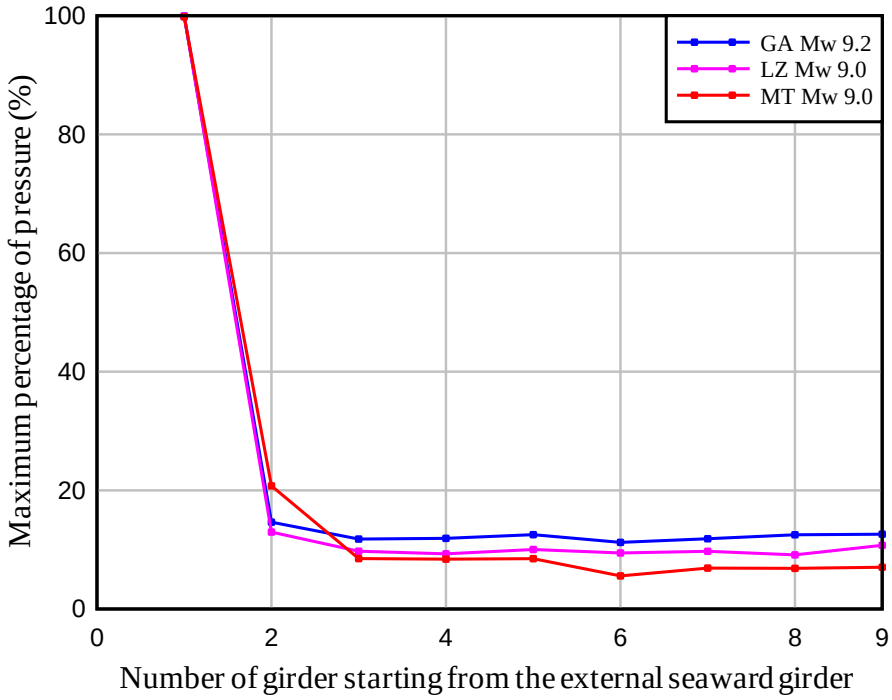

Figure 29 Maximum percentage of pressure distribution under each girder along the cross-section at Drift Creek Bridge

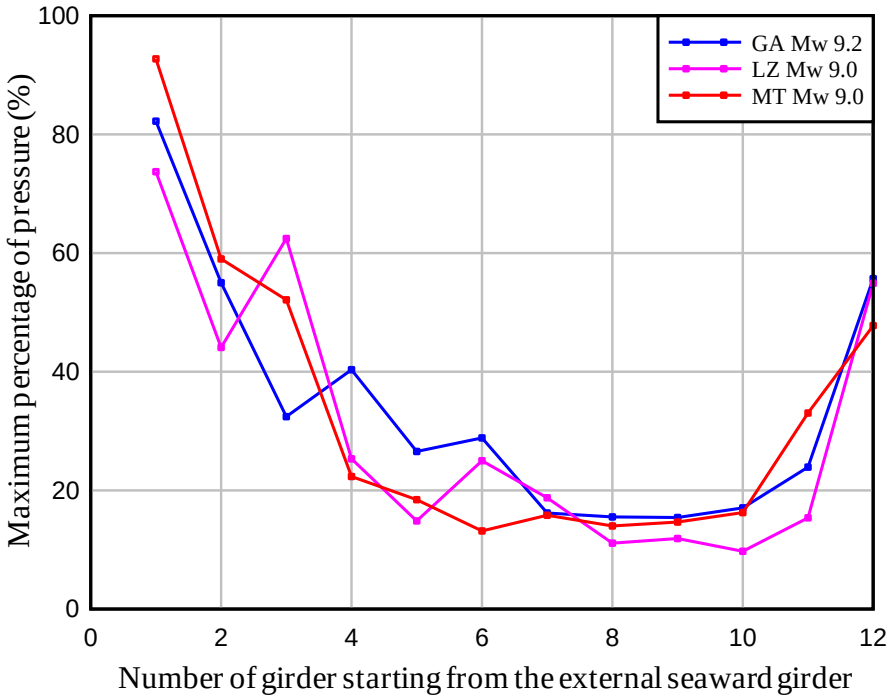

Figure 30 Maximum percentage of pressure distribution under each girder along the cross-section at Millport Slough Bridge

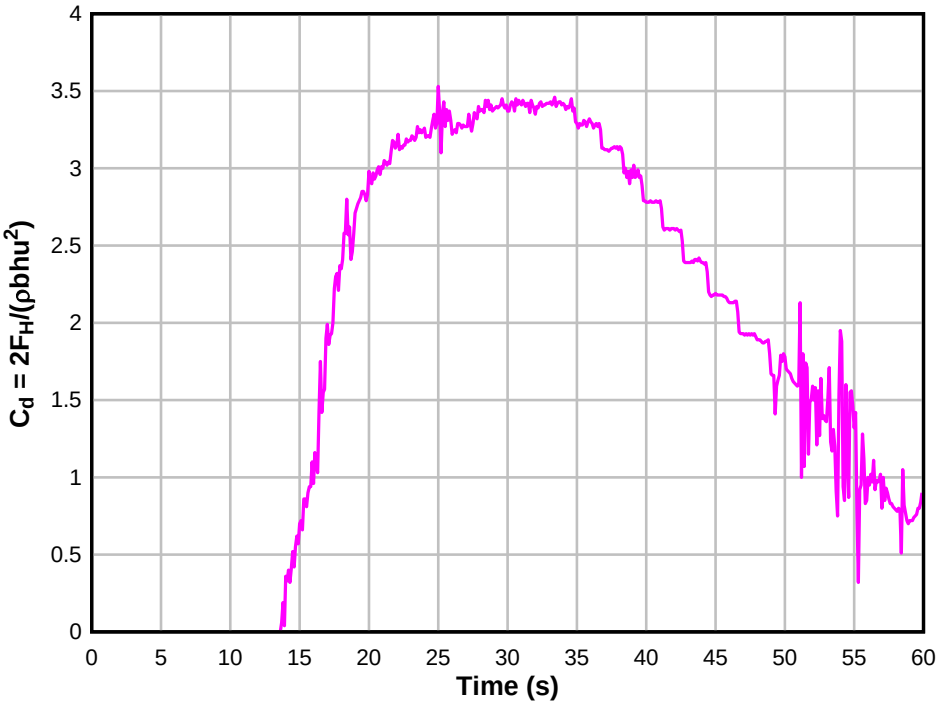

Figure 31 Empirical drag coefficients for Spencer Creek Bridge

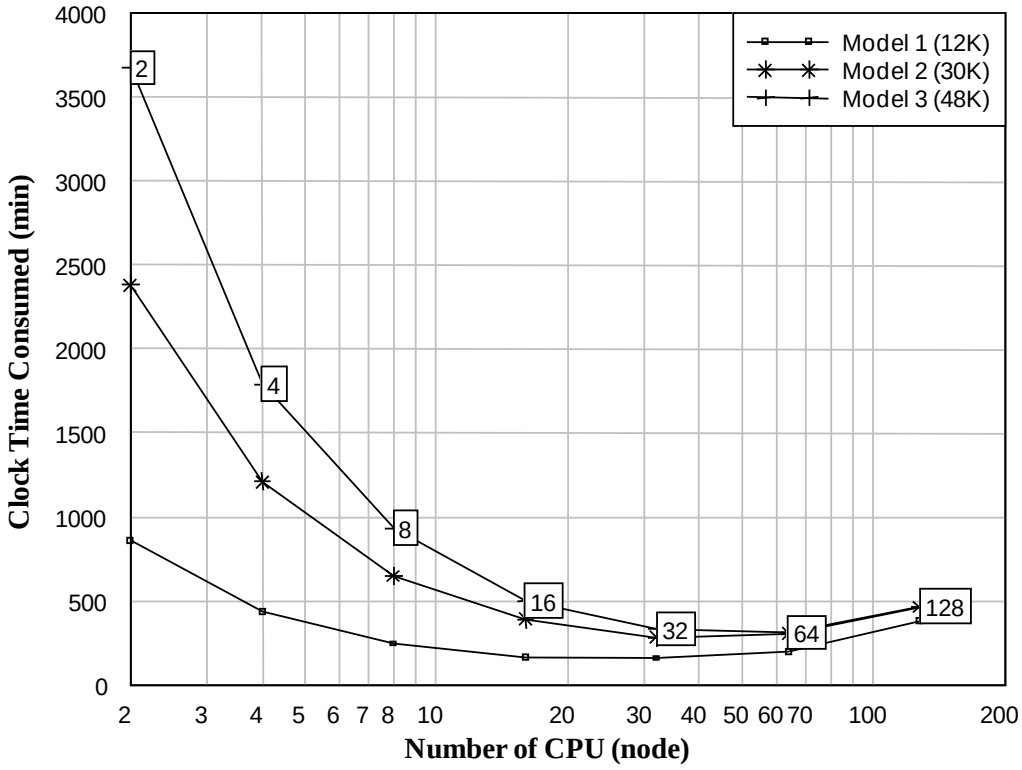

Figure 32 Relationships between consumed computational time and number of computer CPU

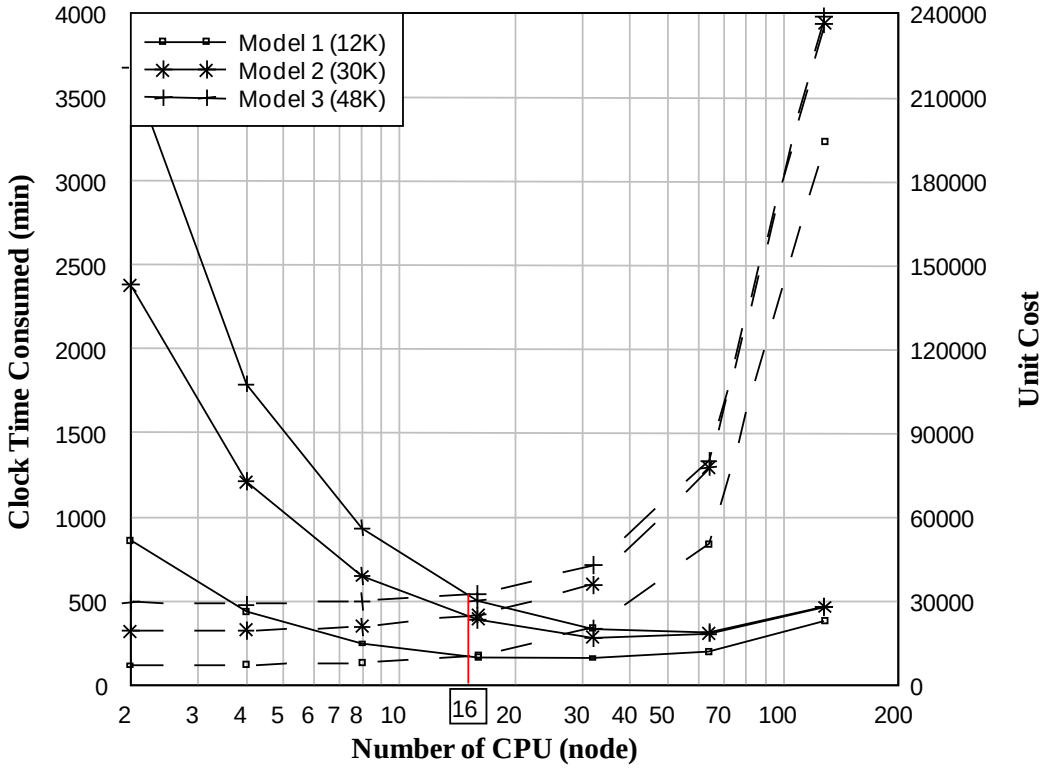

Figure 33 Relationships between computational time, unit cost, and number of computer CPU

General Conclusion

The Oregon coast is vulnerable to 500-year seismic events in Cascadia Subduction Zone that could generate large tsunamis. The bridges along the coast were not designed for such large seismic and tsunami loads. Major damages on these bridges would cause traffic disruption in the area. Unlike seismic loads, the literature of tsunami forces on bridge superstructures is very sparse at this time; thus, a better understanding of interaction between tsunamis and bridge superstructures is of major interest to the practicing engineering community. In this context, this thesis presented a manuscript describing a study of responses of four selected bridge superstructures under controlled tsunami loads and development of guidelines for estimating tsunami forces on bridge superstructures.

Numerical models of tsunami impact on bridge superstructures were developed by using a finite-element code, LS-DYNA software, in this research. At Schooner Creek Bridge, simulation models of two types of bridge superstructure – deck-girder and box section – were created to study an effect of different type of bridge superstructure under identical tsunami conditions. The results indicate that both horizontal force and vertical force on box section bridge type are significantly higher than the forces on deck-girder section, given similar tsunami conditions; thus, the box section bridge type is not recommended in tsunami run-up zone. The numerical results also suggested that an existing of bridge rails could increase horizontal and vertical tsunami forces up to 20% and 15%, respectively. Furthermore, the results from the simulation model of the selected bridges suggested major parameters that must be considered for estimating

tsunami forces on bridge superstructures are the reference bridge elevation, maximum water surface elevation (h_{max}), maximum horizontal water velocity ($u_{x,max}$), and flux momentum ($(\Delta hu^2)_{max}$). Note that the maximum flux momentum is not equal to maximum water elevation times maximum horizontal velocity squared ($(\Delta hu^2)_{max} \neq \Delta h_{max} u_{x,max}^2$). These parameters could be obtained directly from the provided tsunami flow fields (u, h). The reference bridge elevation underside bridge superstructure is an important parameter that must be considered since tsunami forces on the superstructures are generated only when water elevation is higher than the bridge elevation, which is the case when the tsunamis are encountered by the bridge superstructure. If the elevation of bridge superstructure is high enough, the design engineers do not have to concern about the tsunami forces on the bridge superstructures, as we have seen in the Siletz River Bridge case.

The time-history results of the bridge superstructures obtained from the numerical models were used to evaluate appropriate empirical coefficients for calculating tsunami forces on bridge superstructures. The drag coefficient, used in estimation of the horizontal hydrodynamic force, is recommended here as $C_d = 1$. The adjusted horizontal water velocity, used in estimation of the vertical uplift force, near the bridge superstructure is approximately 3.5 times the provided horizontal velocity of tsunami without an obstruction.

The revisited case study of the Spencer Creek Bridge indicates that the guidelines developed in this thesis provide forces (horizontal and vertical) within a factor of 2 from the reference. This clearly demonstrates the applicability of the present

guidelines although the longitudinal girders are not present in the previous model (since the cross-beam was deeper and hence was the only structural member modeled).

The recommended approach is intended to be served as a preliminary guidance for estimating tsunami forces on bridge superstructures. It is not intended to be conservative and it precludes uncertainties in the occurrence of the tsunami phenomena; therefore, an appropriate factor of safety must be included in these equations.

Even though the recommended approach for estimating tsunami forces on bridge superstructure developed in this thesis is expected to be applicable for similar situation, additional data is required to confirm the purposed empirical coefficients. Moreover, the tsunami forces used in this study base on the time-history results calculated from the numerical models only; thus, a verification of the load results with laboratory experimental is needed to confirm the predicted results. To extend this research, three dimensional models with flexible bridge should be developed for a better understanding of an interaction between fluid and the structure, and to study an effect of longitudinal span length of the bridge.

Bibliography

Arnason, H. *Interaction between an Incident Bore and a Free-Standing Coastal Structure.* PhD Thesis, Seattle: University of Washington, 2005.

Bea, R.G., Xu T., Stear J., and and Ramos R. "Wave Forces on Decks of Offshore Platforms." *Journal of Waterway, Port, Coastal and Ocean Engineering*, 1999: 136-144.

Belytschko, T., B Moran, and W. K. Liu. *Nonlinear Finite Elements for Continua and Structures.* Chichester, NY: John Wiley, c2000, 2000.

Chen, Q., L. Wang, and H. Zhao. "Hydrodynamic Investigation of Coastal Bridge Collapse during Hurricane Katrina." *Journal of Hydraulic Engineering*, 2009: 175-186.

Cuomo, Giovanni, K. Shimosako, and S. Takahashi. "Wave-in-deck loads on coastal bridges and the role of air." *Coastal Engineering*, 2009: 793-809.

Douglass, S. L., Q. Chen, and J. M. Olsen. *Wave Forces on Bridge Decks.* Washington: Federal Highway Administration, 2006.

Francis, M. J., and H. Yeh. *Tsunami Inundation Scour of Roadways, Bridges and Foundations.* EERI/ FEMA NEHRP Professional Fellowship Report, 2006.

Goldfinger. "Deep-water turbidites as Holocene earthquake proxies: the Cascadia subduction zone and Northern San Andreas Fault systems." *Annals of Geophysics*, 2003: 1169-1194.

Hallquist, John O. *LS-DYNA Theory Manual.* Livermore, CA: Livermore Software Technology Corporation, 2006.

Haritos, N., T. Ngo, and P. Mendis. "Evaluating Tsunami Wave Forces on Structures." *Monash University*. Melbourne, Australia, 2005.

Hsiao, S., and T. Lin. "Tsunami-like solitary waves impinging and overtopping an impermeable seawall: Experiment and RANS modeling." *Coastal Engineering*, 2010: 1-18.

Huang, W., and H. Xiao. "Numerical Modeling of Dynamic Wave Force Acting on Escambia Bay Bridge Deck during Hurricane Ivan." *Journal of Waterway, Port, Coastal, and Ocean Engineering*, 2009: 164-175.

Jung, J. K. *Using a Finite-Element Based Software LS-DYNA for Modeling and Simulation of Nonlinear Contact/Impact Structural and Fluid Mechanics Problems.* MS project report, Corvallis, OR: Oregon State University.

Livermore Software Technology Corporation (LSTC). *LS-DYNA Keyword User's Manual Volume I.* Livermore, CA: Livermore Software Technology Corporation (LSTC), 2007 Version 971.

Mcconnell, K., W. Allsop, and I. Cruickshank. *Piers, jetties and related structures exposed to waves Guidelines for hydraulic loadings.* London: Thomas Telford Publishing, 2004.

Nimmala, S. B., Solomon C. Y., K. F. Cheung, and Yong W. *Tsunami Design Criteria for Coastal Infrastructure: A case study for Spencer Creek Bridge, Oregon.* Technical Report, Salem: Oregon Department of Transportation (ODOT), 2006.

Oregon Department of Transportation, Bridge Engineering Section. *Seismic Vulnerability of Oregon State Highway Bridges.* Oregon Department of Transportation, 2009.

Palermo, D., I. Nistor, Y. Nouri, and A. Cornett. "Tsunami loading of near-shoreline Structures: a primer." NRC Research Press, 2009. 1804-1815.

Reid, John D. *LS-DYNA Examples Manual.* Livermore, CA: Livermore Software Technology Corporation, 2001.

Tichelaar, B. W., and L. J. Ruff. "Depth of seismic coupling along subduction zone." *Journal of Geophysical Research*, 1993: 15829-15831.

Winston, H. *Tsunami Design Criteria Analysis of Coastal Highway Bridges.* Master Report, Corvallis: Oregon State University, 2010.

Yeh, H. "Design Tsunami Forces for Onshore Structure." *Journal of Disaster Research Vol.2 No.6*, 2007: 531-536.

Yeh, H. "Maximum Fluid Forces in The Tsunami Runup Zone." *Journal of Waterway, Port, Coastal, and Ocean Engineering*, 2006: 496-500.

Yeh, H., I. Robertson, and J. Preuss. *Development of Design Guidelines for Structures that Serve as Tsunami Vertical Evacuation Sites.* Olympia: Washington State Department of Natural Resources, 2005.

Zhang, W. *An Experimental Strudy and a Three-Dimensional Numerical Wave Basin Model of Solitary Wave Impact on a Vertical Cylinder.* Master Thesis, Corvallis: Oregon State University, 2009.

Zienkiewicz, O. C., R.L. Taylor, and P. Nithiarasu. *The finite element method for fluid dynamics.* Oxford; Boston: Elsevier Butterworth-Heinemann, 2005.

Appendices

Appendix A Simulation Models

Appendix A-1 : Model Boundary Conditions

The two dimensional model can be thought of a three dimensional rectangular box model with one-inch thickness in z-direction. The box composes of water and air material parts with a bridge part inside. Boundary conditions of the box must be specified correctly at eight corner nodes, eight edges, two surfaces of the box, and the connection between water and air material to prevent leakage of fluid materials. The eight corner nodes of water part are constrained in x, y, and z translational. Four edges aligned along x-axis are constrained in y and z translational. Two edges aligned along y-axis at the water part and two edges at the connection between water and air parts are constrained in x and z translational. Nodes on two x-y plane surfaces are constrained in z translational. Nodes on two edges along y-axis at the right border of air material part must not be constrained in x translational as they are intentionally leave as a open channel for water and air to flow out. A demonstration of boundary set up is shown in Figure 34. Fluid elements on this open channel, orange area in Figure 34, are specified as a non-reflecting boundary condition to prevent leakage of water from the open channel at the beginning of simulation and still allow water and air to flow out freely. Note that general parameters and formulations set up in each simulation model are similarly specified for all three bridges. The differences between each model are bridge cross-section, and the input tsunami flow fields.

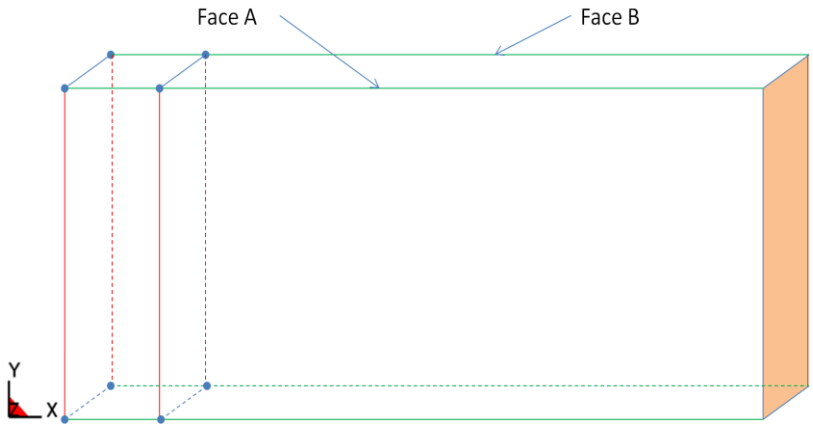

Figure 34 Boundary conditions: ●, constrained in x, y, and z translational; ——, constrained in x, and z translational; ——, constrained in y, and z translational; Face A and B, constrained in z translational.

Appendix A-2 : Model Construction

As mentioned earlier, a numerical model consists of two major material part: a fluid-like part (water and air), and a rigid structure part (bridge). The unit system used in construction of the numerical models is the English system for convenient of design engineers. The FSI numerical models were analyzed by an ALE solver provided in LS-DYNA. The ALE solver involves a Lagrangian step followed by an advection step. The advection step stops the calculation when mesh distortion is occurred and then smoothes the mesh. After the smoothing mesh process, it remaps the solution from the distorted to smoothed meshes. By using a combination of the Lagrangian-Eulerian coupling algorithm and the ALE solver, the interaction between a Lagrangian material (Bridge) and an Eulerian material (Fluid: water and air) could be taken care of.

The Eulerian fluid parts (water and air) are generally modeled using *MAT_NULL and an accompanying by equation of stated (*EOS) as recommended by LS-DYNA user manual. The null material was chosen to represent the fluid material because it has no yield strength and behave in a fluid-like manner.

The equation of state has to be specified along with the fluid-like materials to simulate their behaviors of water and air. The fluid properties of water are usually defined by the bulk modulus of the water. The relation between the change of volume and pressure was assumed to be a linear in this study. Therefore, *EOS LINEAR POLYNOMIAL keyword card is used in development of the numerical model. The fluid pressure is given by the following equation:

$$P = C_o + C_1\mu + C_2\mu^2 + C_3\mu^3 + (C_4 + C_5\mu + C_6\mu^2)E$$

where $\mu = \frac{\rho}{\rho_0} - 1$, and ρ_0 is a reference density defined in the *MAT_NULL keyword card. Due to the linear assumption, the constant parameter of the nonlinear term is assumed to be zero. Therefore, the pressure is now given by:

$$P = C_1\mu$$

where C1 is the bulk modulus of water.

$$C_1 = \rho \times c^2$$

where ρ is density of the water, and c is the speed of sound in the water.

Note that the choice of speed of sound in the water could affect the integration time step in the calculation. In the study of the smoothed particle hydrodynamics (SPH) modeling of wave propagation by Dalrymple and Rogers (2006), it was concluded that the speed of sound could be set lower than its average value without affecting the accuracy of fluid motion but could significantly reduce the computation time by larger the integration time step. The paper suggests that the minimum modified speed of sound should be about ten times greater than the maximum expected water flow speed. However, a very small speed of sound could cause stiffness problems in computation in LS-DYNA.

To model an air material in the simulation model, there are two alternative ways to specify the equation of state along with the null material to simulate the behavior of air. The first way is to use *EOS_LINEAR_POLYNOMIAL keyword card. The second way is to use *EOS_IDEAL_GAS keyword card. The *EOS_LINEAR_POLYNOMIAL was used in this research with the gamma law equation of state by setting $C_4 = C_5 = \gamma - 1$

where γ is the ratio of specific heat capacity, and set other parameters to be zero.

Numerical models of the bridge superstructures are demonstrated in Figure 35 to Figure 37. The selected input tsunami conditions – water surface elevation and horizontal velocity of water – are shown in Figure 38 to Figure 48.

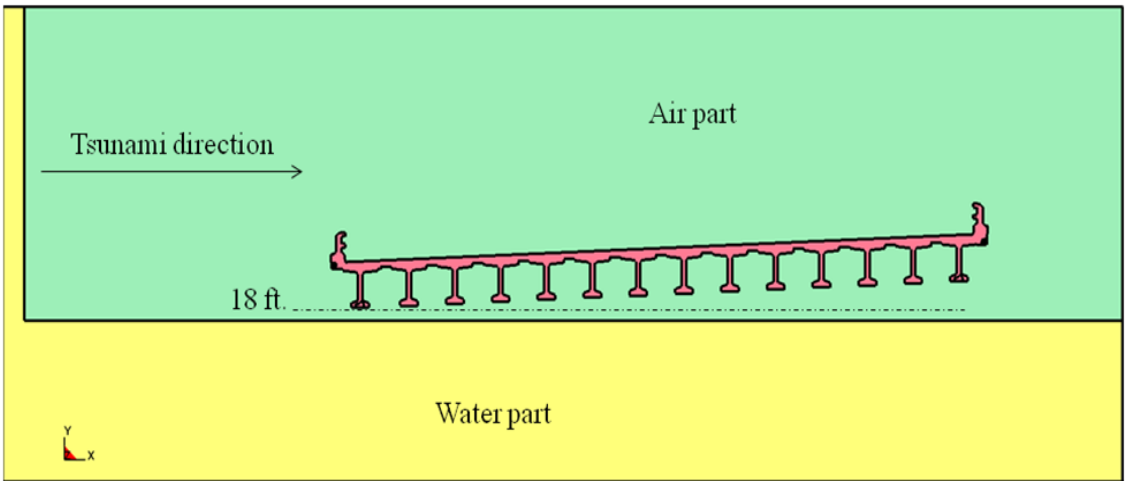

Figure 35 Simulation model of Schooner Creek Bridge (deck-girder) cross-section with one-inch thickness in z-direction

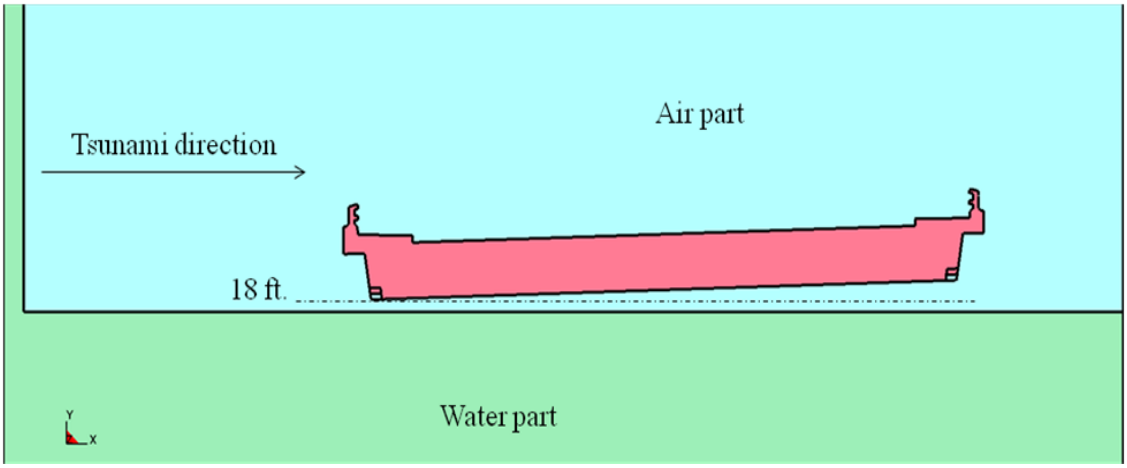

Figure 36 Simulation model of Schooner Creek Bridge (box-section) cross-section with one-inch thickness in z-direction

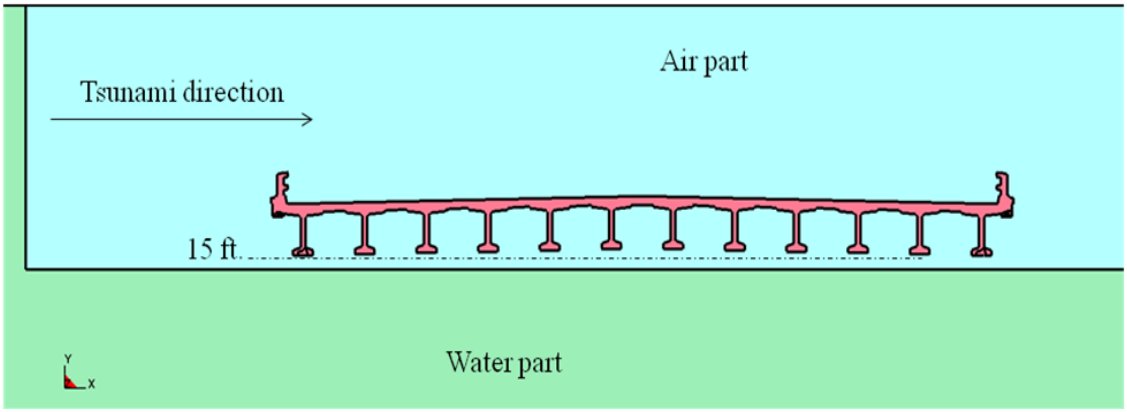

Figure 37 Simulation model of Millport Slough Bridge cross-section with one-inch thickness in z-direction

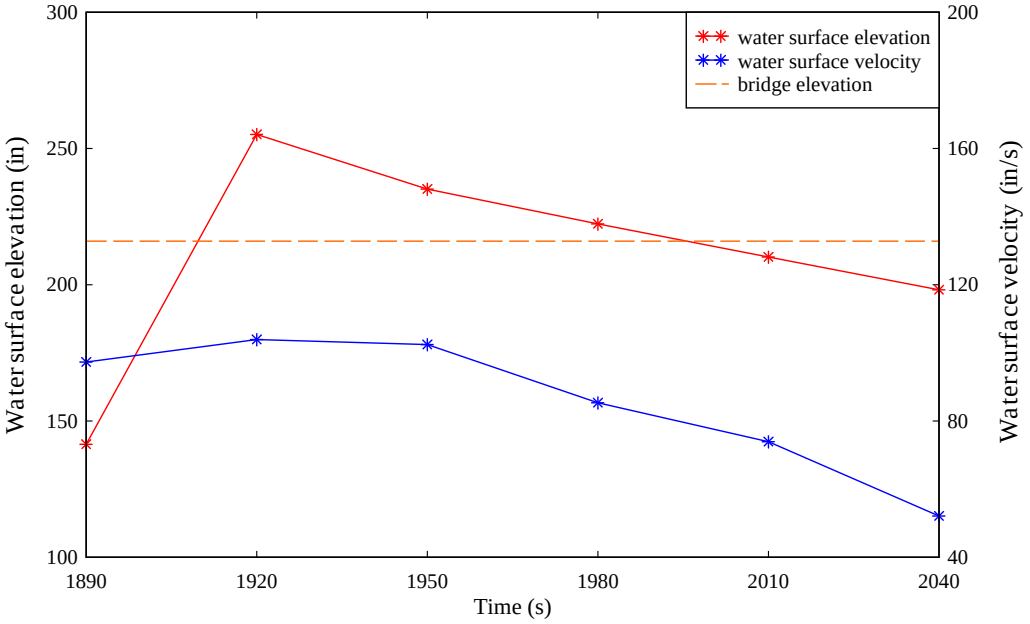

Figure 38 Input conditions for simulation models of Schooner Creek Bridge under GA M_w 9.0 tsunami scenario

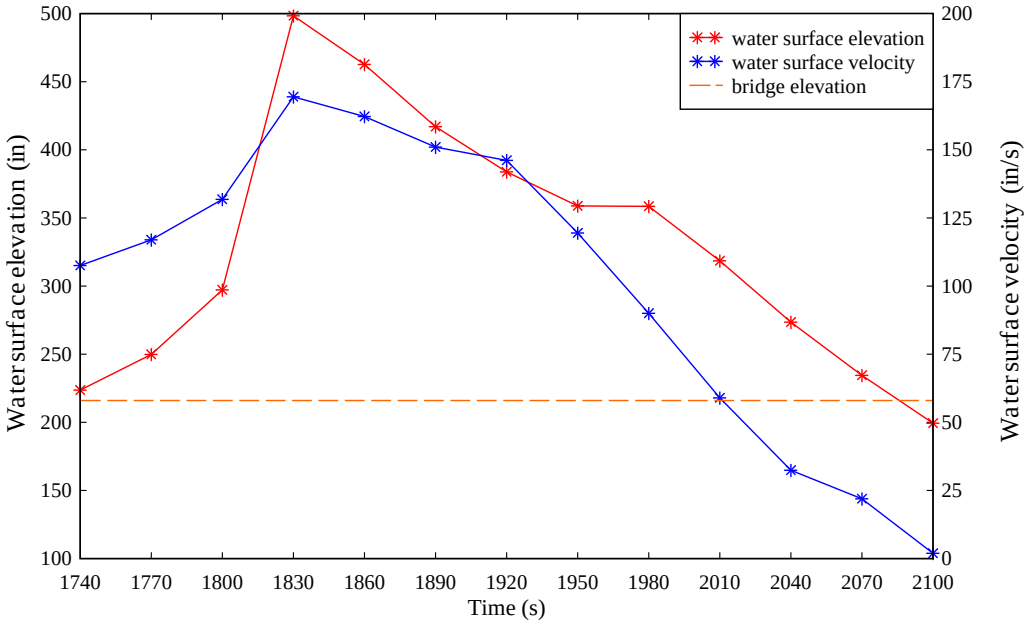

Figure 39 Input conditions for simulation models of Schooner Creek Bridge under GA M_w 9.2 tsunami scenario

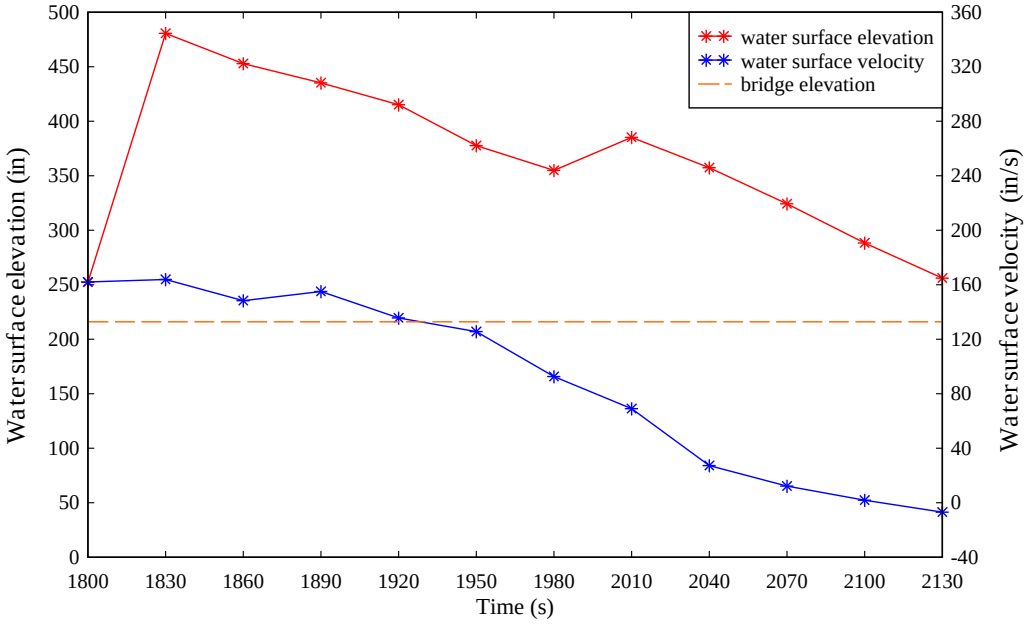

Figure 40 Input conditions for simulation models of Schooner Creek Bridge under LZ M_w 9.0 tsunami scenario

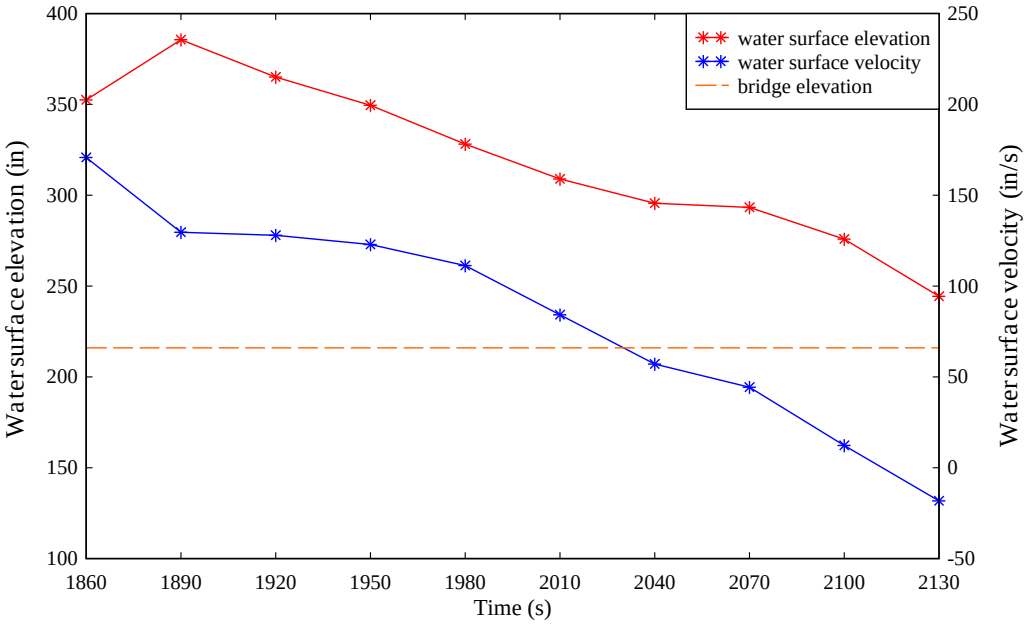

Figure 41 Input conditions for simulation models of Schooner Creek Bridge under MT M_w 9.0 tsunami scenario

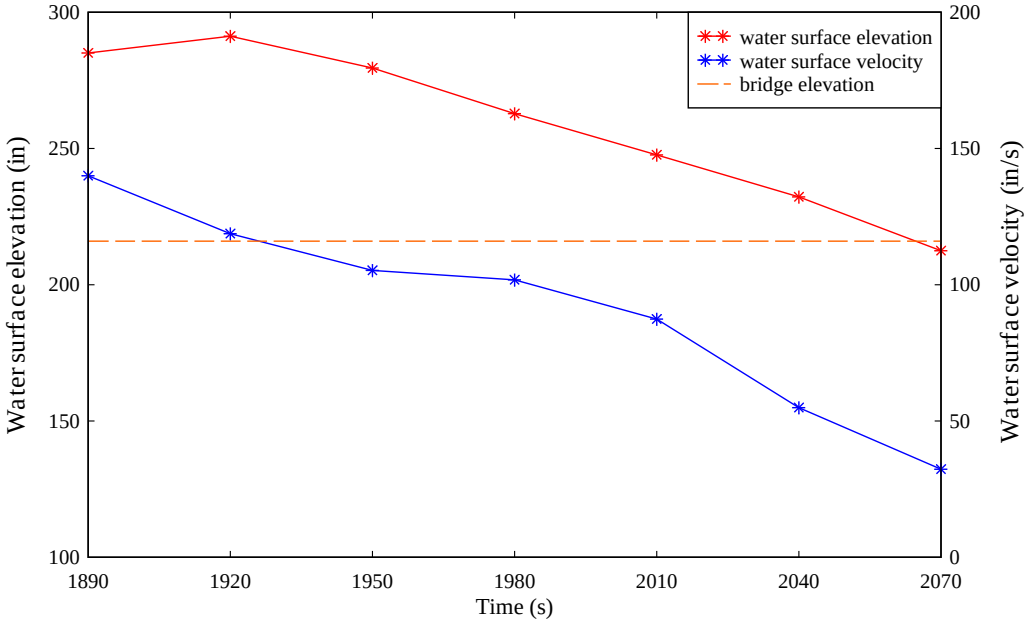

Figure 42 Input conditions for simulation models of Schooner Creek Bridge under TZ M_w 9.0 tsunami scenario

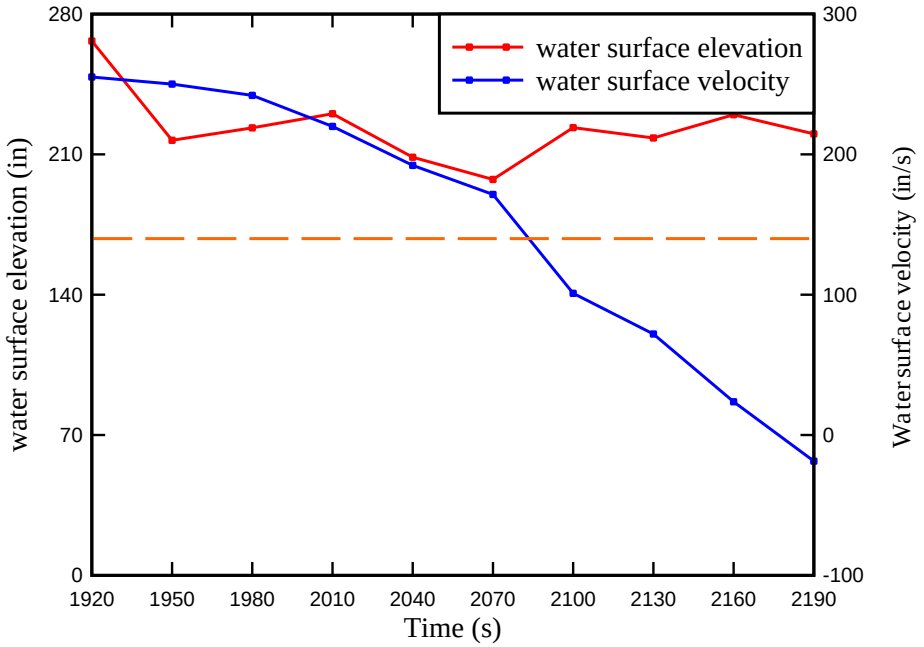

Figure 43 Input conditions for simulation models of Drift Creek Bridge under GA M_w 9.2 tsunami scenario

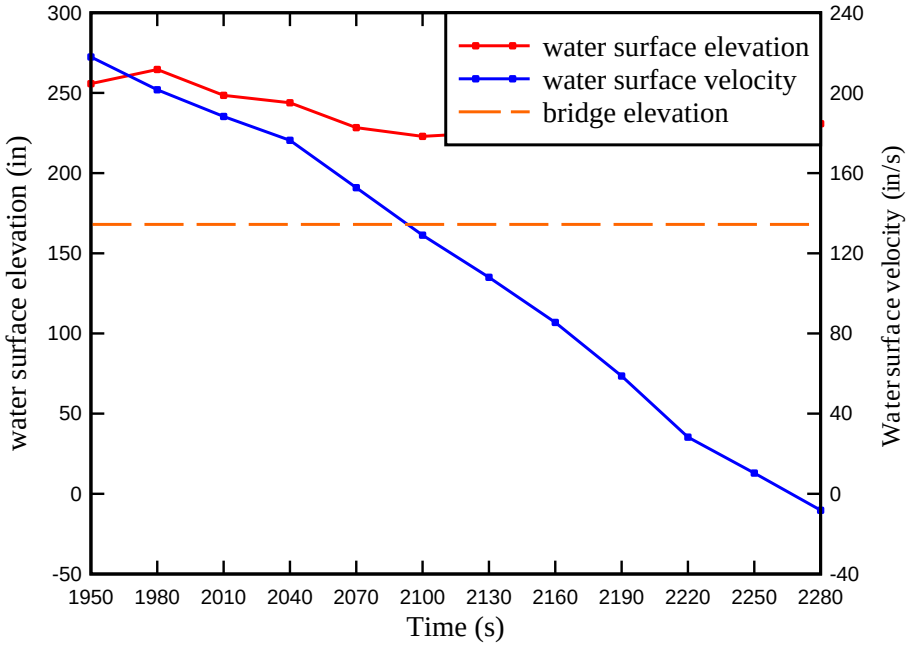

Figure 44 Input conditions for simulation models of Drift Creek Bridge under LZ M_w 9.0 tsunami scenario

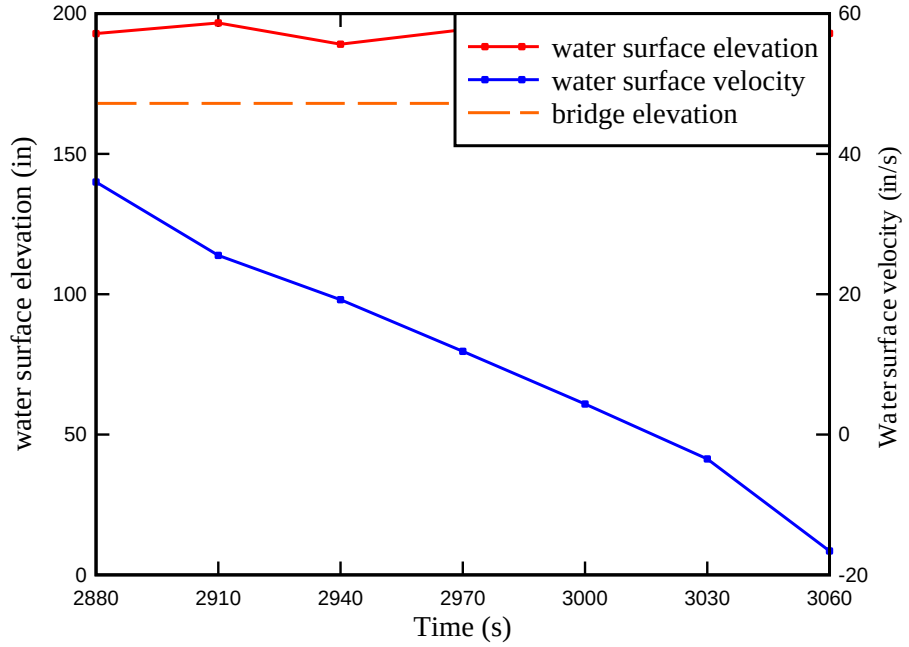

Figure 45 Input conditions for simulation models of Drift Creek Bridge under MT M_w 9.0 tsunami scenario

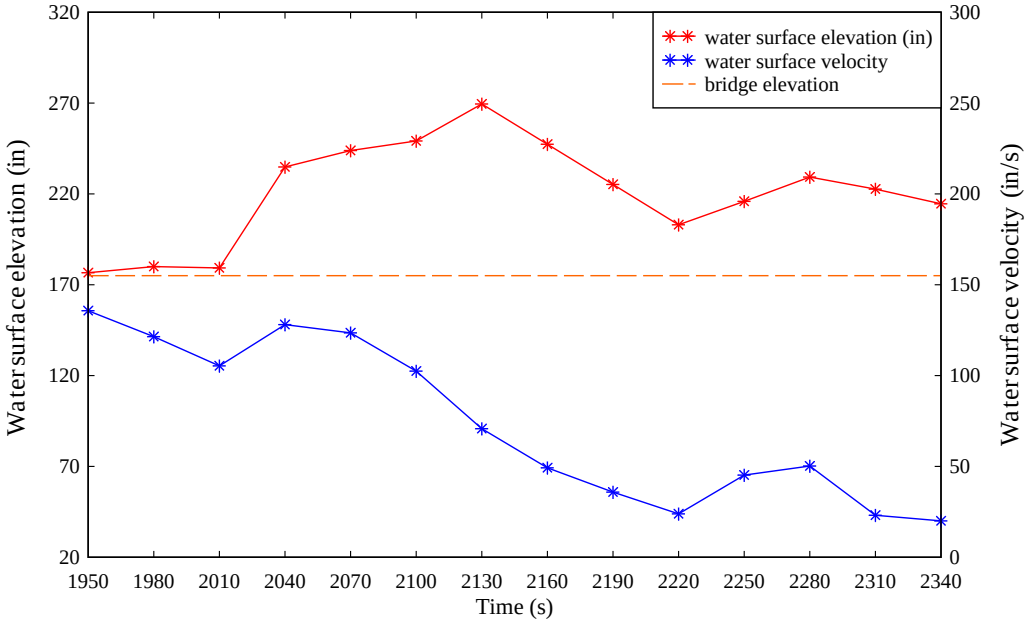

Figure 46 Input conditions for simulation models of Millport Slough Bridge under GA M_w 9.2 tsunami scenario

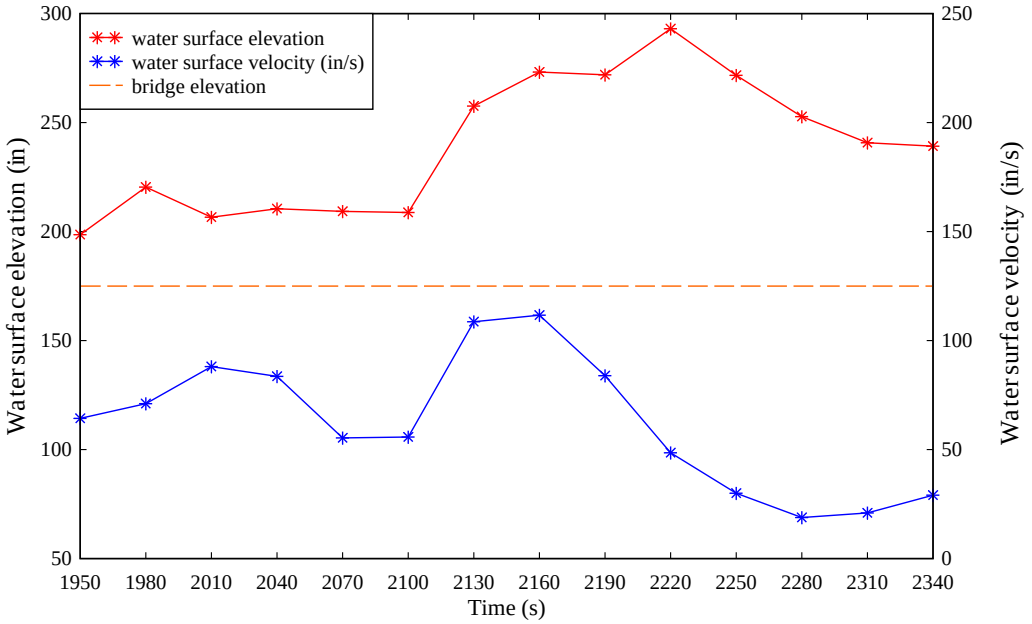

Figure 47 Input conditions for simulation models of Millport Slough Bridge under LZ M_w 9.0 tsunami scenario

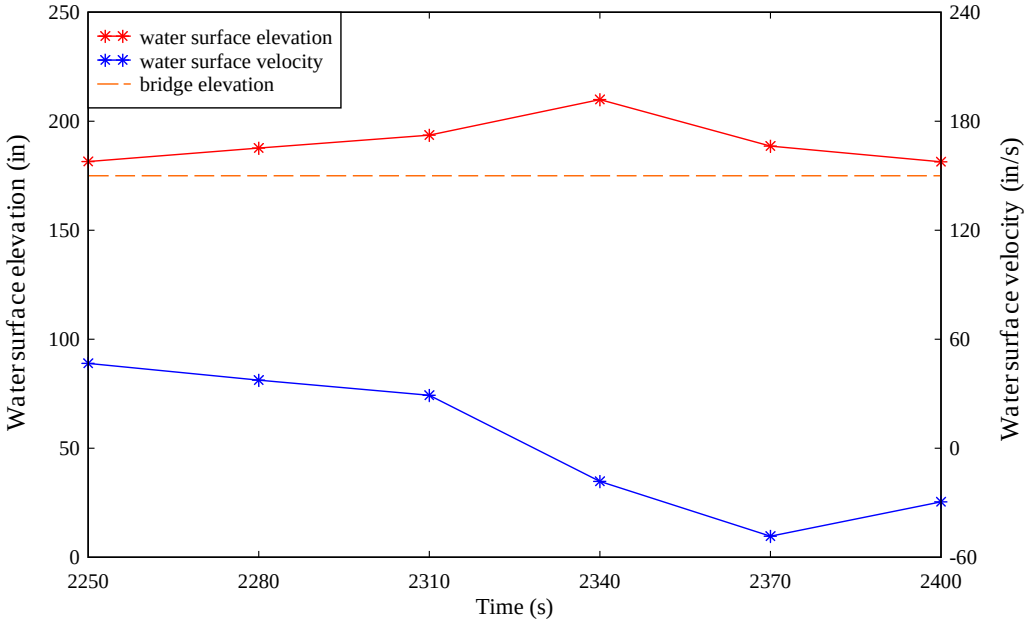

Figure 48 Input conditions for simulation models of Millport Slough Bridge under MT M_w 9.0 tsunami scenario

Appendix A-3 : Simulated tsunami impact on selected bridge superstructures

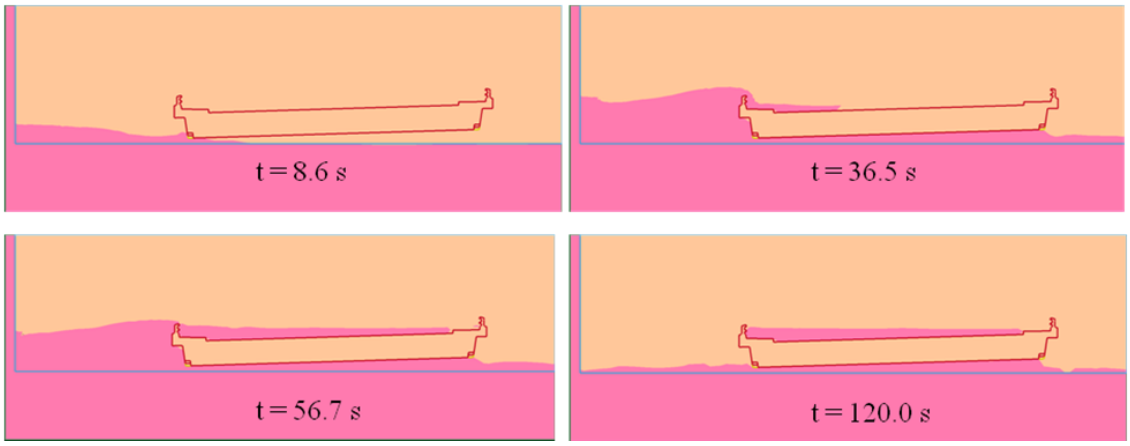

Figure 49 Captured of Schooner Creek Bridge (box-section) under GA M_w 9.0 tsunami scenario

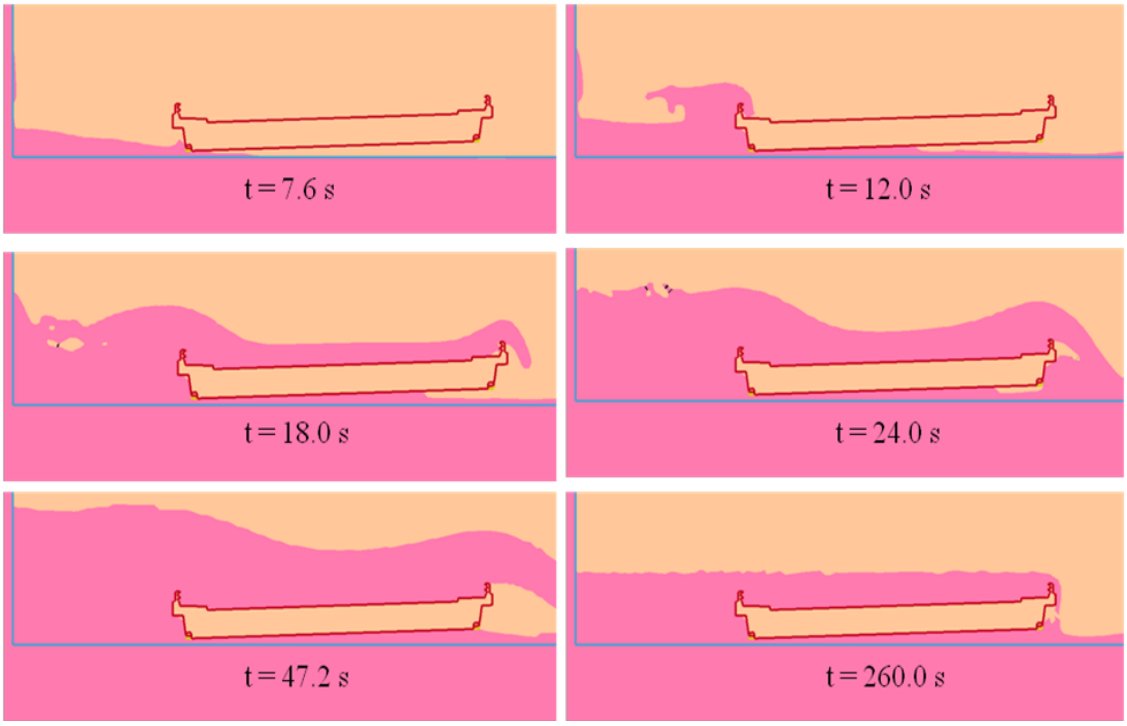

Figure 50 Captured of Schooner Creek Bridge (box-section) under LZ M_w 9.0 tsunami scenario

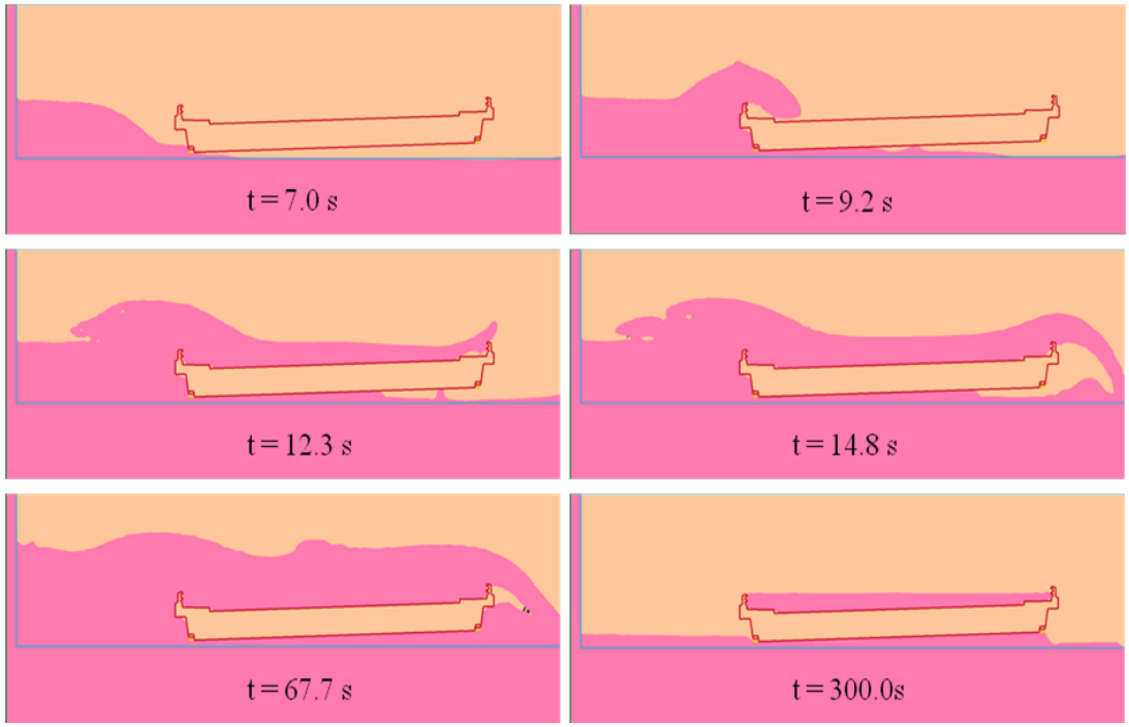

Figure 51 Captured of Schooner Creek Bridge (box-section) under MT M_w 9.0 tsunami scenario

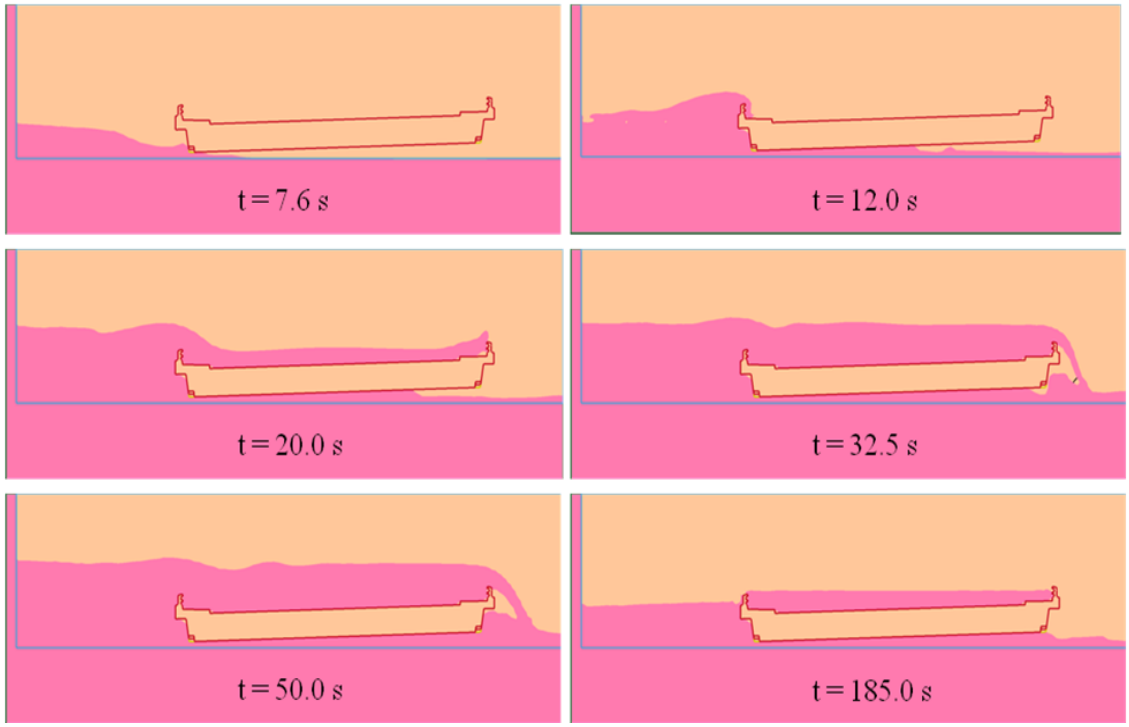

Figure 52 Captured of Schooner Creek Bridge (box-section) under TZ M_w 9.0 tsunami scenario

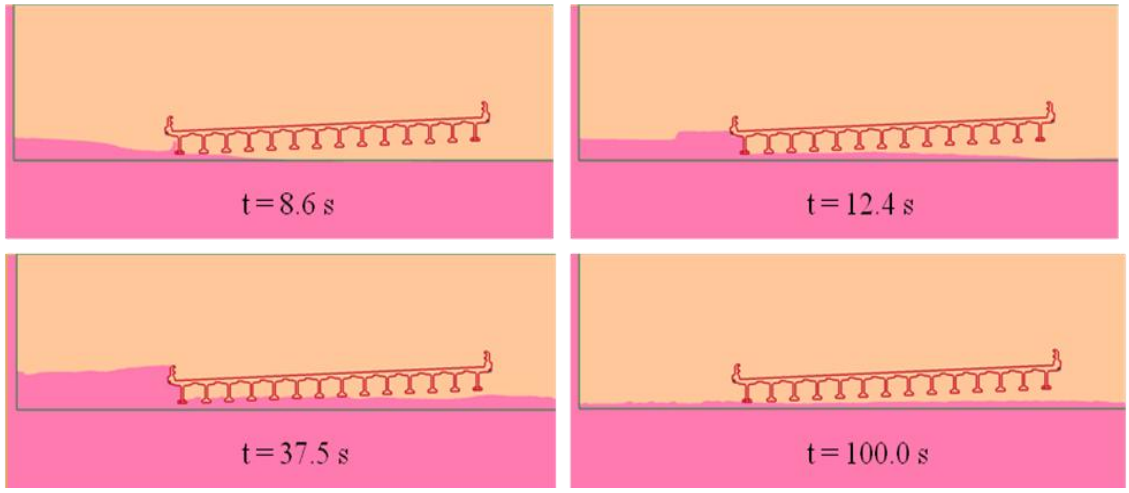

Figure 53 Captured of Schooner Creek Bridge (deck-girder) under GA M_w 9.0 tsunami scenario

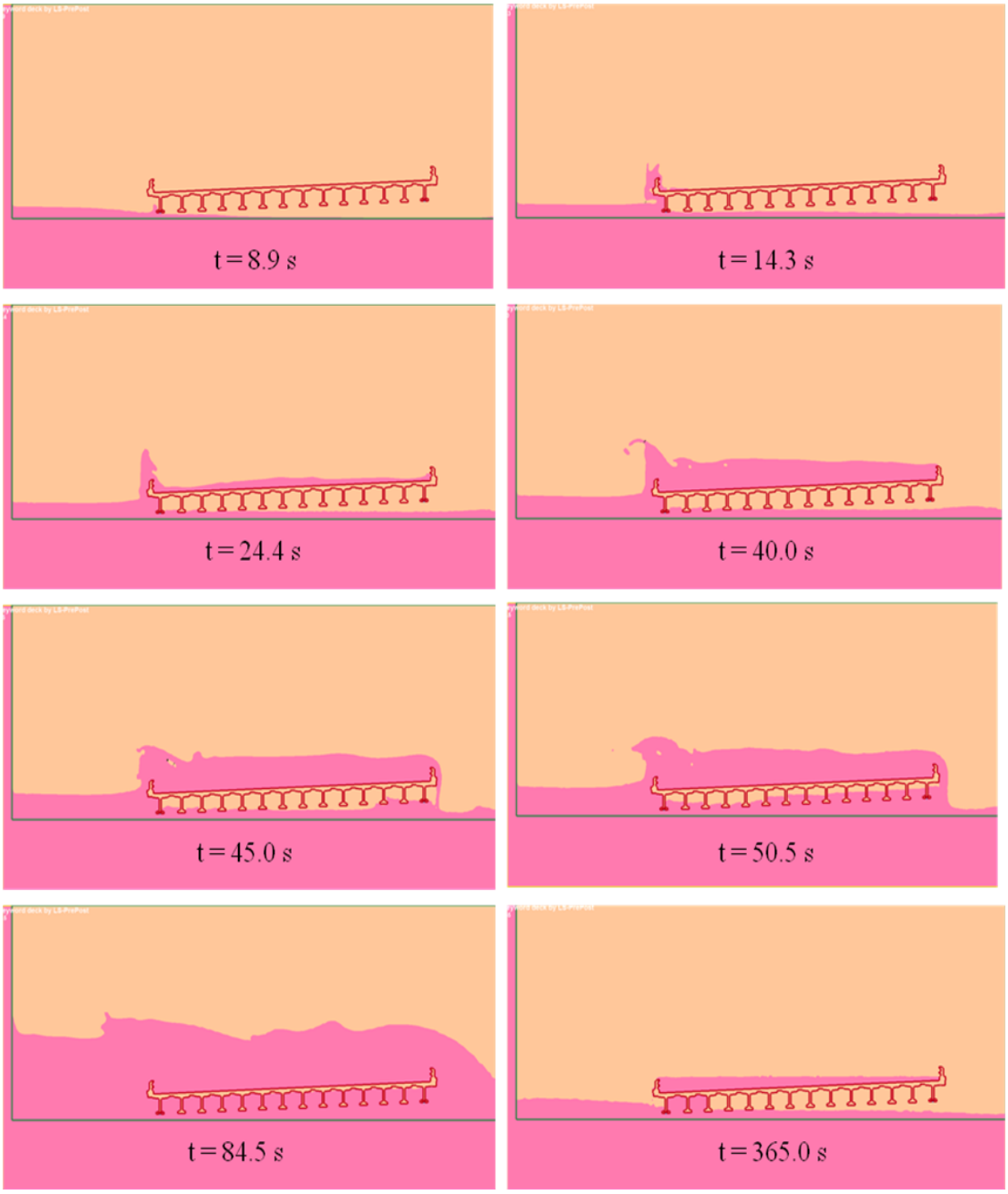

Figure 54 Captured of Schooner Creek Bridge (deck-girder) under GA M_w 9.2 tsunami scenario

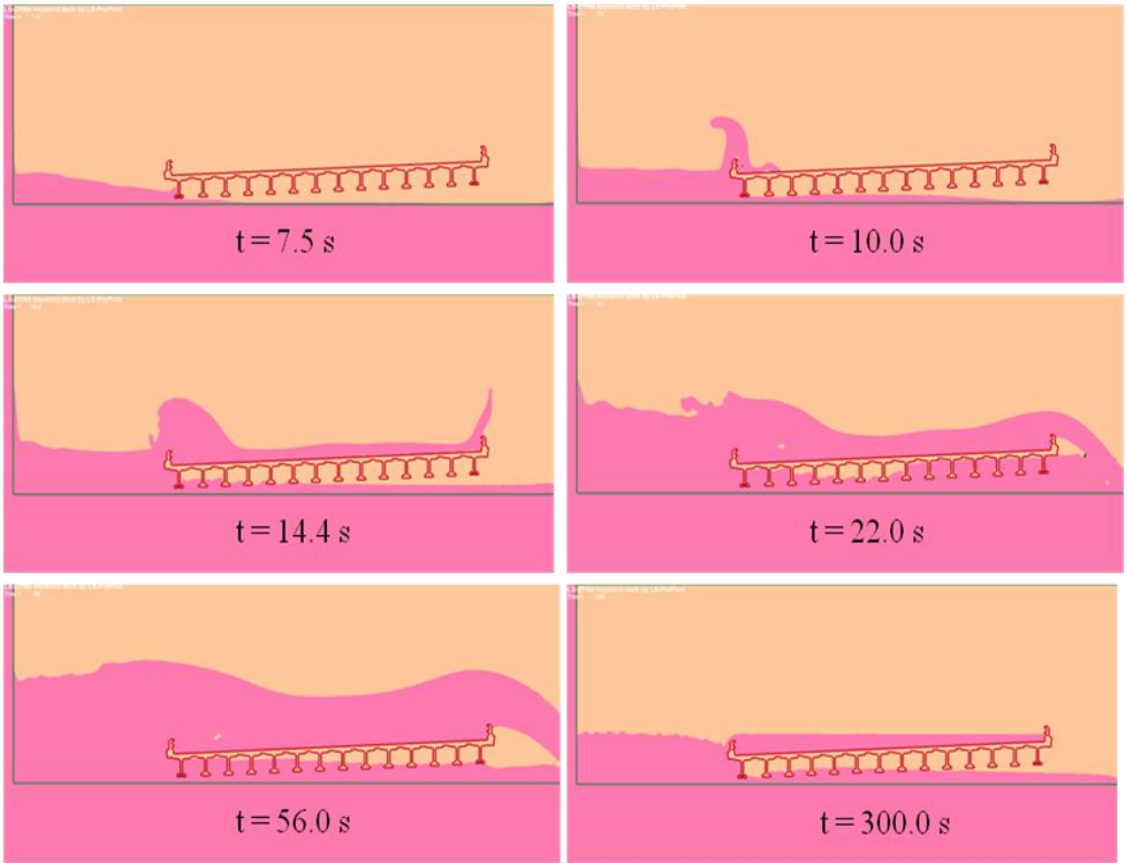

Figure 55 Captured of Schooner Creek Bridge (deck-girder) under LZ M_w 9.0 tsunami scenario

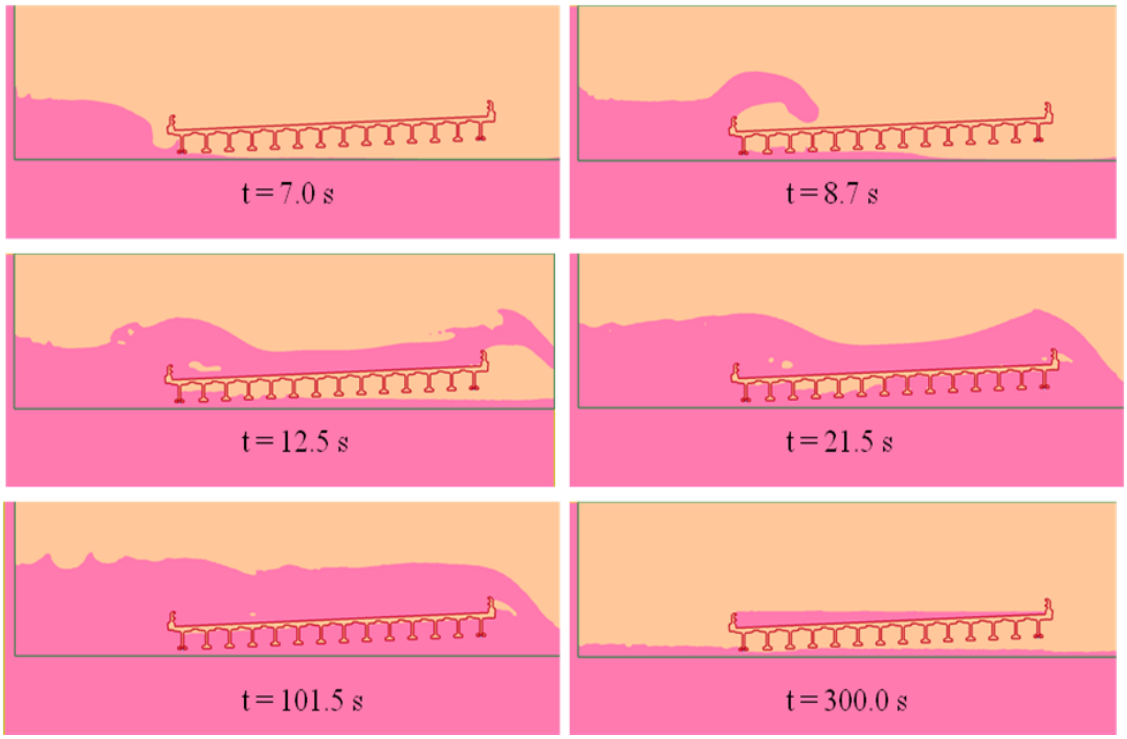

Figure 56 Captured of Schooner Creek Bridge (deck-girder) under MT M_w 9.0 tsunami scenario

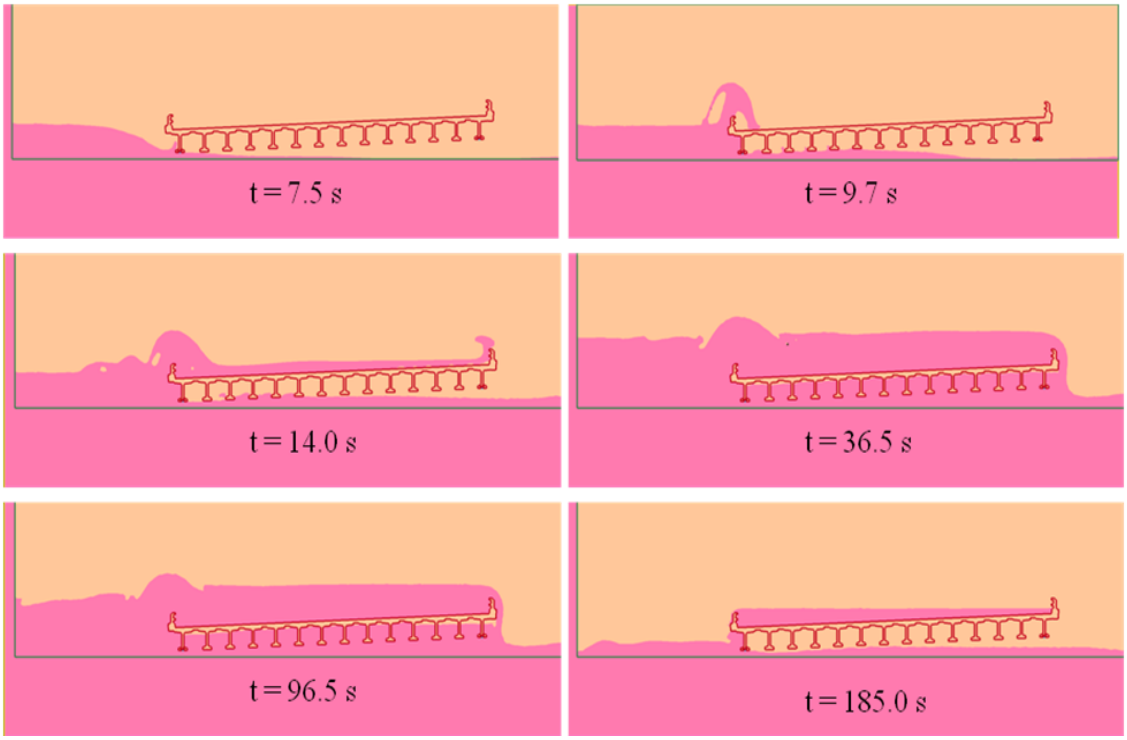

Figure 57 Captured of Schooner Creek Bridge (deck-girder) under TZ M_w 9.0 tsunami scenario

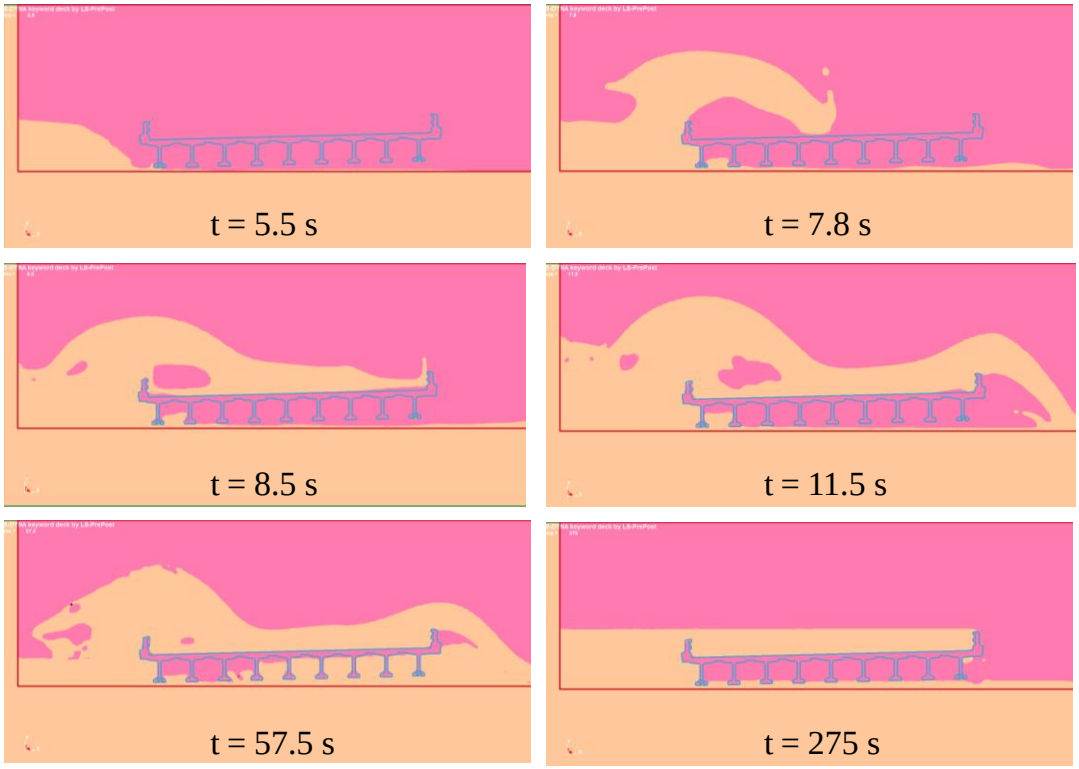

Figure 58 Captured of Drift Creek Bridge under GA M_w 9.2 tsunami scenario

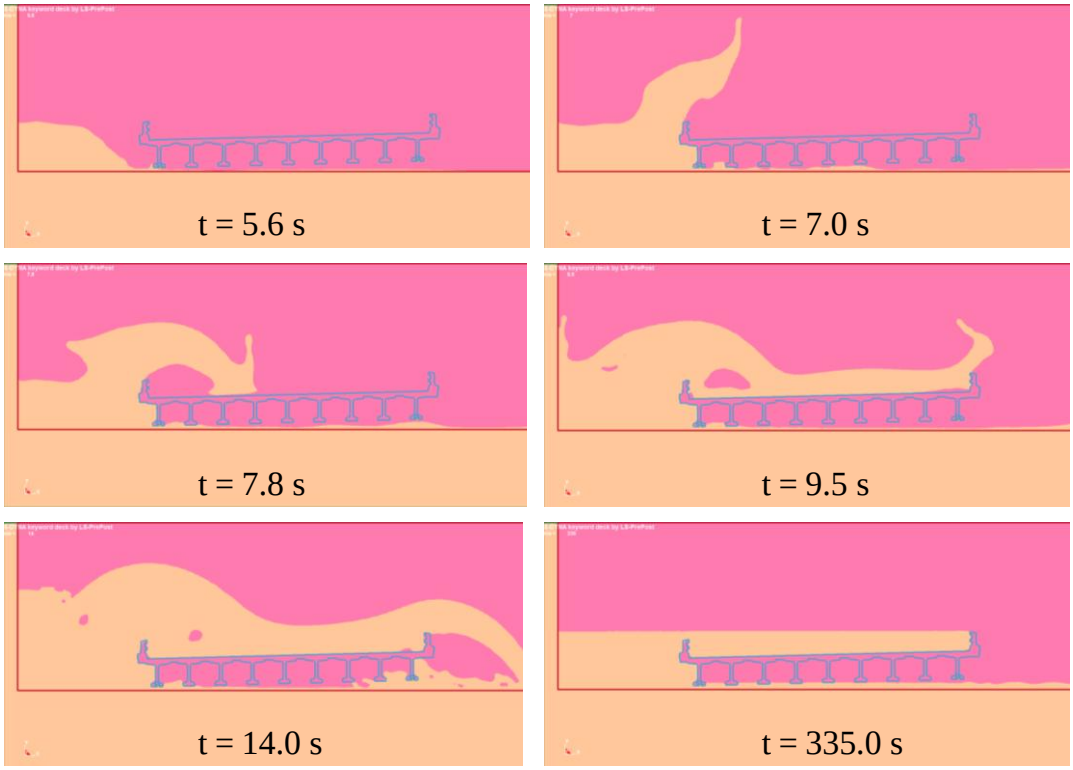

Figure 59 Captured of Drift Creek Bridge under LZ M_w 9.0 tsunami scenario

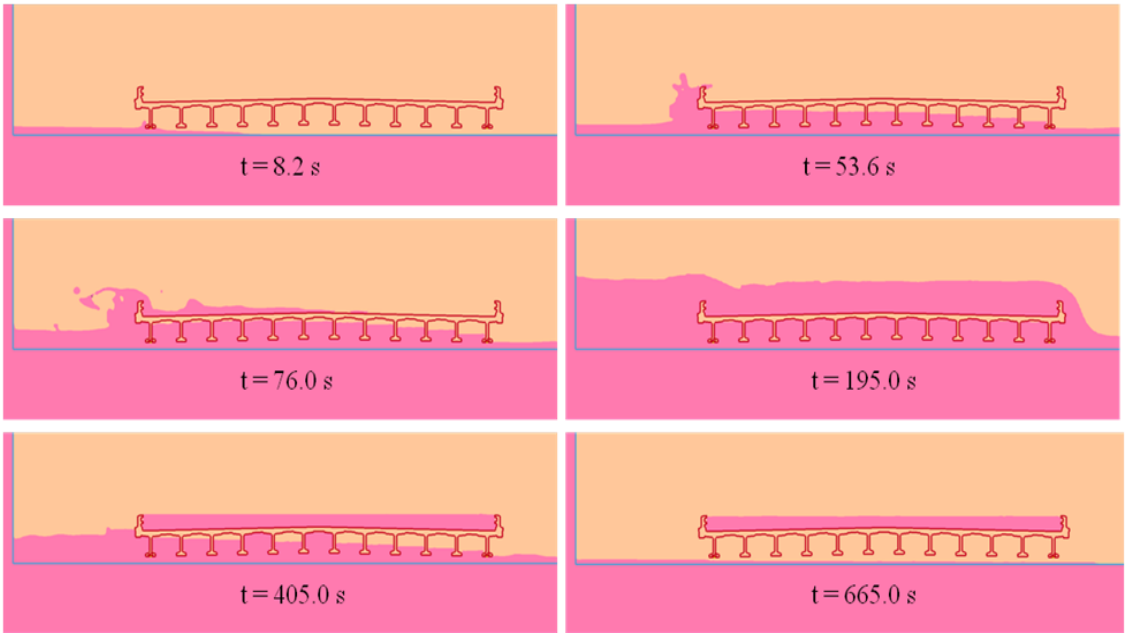

Figure 60 Captured of Millport Slough Bridge under GA M_w 9.2 tsunami scenario

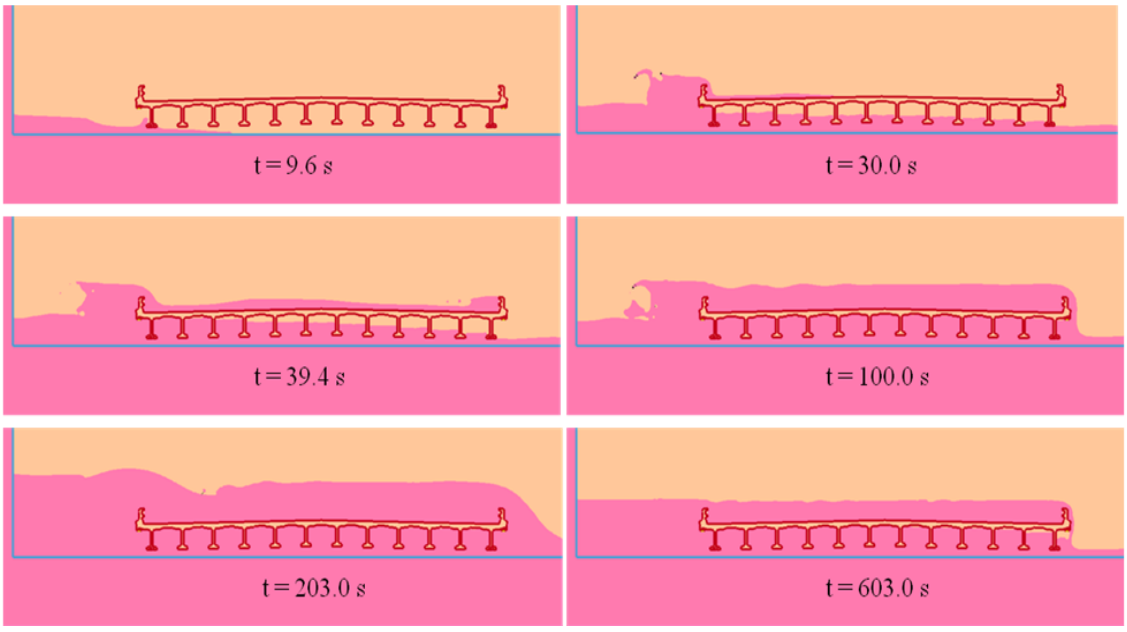

Figure 61 Captured of Millport Slough Bridge under LZ M_w 9.0 tsunami scenario

Appendix B Tsunami Time-History Forces of the Selected Bridge Superstructures

This section presents tsunami time-history results, horizontal and vertical forces time-histories, of the selected bridges under the selected tsunami scenarios. The time-history results of the Schooner Creek Bridge under five selected tsunami scenarios – GA M_w 9.0, GA M_w 9.2, LZ M_w 9.0, MT M_w 9.0, and TZ M_w 9.0 – are shown in Figure 62 to Figure 71. The time-history results of the Drift Creek Bridge and the Millport Slough Bridge under three selected tsunami scenarios – GA M_w 9.2, LZ M_w 9.0, and MT M_w 9.0 – are shown in Figure 75 to Figure 76.

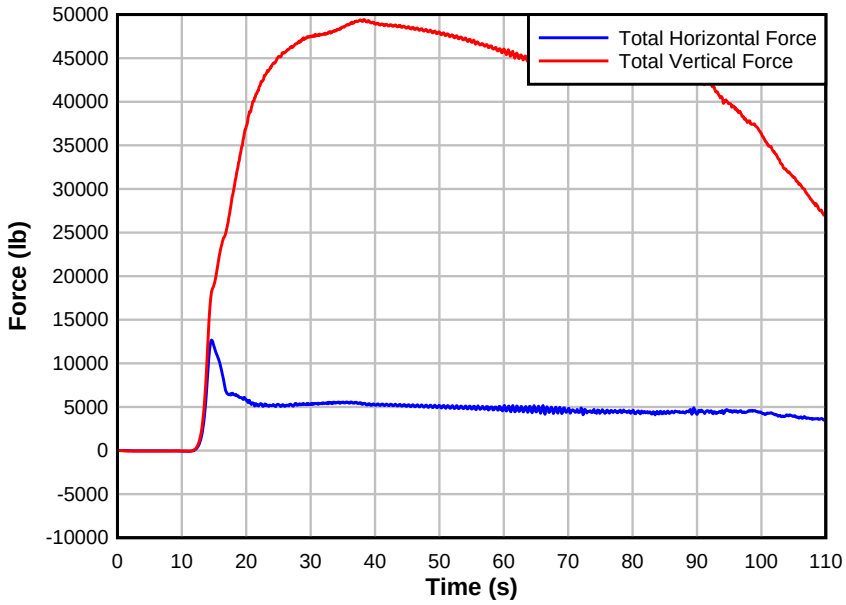

Figure 62 Time-history forces of Schooner Creek Bridge (box-section) under GA M_w 9.0 tsunami conditions

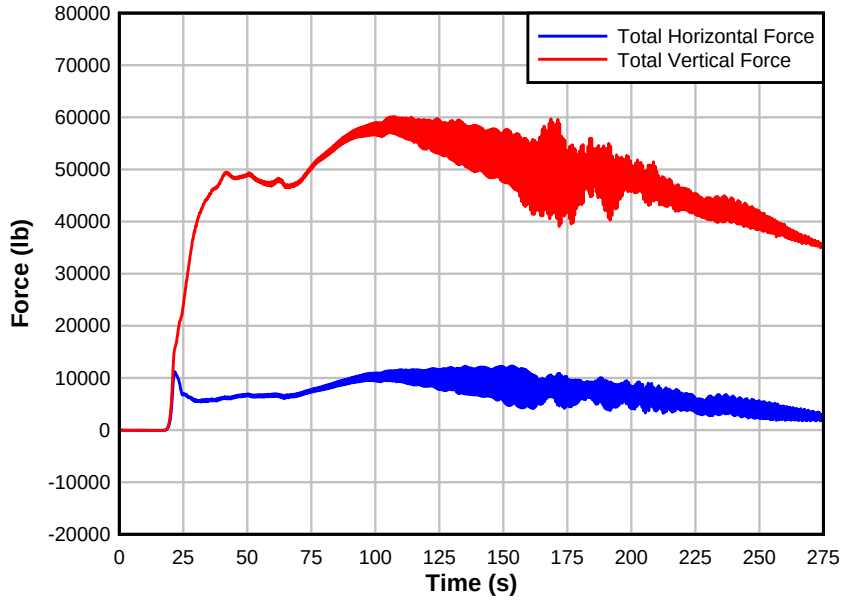

Figure 63 Time-history forces of Schooner Creek Bridge (box-section) under GA M_w 9.2 tsunami conditions

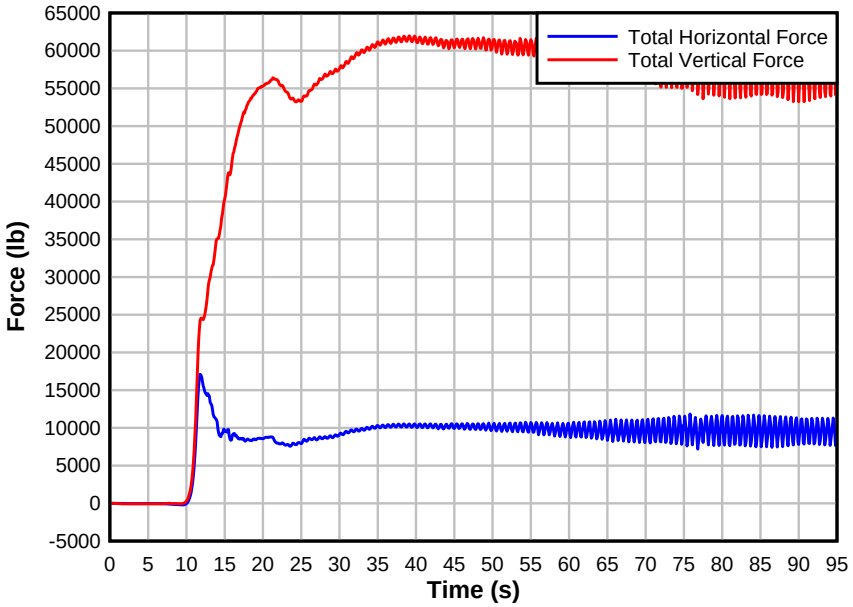

Figure 64 Time-history responses of Schooner Creek Bridge (box-section) under LZ M_w 9.0 tsunami conditions

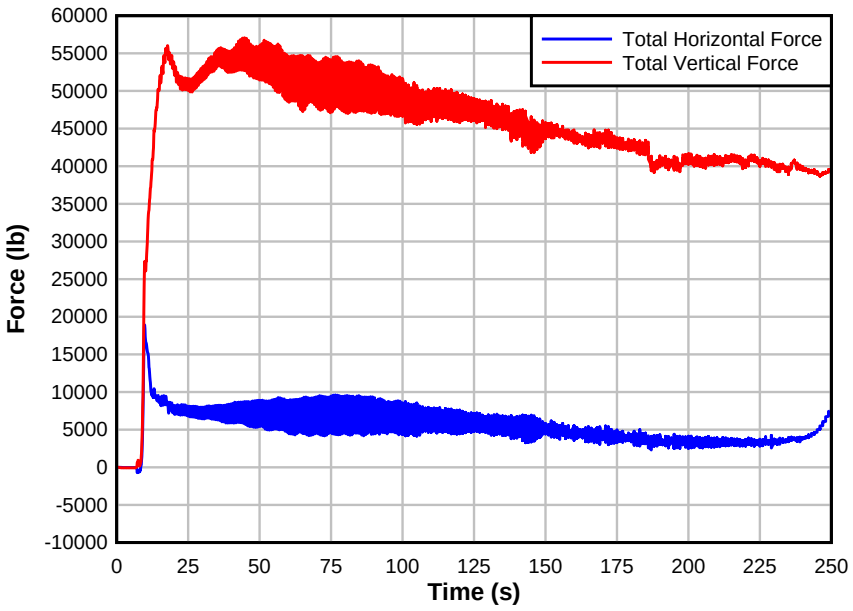

Figure 65 Time-history forces of Schooner Creek Bridge (box-section) under MT M_w 9.0 tsunami conditions

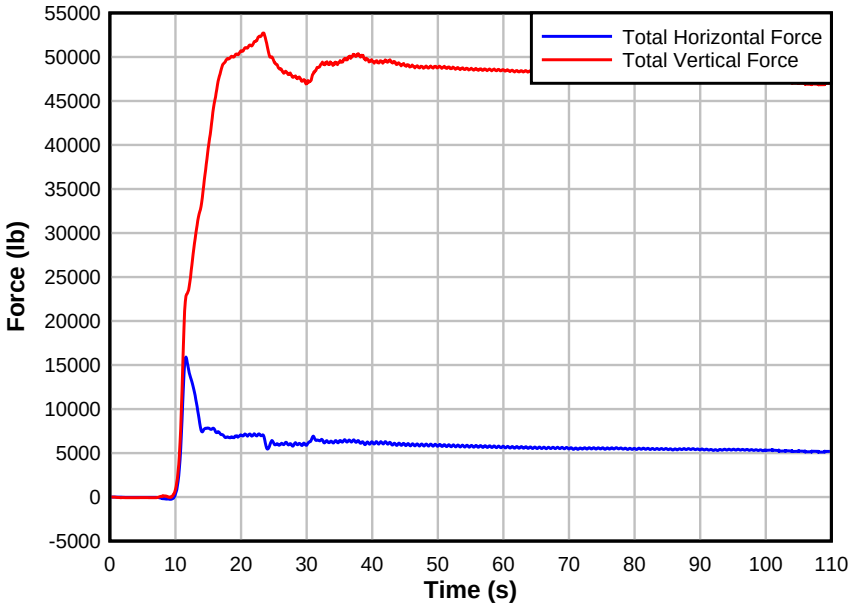

Figure 66 Time-history forces of Schooner Creek Bridge (box-section) under TZ M_w 9.0 tsunami conditions

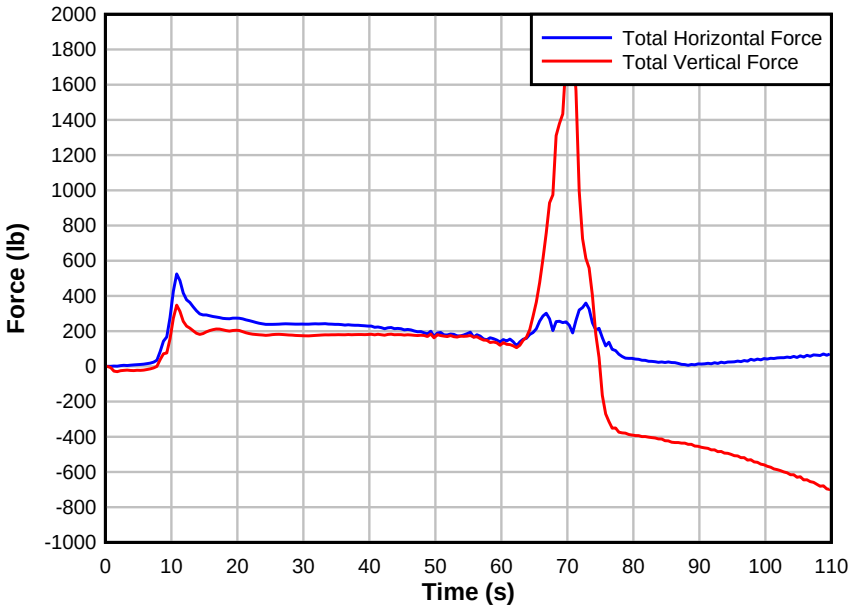

Figure 67 Time-history forces of Schooner Creek Bridge (deck-girder) under GA M_w 9.0 tsunami conditions

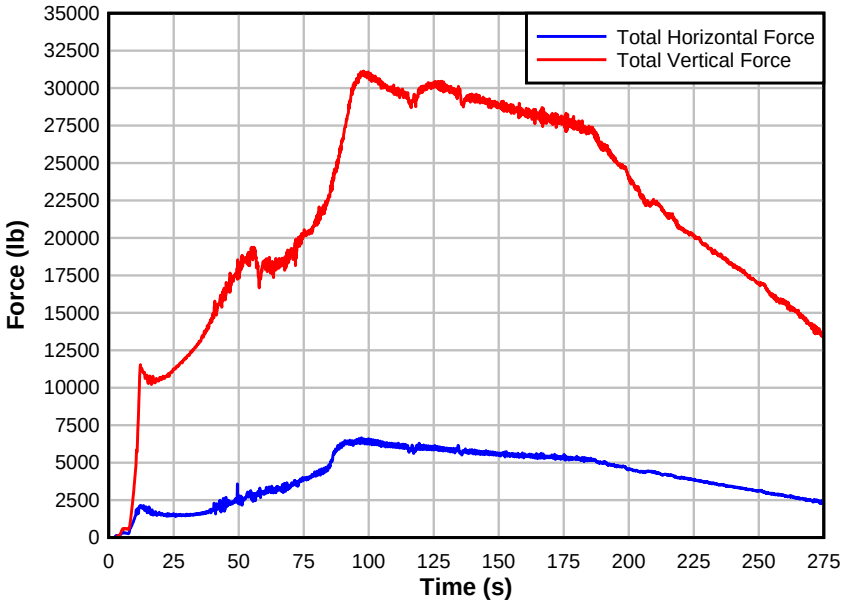

Figure 68 Time-history forces of Schooner Creek Bridge (deck-girder) under GA M_w 9.2 tsunami conditions

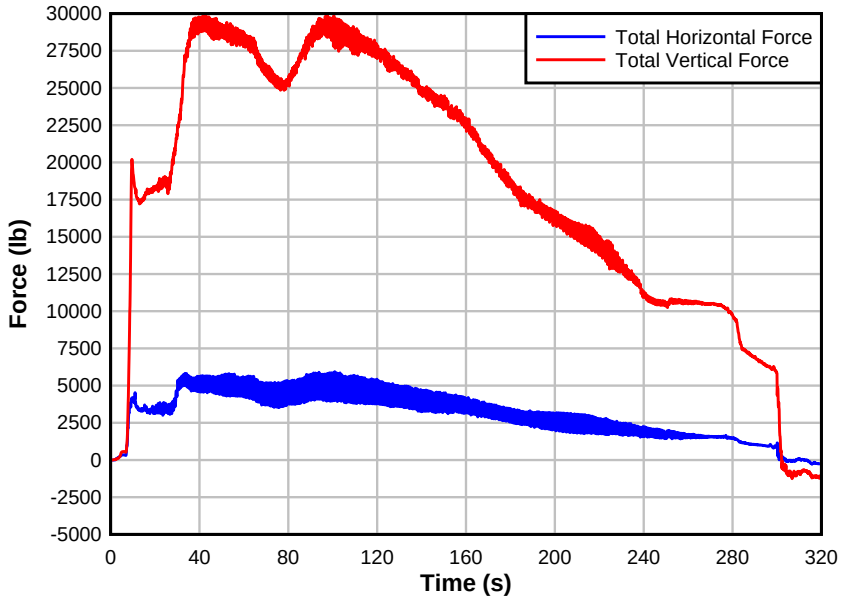

Figure 69 Time-history forces of Schooner Creek Bridge (deck-girder) under LZ M_w 9.0 tsunami conditions

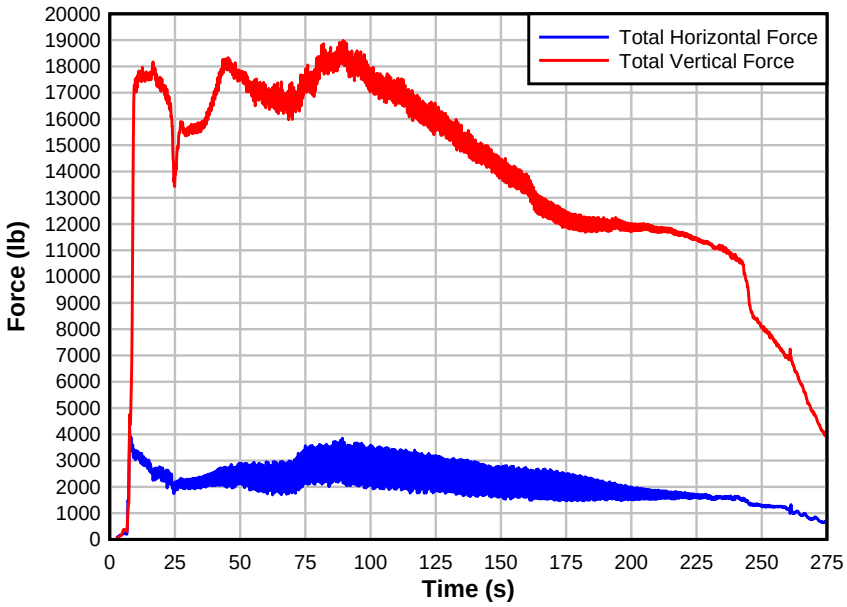

Figure 70 Time-history forces of Schooner Creek Bridge (deck-girder) under MT M_w 9.0 tsunami conditions

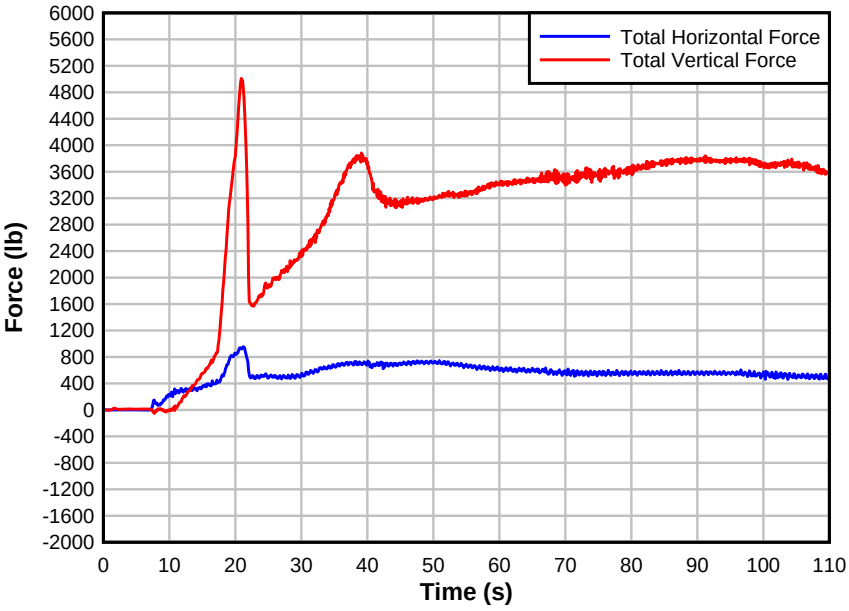

Figure 71 Time-history forces of Schooner Creek Bridge (deck-girder) under TZ M_w 9.0 tsunami conditions

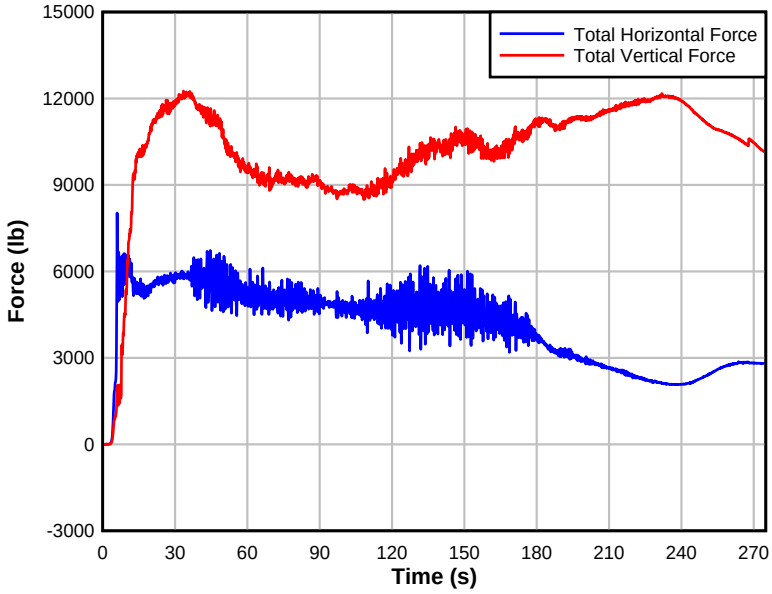

Figure 72 Time-history forces of Drift Creek Bridge under GA M_w 9.2 tsunami conditions

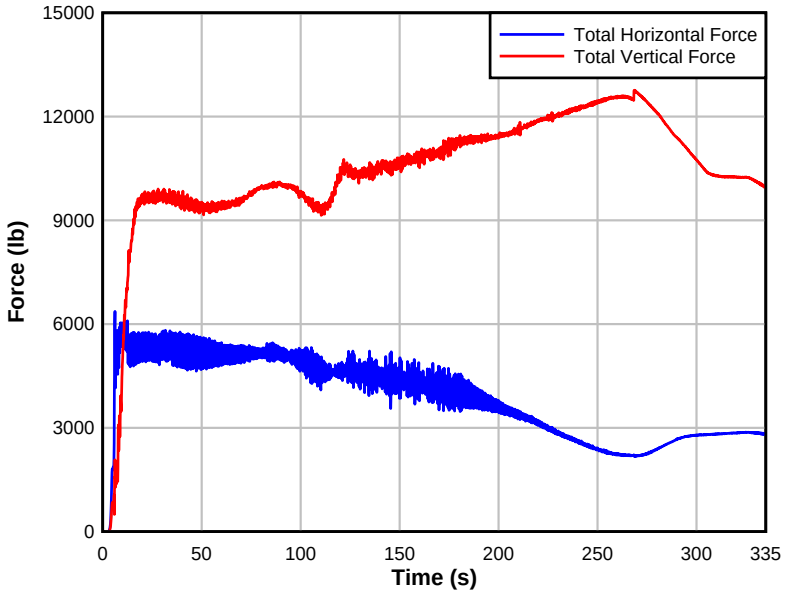

Figure 73 Time-history forces of Drift Creek Bridge under LZ M_w 9.0 tsunami conditions

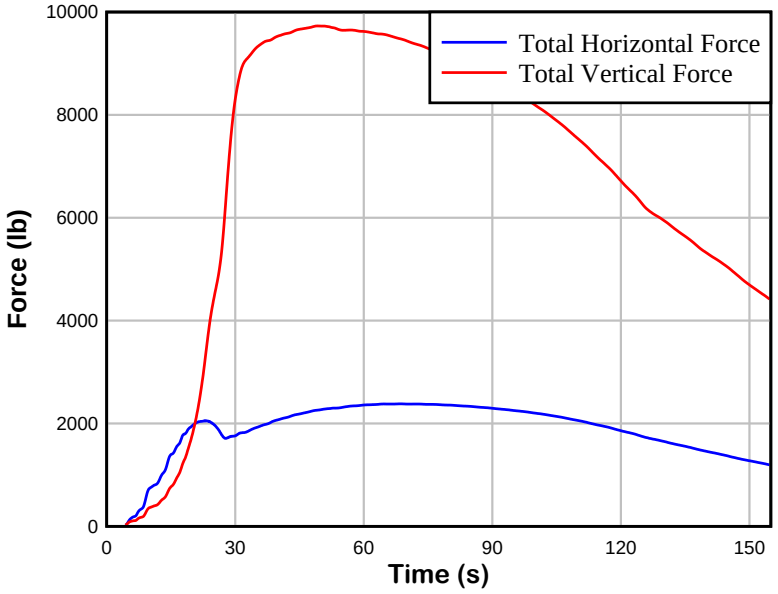

Figure 74 Time-history forces of Drift Creek Bridge under MT M_w 9.0 tsunami conditions

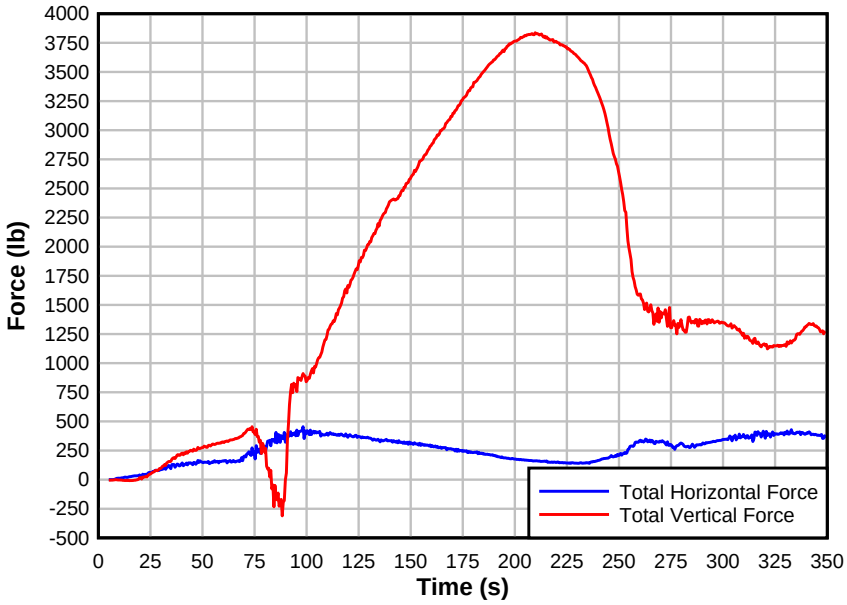

Figure 75 Time-history forces of Millport Slough Bridge under GA M_w 9.2 tsunami conditions

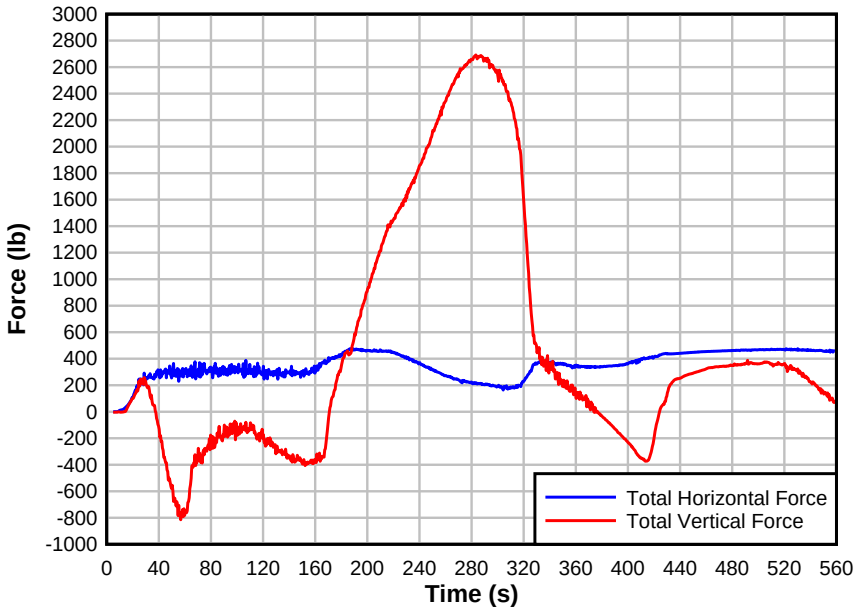

Figure 76 Time-history forces of Millport Slough Bridge under LZ M_w 9.0 tsunami conditions

Appendix C Example Calculations of Tsunami forces on Bridge Superstructure

This section shows example of tsunami forces calculations by using the existing method mentioned earlier in the paper. The example calculations are based on the deck-girder section at Schooner Creek Bridge under the tsunami loads generated by the GA rupture configuration at moment magnitude 9.2.

The bridge deck cross-section properties are given here as follows: underside of bridge deck elevation = 264 in.; underside of girder elevation = 216 in.; elevation of c.g. of the cross-section = 250 in.; number of girders = 14; subjected area normal to horizontal force (Ah) = 93.5 in^2; subjected area normal to vertical force (Av) = 903 in^2; bridge deck volume = 8970 in^3. The subjected areas and volume of bridge deck are based on one inch thickness of bridge cross-sectional. The required tsunami condition data is also provided here as follows: unit weight of water = 62 lb/ft^3; maximum water surface elevation = 498.4 in.; maximum horizontal velocity of water = 169.45 in/s^2; maximum vertical velocity of water = 6.71 in/s^2; maximum water acceleration = 1.33 in/s^2; maximum flux momentum (hu^2, $_{max}$) = 7418.2 x 10^3 in^3/s^2.

Given :

Bridge Properties

$h_{br} := 216in$ $N := 14$ $b := 1in$

$A_v := 903in^2$ $A_h := 93.5in^2$ $V := 8970in^3$

Tsunami Conditions

$h_{max} := 498.4in$ $u_x := 169.45\frac{in}{s}$ $u_v := 6.71\frac{in}{s}$

$a_{max} := 1.33\frac{in}{s^2}$ $flux_{max} := 7418.2\cdot 10^3\frac{in^3}{s^2}$

General Condtions

$g := 386\frac{in}{s^2}$ $\gamma_w := 62\frac{lb}{ft^3}$ $\gamma_s := 1.2\cdot\gamma_w = 74.4\frac{lb}{ft^3}$

$\rho_s := 1.2\cdot\frac{\gamma_w}{g} = 2.313\frac{lb\cdot s^2}{ft^4}$

1. Douglass et al. (2006)'s method for estimating wave forces on bridge decks

$C_r := 0.4$ $C_{h.va} := 1$ $C_{h.im} := 6$

$C_{v.va} := 1$ $C_{v.im} := 3$

$\Delta z := h_{max} - h_{br} = 23.533\,ft$

$$F_{H.Douglass} := \left[\left[1 + C_r \cdot (N - 1)\right] \cdot C_{h.va} + C_{h.im}\right] \cdot \gamma_s \cdot \Delta z \cdot A_h = 1.387 \times 10^4\,lb$$

$$F_{V.Douglass} := \left(C_{v.va} + C_{v.im}\right) \cdot \gamma_s \cdot \Delta z \cdot A_v = 4.392 \times 10^4\,lb$$

2. FEMA P646 (2008), Guidelines for Design of Structures for Vertical Evacuation from Tsunamis

$C_d := 2$ $C_u := 3$

Hydrostatic Force: $F_{hs} := \gamma_s \cdot \Delta z \cdot A_h = 1.137 \times 10^3\,lb$

Hydrodynami Force: $F_d := 0.5 \rho_s \cdot C_d \cdot b \cdot flux_{max} = 827.447\,lb$

Impulsive Force: $F_i := 1.5 F_d = 1.241 \times 10^3\,lb$

$$F_{H.FEMA} := F_{hs} + F_d + F_i = 3.205 \times 10^3\,lb$$

Buoyant Force: $F_b := \gamma_s \cdot V = 386.208\,lb$

Uplift Force: $F_u := 0.5 C_u \cdot \rho_s \cdot A_v \cdot u_v^2 = 6.802\,lb$

$$F_{V.FEMA} := F_b + F_u = 393.011\,lb$$

3. Performance-Based Tsunami Engineering (PBTE): Tsunami bore on vertical wall and slab

Bridge Longitudinal Span Length: $L := 297.083\,ft$

Width to inundation depth ratio: $R := \frac{L}{\Delta z} = 12.624$

$$C_{d.PBTE} := \begin{cases} 1.25 \text{ if } 1 < R < 12 \\ 1.3 \text{ if } 12 < R < 20 \end{cases} = 1.3$$

Hydrodynamic Force: $F_{d.PBTE} := 0.5\,\rho_s \cdot C_{d.PBTE} \cdot b \cdot \Delta z \cdot u_x^2 = 587.899\,lb$

Hydrostatic Force: $F_{hs.PBTE} := 0.5\,\rho_s \cdot g \cdot b \cdot \Delta z^2 = 1.717 \times 10^3\,lb$

$$F_{H.PBTE} := F_{d.PBTE} + F_{hs.PBTE} = 2.305 \times 10^3\,lb$$

$$\beta := \frac{\Delta z}{h_{max}} = 0.567$$

$$C_{u.PBTE} := \begin{cases} \beta \cdot \frac{3}{0.5} \text{ if } \beta < 0.5 \\ 3 \text{ if } 0.5 < \beta < 1.5 \end{cases} = 3$$

Buoyant Force: $F_{b.PBTE} := \gamma_s \cdot V = 386.208\,lb$

Uplift Force: $F_{u.PBTE} := 0.5\,C_{u.PBTE}\,\rho_s \cdot u_x^2 \cdot A_v = 4.338 \times 10^3\,lb$

$$F_{V.PBTE} := F_{b.PBTE} + F_{u.PBTE} = 4.724 \times 10^3\,lb$$

4. The Recommended Approch for estimating tsunami forces on bridge superstructures

$C_{d.recommend} := 1$

Hydrostatic Force: $F_{hs.recommend} := \left[1 + C_r \cdot (N - 1)\right] \cdot \gamma_s \cdot \Delta z \cdot A_h = 7.049 \times 10^3 \, lb$

Hydrodynamic Force: $F_{d.recommend} := 0.5 C_{d.recommend} \cdot \rho_s \cdot b \cdot flux_{max} = 413.724 \, lb$

$F_{H.recommended} := F_{hs.recommend} + F_{d.recommend} = 7.462 \times 10^3 \, lb$

$u_{x.out} := 3.5 u_x = 49.423 \frac{ft}{s}$

Buoyant Force: $F_{b.recommend} := \gamma_s \cdot \Delta z \cdot A_v = 1.098 \times 10^4 \, lb$

Uplift Force: $F_{u.recommend} := 0.5 \rho_s \cdot u_{x.out}^2 \cdot A_v = 1.771 \times 10^4 \, lb$

$F_{V.recommend} := F_{b.recommend} + F_{u.recommend} = 2.869 \times 10^4 \, lb$

Appendix D A case study of the Spencer Creek Bridge, Oregon – revisited:

As mentioned earlier, this research is an extension of the case study of the Spencer Creek Bridge conducted by Nimmala et al. (2006). Differ from the selected bridges in this research, the Spencer Creek Bridge is located at a different area on the Oregon Coast subjected to different tsunami load pattern. Since the bridge location is open to the Pacific, the tsunamis quickly travel across the bridge without trapping water as presented in the Siletz Bay area. Other than the bridge location and tsunami pattern, the cross-section of the Spencer Creek Bridge is quite unique. The bridge superstructure consists of deck with crossbeam supporting the deck, and arch structure as shown in Figure 77 and Figure 78

.

Figure 77 Model of Spencer Creek Bridge [ref: ftp://ftp.wsdot.wa.gov/public/Bridge/WBES2007]

Figure 78 Spencer Creek Bridge [ref: http://bridgehunter.com/photos/]

The tsunami sources for numerical models of the Spencer Creek Bridge were provided by Professor Cheung and associate from University of Hawaii. The provided tsunami data were obtained from two different numerical models, Cornell model and FVWAVE model. Nimmal et al. (2006) performed finite-element based numerical models of tsunami impact on the Spencer Creek Bridge under provided tsunami conditions from both Cornell and FVWAVE models. The numerical results by Nimmala et al. (2006) are shown in Figure 79 and Figure 80. These results are revisited in this research to help in studying the application of the recommended formulation, provided in section 5 in the manuscript, to a bridge superstructure with different geometry.

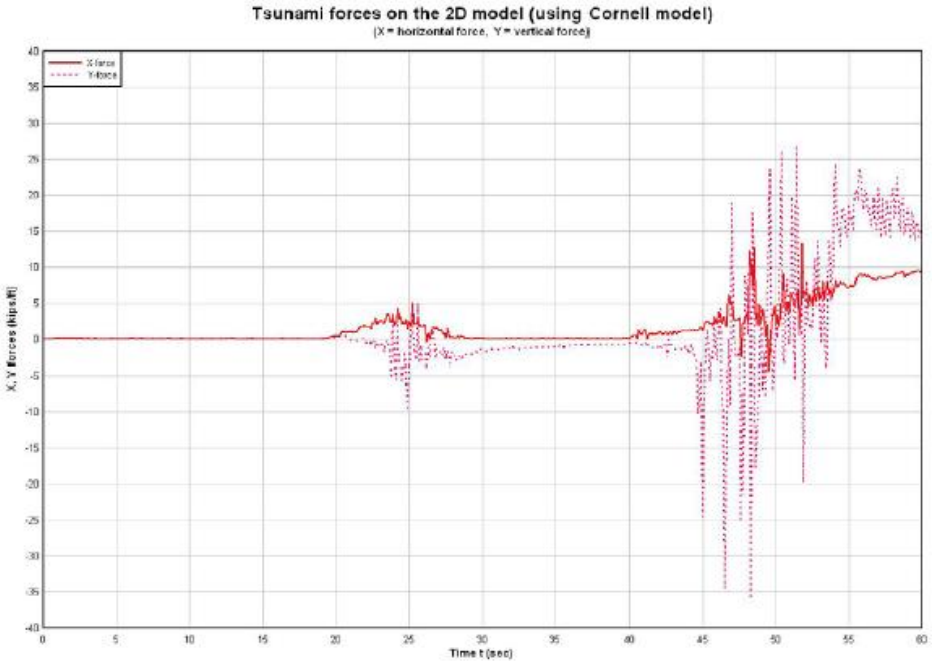

Figure 79 Horizontal and vertical force time-histories based on Cornell tsunami model

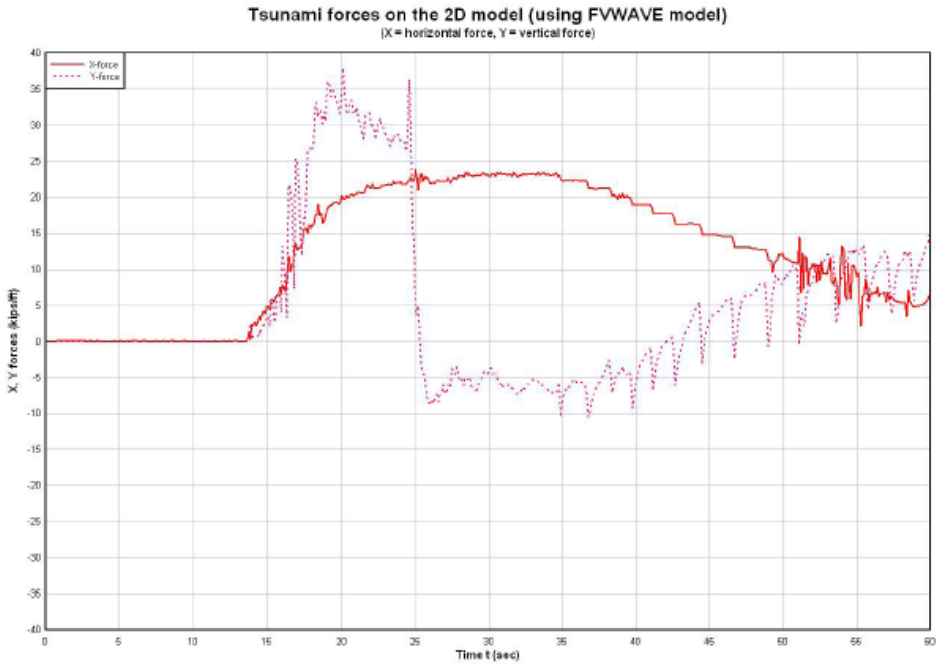

Figure 80 Horizontal and vertical force time-histories based on FVWAVE tsunami model

An example calculation of tsunami forces on deck of the Spencer Creek Bridge is described in this section. In this case, the bridge superstructure consists of deck and crossbeam without girder. Therefore, the term that accounting for distributing forces on the internal girders must be canceled; or, the bridge superstructure can be thought of bridge deck with single girder (N =1).

Given :

Bridge Properties

$h_{br} := 50ft$ $N := 1$ $b := 3in$

$A_v := 1920in^2$ $A_h := 215.76in^2$ $V := 124800in^3$

Tsunami Conditions

$h_{max} := 669.2in$ $u_x := 321.0\frac{in}{s}$ $u_v := 16.6\frac{in}{s}$

$a_{max} := 844.2\frac{in}{s^2}$ $flux_{max} := 639510^3\frac{in^3}{s^2}$

General Condtions

$g := 386\frac{in}{s^2}$ $\gamma_w := 62\frac{lb}{ft^3}$ $\gamma_s := 1.2\gamma_w = 74.4\frac{lb}{ft^3}$

$\rho_s := 1.2\frac{\gamma_w}{g} = 2.313\frac{lb\cdot s^2}{ft^4}$

1. Douglass et al. (2006)'s method for estimating wave forces on bridge decks

$C_r := 0.4$ $C_{h.va} := 1$ $C_{h.im} := 6$

$C_{v.va} := 1$ $C_{v.im} := 3$

$\Delta z := h_{max} - h_{br} = 5.767\,ft$

$$F_{H.Douglass} := \left[\left[1 + C_r \cdot (N-1)\right] \cdot C_{h.va} + C_{h.im}\right] \cdot \gamma_s \cdot \Delta z \cdot \frac{A_h}{b} = 1.8 \times 10^4 \frac{lb}{ft}$$

$$F_{V.Douglass} := \left(C_{v.va} + C_{v.im}\right) \cdot \gamma_s \cdot \Delta z \cdot \frac{A_v}{b} = 9.153 \times 10^4 \frac{lb}{ft}$$

2. FEMA P646 (2008), Guidelines for Design of Structures for Vertical Evacuati from Tsunamis

$C_d := 2$ $C_u := 3$

Hydrostatic Force: $F_{hs} := \gamma_s \cdot \Delta z \cdot A_h = 642.845\,lb$

Hydrodynami Force: $F_d := 0.5 \rho_s \cdot C_d \cdot b \cdot flux_{max} = 2.14 \times 10^3\,lb$

Impulsive Force: $F_i := 1.5 F_d = 3.21 \times 10^3\,lb$

$$F_{H.FEMA} := \frac{\left(F_{hs} + F_d + F_i\right)}{b} = 2.397 \times 10^4 \frac{lb}{ft}$$

Buoyant Force: $F_b := \gamma_s \cdot V = 5.373 \times 10^3\,lb$

Uplift Force: $F_u := 0.5 C_u \cdot \rho_s \cdot A_v \cdot u_v^{\,2} = 88.522\,lb$

$$F_{V.FEMA} := \frac{\left(F_b + F_u\right)}{b} = 2.185 \times 10^4 \frac{lb}{ft}$$

3. Performance-Based Tsunami Engineering (PBTE): Tsunami bore on vertical wall and slab

Bridge Longitudinal Span Length: $L := 210\,ft$

Width to inundation depth ratio: $R := \frac{L}{\Delta z} = 36.416$

$$C_{d.PBTE} := \begin{cases} 1.25 \text{ if } 1 < R < 12 \\ 1.3 \text{ if } 12 < R < 20 \\ 1.4 \text{ if } 20 < R < 32 \\ 1.5 \text{ if } 32 < R < 40 \\ 1.75 \text{ if } 40 < R < 80 \\ 1.8 \text{ if } 80 < R < 120 \\ 2.0 \text{ if } R > 120 \end{cases} = 1.5$$

Hydrodynamic Force: $F_{d.PBTE} := 0.5\rho_s \cdot C_{d.PBTE} b \cdot \Delta z \cdot u_x^2 = 1.79 \times 10^3\,lb$

Hydrostatic Force: $F_{hs.PBTE} := 0.5\rho_s \cdot g \cdot b \cdot \Delta z^2 = 309.266\,lb$

$$F_{H.PBTE} := \frac{\left(F_{d.PBTE} + F_{hs.PBTE}\right)}{b} = 8.395 \times 10^3\,\frac{lb}{ft}$$

$$\beta := \frac{\Delta z}{h_{max}} = 0.103$$

$$C_{u.PBTE} := \begin{cases} \beta \cdot \frac{3}{0.5} \text{ if } \beta < 0.5 \\ 3 \text{ if } 0.5 < \beta < 1.5 \end{cases} = 0.62$$

Buoyant Force: $F_{b.PBTE} := \gamma_s \cdot V = 5.373 \times 10^3\,lb$

Uplift Force: $F_{u.PBTE} := 0.5 C_{u.PBTE} \rho_s \cdot u_x^2 \cdot A_v = 6.846 \times 10^3\,lb$

$$F_{V.PBTE} := \frac{\left(F_{b.PBTE} + F_{u.PBTE}\right)}{b} = 4.888 \times 10^4\,\frac{lb}{ft}$$

4. The Recommended Approch for estimating tsunami forces on bridge superstructures

$C_{d.recommend} := 3.5$

Hydrostatic Force: $F_{hs.recommend} := \left[1 + C_r \cdot (N - 1)\right] \cdot \gamma_s \cdot \Delta z \cdot A_h = 642.845\,lb$

Hydrodynamic Force: $F_{d.recommend} := 0.5\, C_{d.recommend} \cdot \rho_s \cdot b \cdot flux_{max} = 3.745 \times 10^3\,lb$

$$F_{H.recommended} := \frac{\left(F_{hs.recommend} + F_{d.recommend}\right)}{b} = 1.755 \times 10^4\,\frac{lb}{ft}$$

$u_{x.out} := 1.0\, u_x = 26.75\,\frac{ft}{s}$

Buoyant Force: $F_{b.recommend} := \gamma_s \cdot \Delta z \cdot A_v = 5.721 \times 10^3\,lb$

Uplift Force: $F_{u.recommend} := 0.5\, \rho_s \cdot u_{x.out}^2 \cdot A_v = 1.103 \times 10^4\,lb$

$$F_{V.recommend} := \frac{\left(F_{b.recommend} + F_{u.recommend}\right)}{b} = 6.702 \times 10^4\,\frac{lb}{ft}$$

Appendix E Drawing of the Selected Bridges

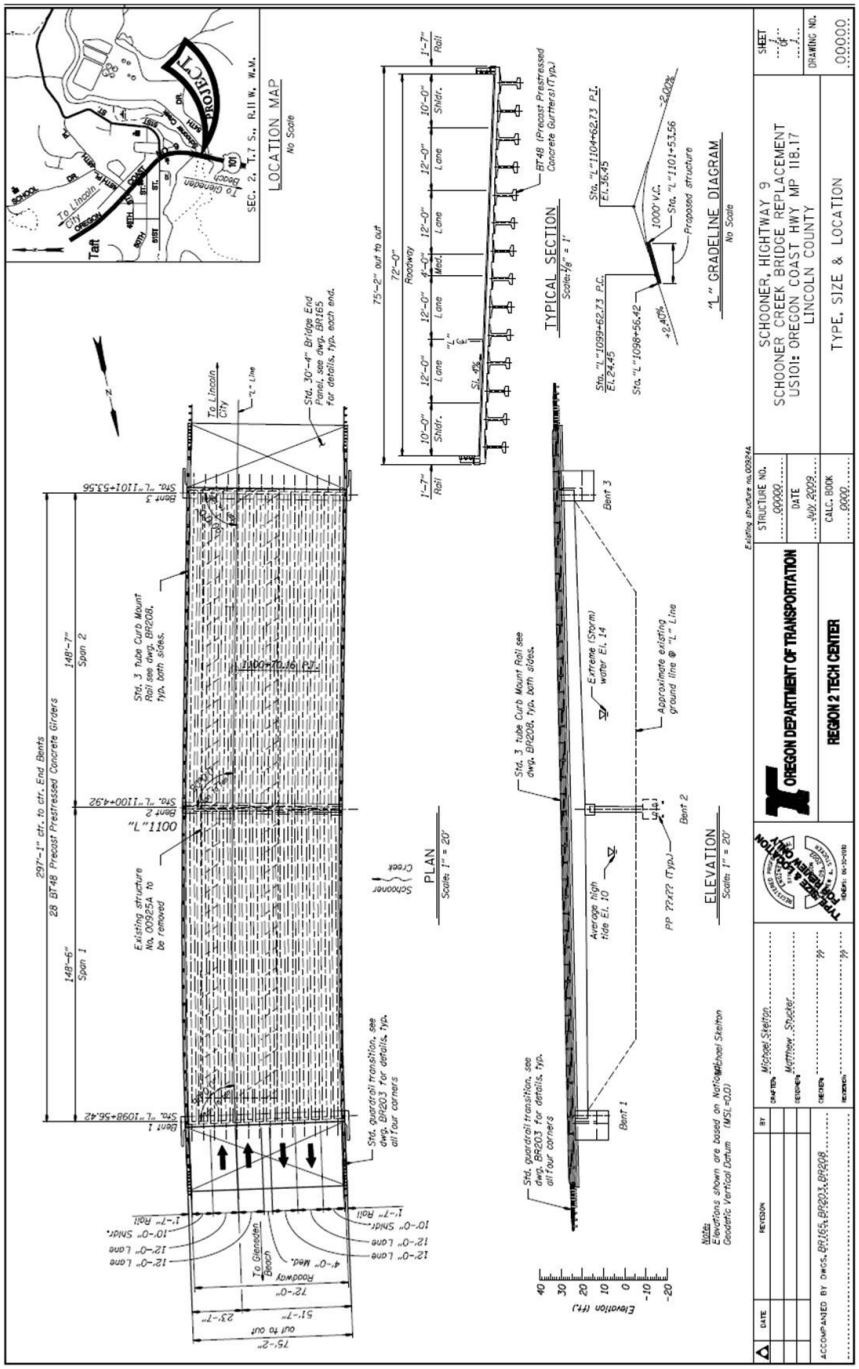

Figure 81 Preliminary drawing of Schooner Creek Bridge (deck-girder)

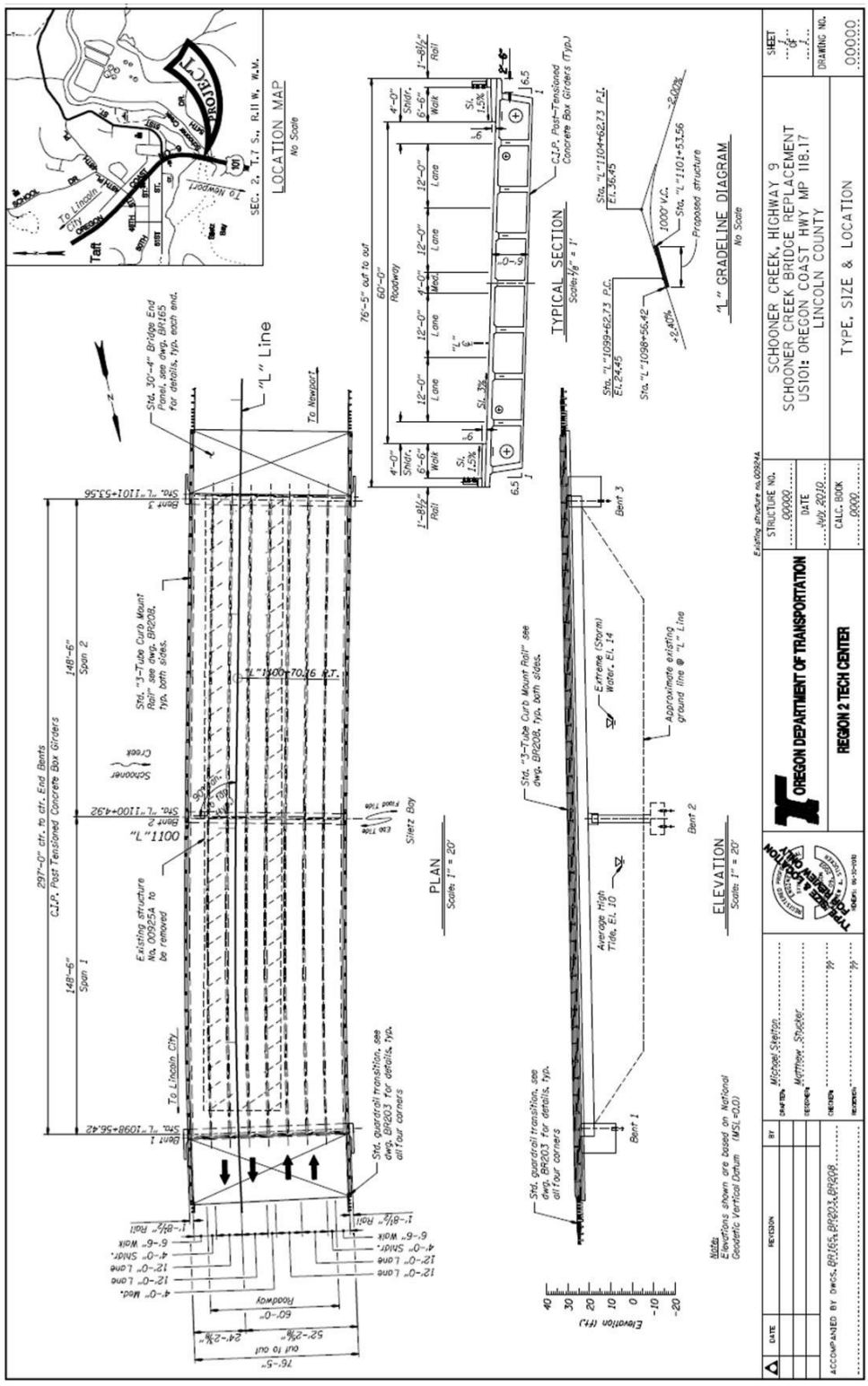

Figure 82 Preliminary drawing of Schooner Creek Bridge (box-section)

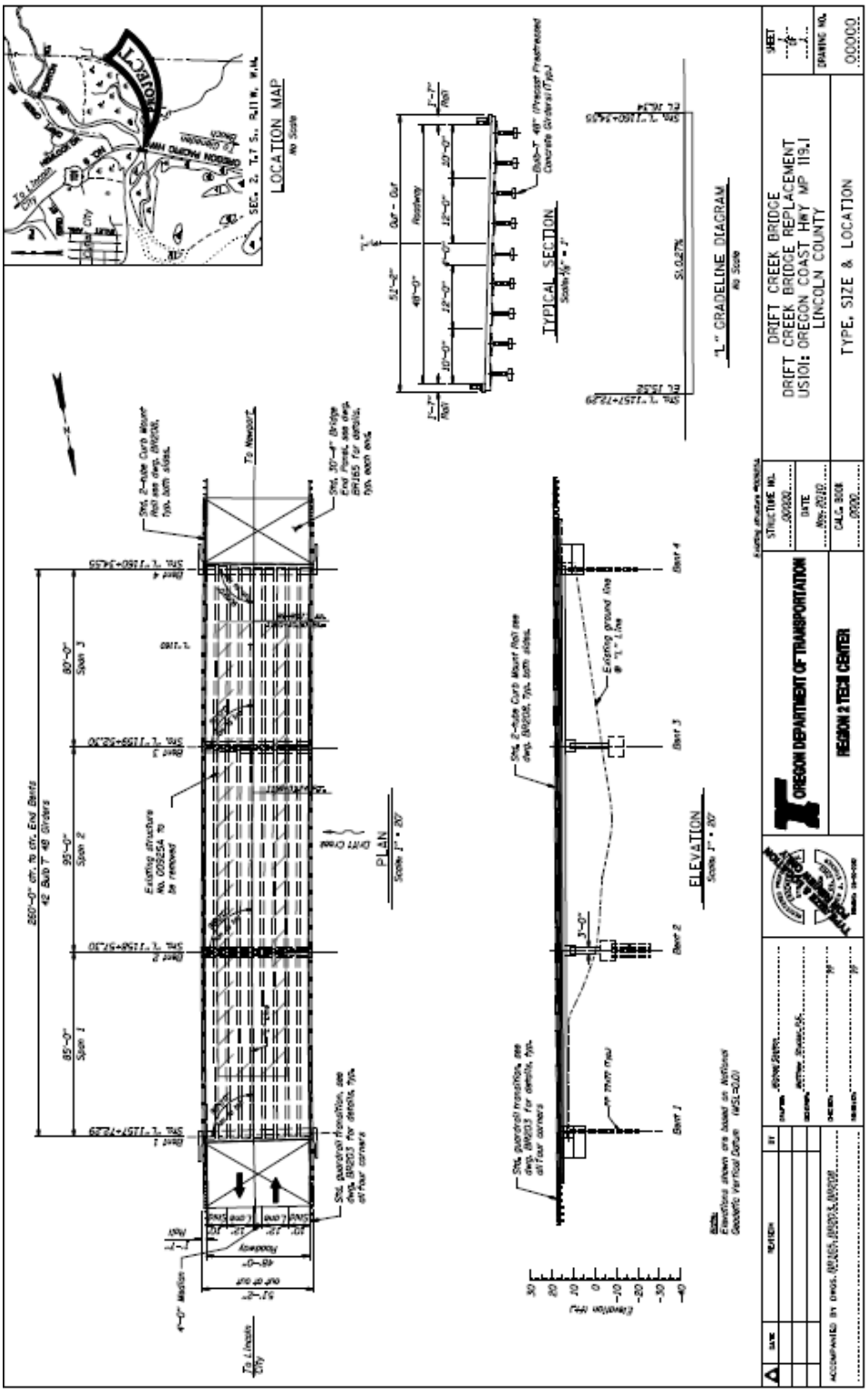

Figure 83 Preliminary drawing of Drift Creek Bridge

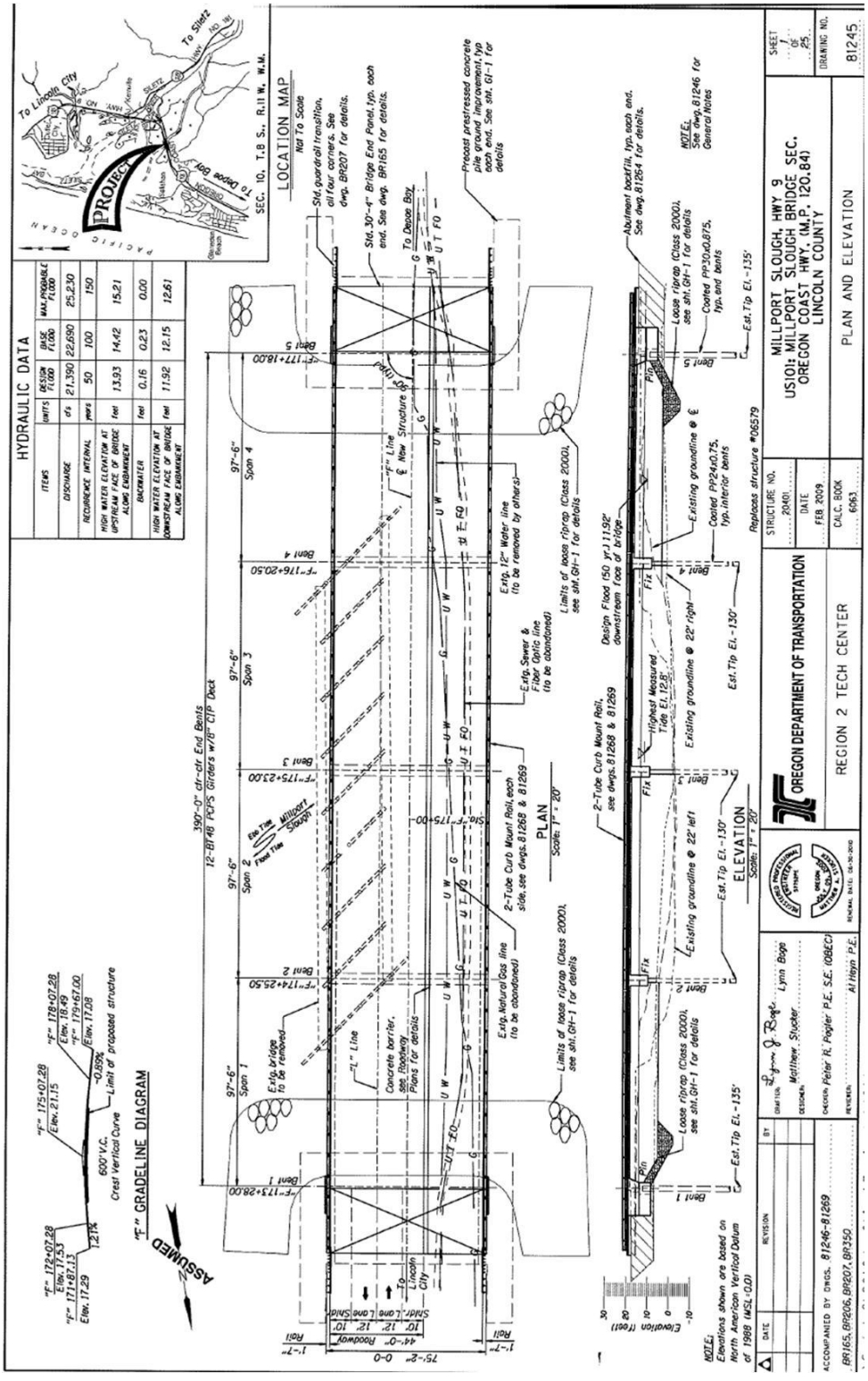

Figure 84 Plan and elevation view of new Millport Slough Bridge

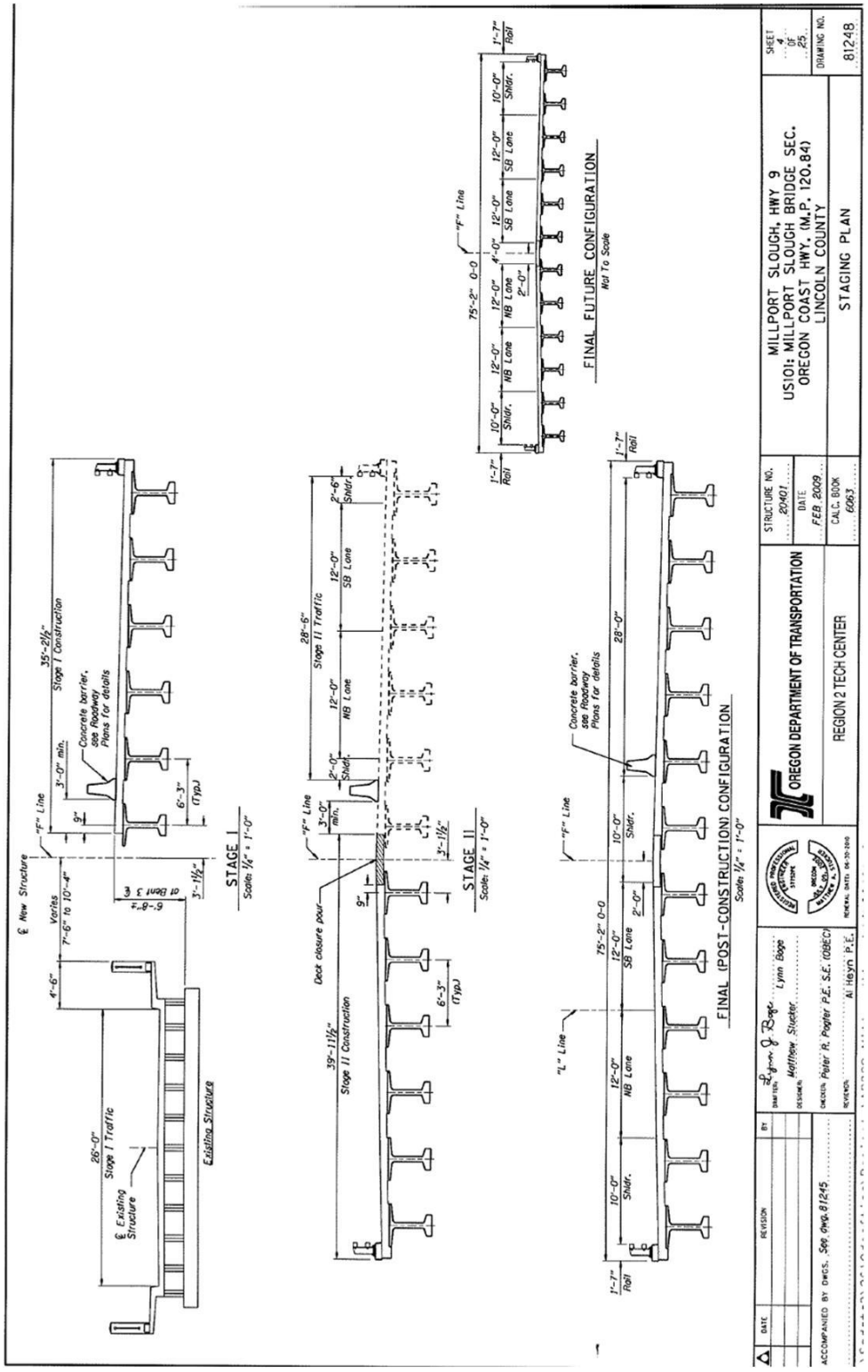

Figure 85 Staging plan of new Millport Slough Bridge

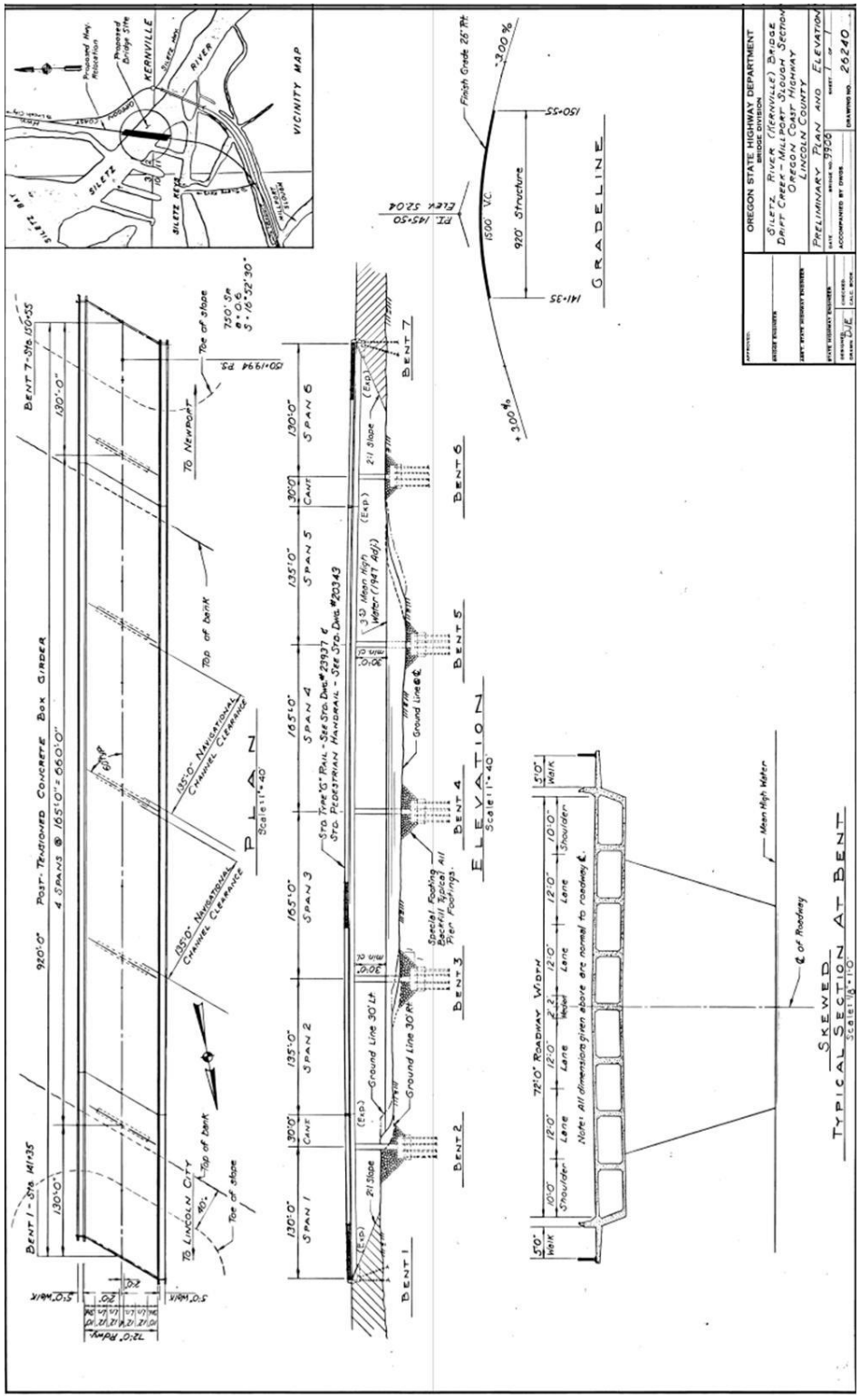

Figure 86 Plan and elevation view of Siletz River Bridge